NPS 69-89-04

NAVAL POSTGRADUATE SCHOOL

Monterey, California

THESIS

M 1832.33

MODEL BASED DESIGN AND VERIFICATION OF A RAPID DIVE CONTROLLER FOR AN AUTONOMOUS UNDERWATER VEHICLE

by

Gordon S. MacDonald

March 1989

Thesis Advisor: A. J. Healey

Approved for public release; distribution is unlimited

Prepared for:
Naval Surface Weapons Center
White Oak, Maryland 20910

T244011

NAVAL POSTGRADUATE SCHOOL
Monterey, California

Rear Admiral R. C. Austin
Superintendent

Harrison Shull
Provost

This report was prepared in conjunction with research conducted for the Naval Surface Warfare Center and funded by the Naval Postgraduate School.

Reproduction of all or part of this report is authorized.

REPORT DOCUMENTATION PAGE

REPORT SECURITY CLASSIFICATION UNCLASSIFIED	1b RESTRICTIVE MARKINGS
SECURITY CLASSIFICATION AUTHORITY	3 DISTRIBUTION / AVAILABILITY OF REPORT Approved for public release; distribution is unlimited
DECLASSIFICATION / DOWNGRADING SCHEDULE	
PERFORMING ORGANIZATION REPORT NUMBER(S) NPS 69-89-04	5 MONITORING ORGANIZATION REPORT NUMBER(S)
NAME OF PERFORMING ORGANIZATION aval Postgraduate School 6b OFFICE SYMBOL (If applicable) Code 69	7a. NAME OF MONITORING ORGANIZATION Naval Postgraduate School
ADDRESS (City, State, and ZIP Code) Monterey, California 93943-5000	7b. ADDRESS (City, State, and ZIP Code) Monterey, California 93943-5000
NAME OF FUNDING / SPONSORING ORGANIZATION aval Surface Weapons Center 8b OFFICE SYMBOL (If applicable)	9. PROCUREMENT INSTRUMENT IDENTIFICATION NUMBER
ADDRESS (City, State, and ZIP Code) hite Oak, Maryland 20910	10 SOURCE OF FUNDING NUMBERS PROGRAM ELEMENT NO. / PROJECT NO / TASK NO / WORK UNIT ACCESSION NO

TITLE (Include Security Classification)
ODEL BASED DESIGN AND VERIFICATION OF A RAPID DIVE CONTROLLER FOR AN UTONOMOUS UNDERWATER VEHICLE

PERSONAL AUTHOR(S)
MacDonald, Gordon S.

a. TYPE OF REPORT echanical Engineer	13b TIME COVERED FROM _____ TO _____	14. DATE OF REPORT (Year, Month, Day) March 1989	15 PAGE COUNT 141

SUPPLEMENTARY NOTATION The views expressed in this thesis are those of the author & do not reflect the official policy or position of the Department of Defense the U. S. Government

COSATI CODES		
FIELD	GROUP	SUB-GROUP

18 SUBJECT TERMS (Continue on reverse if necessary and identify by block number)
Autinomous Underwater Vehicles, Automatic Dive Control, Model Based Compensators

ABSTRACT (Continue on reverse if necessary and identify by block number) Autonomous underwater vehicles are ing considered today by many organizations as a low cost substitute for nned vehicles. Requirements for autonomy emphasize the need for a robust stem controller that can adequately maneuver the vehicle and ensure precise acking of a planned path. This thesis presents the determination of hydro- namic coefficients for vertical motion of a radio controlled underwater hicle based on open loop testing. The equations of motion were manipulated ing software Matrix-x to create satisfactory closed loop control system for pid maneuvering in the vertical plane. Because vehicle data provided by on- ard sensors was limited, both state estimation and disturbance estimation/ mpensation techniques were used, leading to a model based compensator which hanced control. Results show that a satisfactory closed loop control design n be achieved using these modern controller design techniques. The extension the design of steering control is addressed.

DISTRIBUTION / AVAILABILITY OF ABSTRACT ☒ UNCLASSIFIED/UNLIMITED ☐ SAME AS RPT ☐ DTIC USERS	21. ABSTRACT SECURITY CLASSIFICATION UNCLASSIFIED
NAME OF RESPONSIBLE INDIVIDUAL Prof. A. J. Healey	22b TELEPHONE (Include Area Code) (408) 646-2586 22c. OFFICE SYMBOL Code 69Hy

FORM 1473, 84 MAR 83 APR edition may be used until exhausted. All other editions are obsolete

SECURITY CLASSIFICATION OF THIS PAGE

☆ U.S. Government Printing Office: 1986—606-24

Approved for public release; distribution is unlimited.

Model Based Design and Verification of a Rapid Dive Controller for an Autonomous Underwater Vehicle

by

Gordon S. MacDonald
Commander, United States Navy
B.S., United States Naval Academy, 1973

Submitted in partial fulfillment of the requirements for the degree of

MASTER OF SCIENCE IN MECHANICAL ENGINEERING
and
MECHANICAL ENGINEER

from the
NAVAL POSTGRADUATE SCHOOL
March 1989

ABSTRACT

Autonomous Underwater Vehicles are being considered today by many organizations as a low cost substitute for manned vehicles. Requirements for autonomy emphasize the need for a robust system controller that can adequately maneuver the vehicle and ensure precise tracking of a planned path. This thesis presents the determination of hydrodynamic coefficients for vertical motion of a radio controlled underwater vehicle based on open loop testing. The equations of motion were manipulated using software Matrix-x to create a satisfactory closed loop control system for rapid maneuvering in the vertical plane. Because vehicle data provided by on-board sensors was limited, both state estimation and disturbance estimation/compensation techniques were used, leading to a model based compensator which enhanced control. Results show that a satisfactory closed loop control design can be achieved using these modern controller design techniques. The extension to the design of steering control is addressed.

TABLE OF CONTENTS

I. INTRODUCTION..... 1

A. SPECIFIC OBJECTIVES..... 1

B. PREVIOUS WORK..... 3

C. DESIGN APPROACH..... 5

II. VERTICAL MOTION PARAMETER IDENTIFICATION..... 7

A. INTRODUCTION..... 7

B. VALIDATION OF OPEN LOOP EQUATIONS OF MOTION..... 9

C. GENERALIZED DIMENSIONLESS PARAMETERS..... 14

D. PARAMETER SENSITIVITY..... 16

III. INITIAL DESIGN OF VERTICAL MOTION CONTROL..... 19

A. INTRODUCTION..... 19

B. OPEN LOOP CONTROL..... 20

C. DERIVATION OF CLOSED LOOP CONTROL-- CONTINUOUS TIME WITH NO DISTURBANCES..... 23

D. DISCRETE TIME FORM FOR SAMPLED DATA SYSTEM..... 26

E. CLOSED LOOP POLE PLACEMENT..... 30

F. PROTOTYPE VEHICLE PHYSICAL LIMITATIONS..... 31

G. EFFECT OF SENSOR BIAS ON PREDICTED PERFORMANCE..... 32

H. ADDITION OF A STATE OBSERVER..... 34

IV. EFFECT OF EXTERNAL DISTURBANCES AND

THEIR COMPENSATION IN A DISTURBANCE OBSERVER/ESTIMATOR..... 38
A. INTRODUCTION..... 38
B. DISTURBANCE OBSERVER CONCEPT..... 39
C. MODIFIED STATE OBSERVER..... 40
D. DISTURBANCE OBSERVER..... 43
E. SYSTEM RESPONSE..... 47
V. HORIZONTAL EQUATIONS OF MOTION..... 50
A. INTRODUCTION..... 50
B. HORIZONTAL EQUATIONS OF MOTION..... 50
C. STATE SPACE CONFIGURATION..... 55
D. COMPUTOR SIMULATION OF HORIZONTAL MOTION..... 56
VI. TOW TANK TESTING OF VERTICAL MOTION CONTROLLER..... 58
A. INTRODUCTION..... 58
B. CALIBRATION..... 58
C. TEST PROCEDURES AND DATA ACQUISITION..... 60
D. TEST RESULTS..... 61
E. TEST VS. THEORY FOR SELECTED CASES..... 68
VII. CONCLUSIONS AND RECOMMENDATIONS..... 77
A. CONCLUSIONS..... 77
B. RECOMMENDATIONS..... 78

APPENDIX A (MATRIX-X PROGRAM "MOD.MX")..... 80

APPENDIX B (TEST RUN PERFORMANCE CURVES)..... 81
APPENDIX C (MATRIX-X PROGRAM "RMS.MX")..... 90
APPENDIX D (RESULTS OF DATA PROCESSING THROUGH "RMS.MX")..... 91
APPENDIX E (MODEL SENSITIVITY TO M_W)..... 92
APPENDIX F (MATRIX-X PROGRAM "POLE.MX")..... 96
APPENDIX G (DETAILED RESULTS OF POLE OPTIMIZATION STUDY USING "POLE.MX" WITH A 20 HZ SAMPLING RATE)..... 97
APPENDIX H (SELECTED POLE PLACEMENT PERFORMANCE)..... 99
APPENDIX I (SATURATED CLOSED LOOP SYSTEM)..... 102
APPENDIX J (SATURATED SYSTEM RESPONSE)..... 103
APPENDIX K (SATURATED AND BIASED SYSTEM BLOCK DIAGRAM AND RESPONSE). 106
APPENDIX L (OBSERVED SYSTEM BLOCK DIAGRAM)..... 113
APPENDIX M (MATRIX-X PROGRAM "DISTPOLE.MX")... 115
APPENDIX N (AUV HORIZONTAL MOTION SYSTEM BLOCK DIAGRAM)..... 119
APPENDIX O (MATRIX-X PROGRAMS "AUVTURNPLOT" AND "AUVMULTIPLOT")..... 120
APPENDIX P (AUV HORIZONTAL SYSTEM RESPONSE).... 121
APPENDIX Q (MATRIX-X PROGRAM "DEPTHIN.MX" BLOCK DIAGRAM)..... 124
APPENDIX R ("DEPTHIN.MX" PERFORMANCE CURVES)... 125

LIST OF REFERENCES..... 128
INITIAL DISTRIBUTION LIST..... 130

I. INTRODUCTION

A. SPECIFIC OBJECTIVES

In recent years, interest in the use of the Autonomous Underwater Vehicle (AUV) has increased in both the United States Navy and private industry. It is now recognized that these vehicles may perform a variety of missions more efficiently than the traditionally larger, more costly manned vessels. Potential missions include surveillance, search and rescue, decoy, early warning border patrol, and deep oceanographic research. The use of AUV's in this type of work may not only be less expensive, but will also reduce the exposure of human operators to the dangers associated with these types of work.

This study was concerned with the application of advanced control theory and methods for the control of vehicle reflexive maneuvers. These can be considered as the lowest level of control in the overall hierarchy of unmanned vehicle artificial intelligence. Figure 1.1 illustrates how this thesis relates to this hierchy.The design scenario assumed that mission and planning level control had already recognized the need for evasive action and had already decided on a required depth change. This depth change

command was then sent to the maneuvering controller which was responsible for positioning dive planes to complete

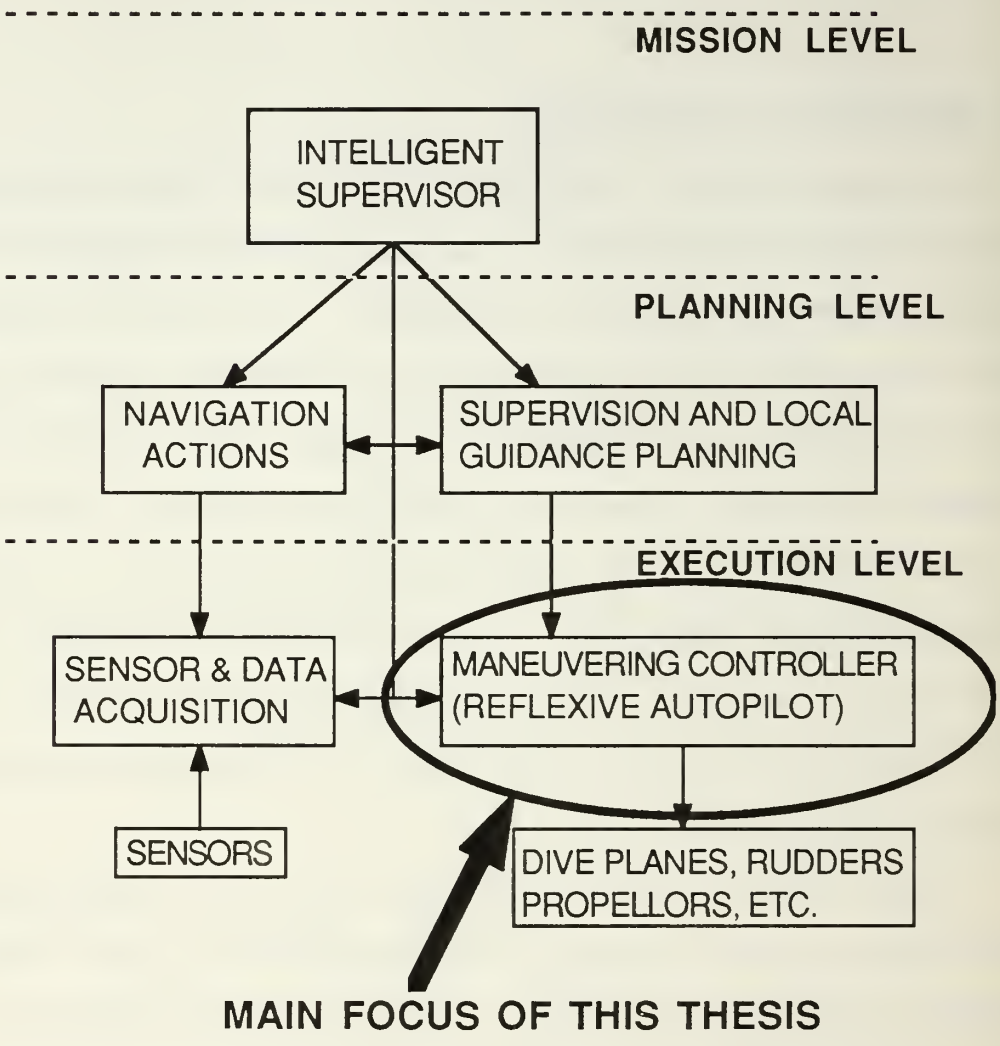

Figure 1.1. Artificial Intelligence Hierarchy

the depth change as rapidly as possible without a loss of vehicle stability or excessive cycling of the associated

mechanical systems. The design of this maneuvering controller was the goal of this study.

The trade-off between vehicle maneuverability and stability is widely recognized by controls engineers. The main objective of this thesis was to investigate the performance of a control system for rapid depth changes, thereby improving the vehicle's maneuverability without an unacceptable loss of inherent stability. There has been progress in recent years in developing control systems capable of handling minor or slow maneuvers. This thesis, however, focused on a controller that could perform quick response collision avoidance maneuvers involving radical depth changes. It further studied the application of state observers and disturbance estimators in the controller design. These observers were used to estimate and account for unmeasured vehicle motion and forces with the intention of developing a robust controller while minimizing onboard equipment and sensors needed to provide real time data.

B. PREVIOUS WORK

Classical controls for submarine vehicles have been used successfully for automating vehicle hovering during missile firing. Global position referencing using an integrated navigation system can provide high accuracy global

placement. However, high accuracy inertial navigation units may be too large and costly for AUV operations.

High speed maneuvering controls for torpedoes have been developed along classical control lines with success. The issue for AUV's, however, is different because of their slow speed range anticipated at around 5 knots cruise speed, with a high degree of maneuverability at even slower speeds. It is expected that recent control technology can help to provide high quality robust maneuvering controls for these vehicles, as well as further information concerning the range of variability of their hydrodynamic/mechanical performance.

The initial assessment of the AUV concept conducted by the Naval Postgraduate School was prepared in October 1987 Healey, Cristi, Smith and McGhee [Ref. 1]. This proposal addressed the institution's capabilities for the design, construction, testing and operation of an AUV research prototype. A suitable model was chosen based on the proposed Swimmer Delivery Vehicle [Ref. 2] and simplified equations of motion for that specific prototype were developed by Boncal [Ref. 3]. The actual prototype was constructed by Brunner in 1988 [Ref.4]. Equipment installed in the prototype included a pressure cell depth sensor and gyros for pitch roll and yaw rate signals. The model itself was 30 inches long, seven inches wide and four

inches high with two shafts powered by two separate DC motors. Open loop controlled tow tank runs provided first estimates of the prototype hydrodynamic coefficients.

C. DESIGN APPROACH

The first step was to verify the hydrodynamic coefficients determined in Reference 4. This was done by comparing open loop test results with the theoretical results obtained using the computer software Matrix-x. The result of this study was the determination of a general set of hydrodynamic coefficients that adequately model the prototype response at different speeds. With an adequate model now in hand, the closed loop controller was developed based on the design objective of completing depth changes within approximately five seconds (Chapter 2).

Building this controller using current design methods would require that onboard sensors provide continuous updated data on vehicle pitch angle and pitch rate as well as depth. The NPGS AUV prototype was built with a depth cell and rate gyro only, with the depth cell being the most noise free sensor. The controller was therefore designed to operate using only one input, depth. Pitchrate and pitch angle were provided by incorporating a state observer/estimator (Chapter 3), to determine the effectiveness of a compensator designed from depth signals only.

An attempt to further enhance the robustness of the controller was conducted (Chapter 4) by adding to the controller an additional observer to account for hydrodynamic disturbances that were not adequately modelled by the equations of motion of Reference 4. Controller design was then verified using tow tank tests of the prototype in Chapter 6.

The techniques used in Chapters 2, 3 and 4 were conducted for analysis of motion in the vertical plane only. An introduction to the application of these techniques for horizontal motion was also discussed.

II. VERTICAL MOTION PARAMETER IDENTIFICATION

A. INTRODUCTION

The basic open loop equations of motion for a submerged vehicle were first derived by Gertler and Hagen [Ref. 5] and were later published by Abkowitz [Ref. 6]. These equations represented the 12 state, nonlinear model of a submarine. Boncal first applied the equations to the NPS AUV prototype vehicle [Ref. 3], following the work at NCSC on the Swimmer Delivery Vehicle simulator [Ref. 2]. Further development of the equations was performed by Brunner [Ref. 4], simplifying them to the four state, linearized, straight path, vertical motion form:

$$\dot{w} = \frac{(Z_W)(U_X)(w)}{(M_{ZDW})} + \frac{(Z_Q)(U_X)(q)}{(M_{ZDW})} + \frac{(Z_D)(U_X^2)(\delta)}{(L)(M_{ZDW})} + \frac{(F_1)}{(M_{ZDW})} \tag{2.1}$$

$$\dot{q} = \frac{(M_W)(U_X)(w)}{(L^2)(I_{YY})} + \frac{(M_Q)(U_X)(q)}{(L)(I_{YY})} + \frac{(M_D)(U_X^2)(\delta)}{(L^2)(I_{YY})} + \frac{(F_2)}{(M_{ZDW})} \tag{2.2}$$

$$\dot{\theta} = q \tag{2.3}$$

$$\dot{z} = w - (U_X)(\Theta) \qquad (2.4)$$

Where the measured variables are shown in Table 2.1, and the dimensionless hydrodynamic parameters are shown in Table 2.2 below.

These parameters were initially estimated by Brunner [Ref. 4] using hydrodynamics theory. In this study, the

TABLE 2.1 NPS AUV PROTOTYPE MEASURED PARAMETERS

q = Pitch Rate
z = Water Depth
Ux = Forward Speed
δ = Dive Plane Angle

TABLE 2.2 AUV PROTOTYPE DIMENSIONLESS HYDRODYNAMIC PARAMETERS

Z_W = Heave Damping
Z_Q = Pitch Cross Coupling
M_W = Heave Cross Coupling
M_Q = Pitch Damping
Z_D = Moment Effect
M_D = Moment Effect ($M_D = 2*Z_D$)
M_{ZDW} = Mass plus Added Mass
I_{YY} = Inertia plus Added Mass

vehicle equations of motion and their respective dimensionless parameters were first verified based on

experimental open loop diving motion observed in a tow tank. Graphical plots of actual vehicle performance as recorded by on-board sensors was compared with similar plots of vehicle performance predicted by Equations 2.1 through 2.4. Values for the nondimensional parameters listed in Table 2.2 were thereby refined. The result was a set of equations that appeared to accurately model the pitchrate response of the NPGS AUV prototype. Experimental and theoretical depth responses did not compare as well as the pitchrates because unmodelled biases and disturbance forces cause large changes in depth response while having little effect on pitchrate response. However, the simulation was determined to be adequate to support the design of the initial controller. The method used in the identification of these parameters is the subject of this chapter.

B. VALIDATION OF OPEN LOOP EQUATIONS OF MOTION

The NPS AUV prototype was subjected to a series of water trials described in Reference 4. In these trials, actual vehicle responses to specific control inputs (dive plane angle) were recorded. Vehicle responses were measured by onboard sensors monitoring vehicle pitch rate and depth. Dive plane commands were generated using a joy stick and a radio transmitter, with signals received from the vehicle

via a tether--a power sensor output cord. These water trials produced ten sets of data that were used in dimensionless parameter identification. Each data set contained three reliable parameters--depth (z), pitch rate (q) and dive plane angle (δ).

The commercial computer software package Matrix-x was used to determine the best values for the non-dimensional parameters Table 2.2. First, the equations were written in the state-space format:

$$\dot{x} = Ax + Bu \qquad (2.5)$$

$$y = Cx + Du \qquad (2.5a)$$

where x, the state variable, was defined as

$$x' = [w \; q \; \Theta \; z]$$

When the elements from Equations (2.1) through (2.4) were substituted into the matrices A, B, C and D of Equations (2.5) and (2.5a), they became:

$$A = \begin{vmatrix} \frac{Z_W U_X}{M_{ZDW}} & \frac{Z_Q U_X}{M_{ZDW}} & 0 & 0 \\ \frac{M_W U_X}{L^2 I_{YY}} & \frac{M_Q U_X}{L I_{YY}} & 0 & 0 \\ 0 & 1 & 0 & 0 \\ 1 & 0 & -U_X & 0 \end{vmatrix} \quad B = \begin{vmatrix} \frac{-Z_Q U_X^2}{L M_{ZDW}} & \frac{F_1}{M_{ZDW}} \\ \frac{M_D U_X^2}{L^2 I_{YY}} & \frac{F_2}{I_{YY}} \\ 0 & 0 \\ 0 & 0 \end{vmatrix}$$

$$C = \begin{vmatrix} 1 & 0 & 0 & 0 \\ 0 & .72 & 0 & 0 \\ 0 & 0 & 1 & 0 \\ 0 & 0 & 0 & 3 \end{vmatrix} \quad D = \begin{vmatrix} 0 & 0 \\ 0 & 0 \\ 0 & 0 \\ 0 & 0 \end{vmatrix}$$

Where:

1. u was the system input (dive plane angle, δ, in this case)
2. y contains the outputs to be analyzed by Matrix-x.

Simplifying, the resultant state-space formulation for the motion of the NPS AUV prototype under open loop control became:

$$\dot{x} = \begin{vmatrix} \dot{w} \\ \dot{q} \\ \dot{\theta} \\ \dot{z} \end{vmatrix} = \begin{vmatrix} p_1 & p_2 & 0 & 0 \\ p_3 & p_4 & 0 & 0 \\ 0 & 1 & 0 & 0 \\ 1 & 0 & -U_X & 0 \end{vmatrix} \begin{vmatrix} w \\ q \\ \theta \\ z \end{vmatrix} + \begin{vmatrix} p_5 & p_6 \\ p_7 & p_8 \\ 0 & 0 \\ 0 & 0 \end{vmatrix} \begin{vmatrix} \delta \\ 1 \end{vmatrix} \qquad (2.6)$$

$$y = \begin{vmatrix} w \\ q \\ \theta \\ z \end{vmatrix} = \begin{vmatrix} 1 & 0 & 0 & 0 \\ 0 & .72 & 0 & 0 \\ 0 & 0 & 1 & 0 \\ 0 & 0 & 0 & 3 \end{vmatrix} \begin{vmatrix} w \\ q \\ \theta \\ z \end{vmatrix} + \begin{vmatrix} 0 & 0 \\ 0 & 0 \\ 0 & 0 \\ 0 & 0 \end{vmatrix} \begin{vmatrix} \delta \\ 1 \end{vmatrix} \qquad (2.6a)$$

Where :

$$p_1 = \frac{Z_w U_X}{M_{ZDW}} \qquad p_2 = \frac{Z_Q U_X}{M_{ZDW}} \qquad p_3 = \frac{M_w U_X}{L^2 I_{YY}}$$

$$p_4 = \frac{M_Q U_X}{L I_{YY}} \qquad p_5 = \frac{-Z_Q U_X^2}{L M_{ZDW}} \qquad p_6 = \frac{F_1}{M_{ZDW}}$$

$$p_7 = \frac{M_D U_X^2}{L^2 I_{YY}} \qquad p_8 = \frac{F_2}{I_{YY}}$$

In the above development, the force F_1 and the moment F_2 were included to represent the influence of unmodelled

factors and disturbance loads such as those from power cord drag, suction forces and other external effects lumped to the input. While these effects are not generally constant, they were modelled here as constants to begin with.

Equations (2.6) and (2.6a) were then analyzed by the Matrix-x program "MOD.MX" (see Appendix A). This program produced plots of actual vehicle motion overlaid on plots of predicted vehicle motion. The actual motion curves were generated from the onboard sensor data. The predicted motion curves were generated by the system mathematical model, Equations (2.6) and (2.6a). Different values for the parameters of Table 2.2 were inserted into the mathematical model equations until a set of "best" values was found. The best values for the dimensionless parameters were those that generated predicted performance curves that fit closest to the actual performance curves. While an optimization criterion such as minimization of sum of squared errors was not used, "best" fit was used in the context of visually matching peaks, rise times, zero crossings, average values, etc.

Initially, ten of the separate water trials run in Reference 4 were examined individually. A separate set of best fitting dimensionless parameters was determined for each separate water trial run. This resulted in ten separate sets of "best" parameters values. See Appendix B

for the resultant parameters and their respective performance curves. Realization of these parameters verified that the equations of motion did provide a reasonably accurate model of the vehicle response characteristics.

C. GENERALIZED DIMENSIONLESS PARAMETERS

The determination of best fit parameters for separate test runs served to validate the system model, Equations (2.1) through (2.4). A more generalized set of parameter values was required, however, in order to use the system model to predict actual vehicle response under varying conditions, and it was of interest to know the range of their variability and sensitivity to input levels and functional form.

To accomplish this, another Matrix-x program, "RMS.MX" was written to determine the root mean squared error between actual vehicle performance curves and the predicted performance curves that were generated by the "MOD.MX" program. See Appendix C. The objective was now to determine the values of a more generalized set of parameters that could be applied to more than just one specific water trial run. Three experimental sets of generalized parameters were examined. Each set of parameters was analyzed by "RMS.MX" to determine which

set resulted in the smallest root mean square error between actual and predicted performance. The following experimental sets were analyzed:

Set #1. A "nominal" set that was originally used in the analogue simulation of the vehicle responses [Ref.4].
Set #2. An "average" set of parameters--the statistical average of the ten sets of best fit parameters determined previously in Section A.
Set #3. Three separate sets of parameters--one for each of the three vehicle speeds used in the water trials of Reference 4.

See Appendix D for the detailed results of processing methods 1,2, and 3 through "RMS.MX". The root mean square errors that "RMS.MX" calculated for each of the three experimental sets were as follows:

Set #1. Nominal parameters : pitch rate error = .1287 volts, depth error = 11.1738 volts.
Set #2. Average set : pitch rate error = .0304 volts, depth error = 4.7161 volts.
Set #3. One set for each speed : pitch rate error = .0233 volts, depth error = 3.9130 volts.

It was determined that Set #3--separate parameter values for each vehicle speed--resulted in the least error between actual and predicted performance curves. Based on these computer simulations, the following values for the dimensionless values listed above were to be used in subsequent computer simulations of the vehicle:

SPEED	Z_W	Z_Q	M_W	M_Q	Z_D	M_D	M_{ZDW}	I_{YY}	F_1	F_2
1.2	-1.5	0	0	-.19	0	.18	1.005	.072	.11	0
1.8	-1.5	0	0	-.15	0	.38	1.005	.072	.11	0
2.1	-1.5	0	0	-.15	0	.253	1.005	.072	.11	0

To account for variations in onboard sensor null points, additional biases were added to the predicted curves for depth and pitch rate. They were:

SPEED	DEPTH BIAS	PITCH RATE BIAS
1.2	2.6	.07
1.8	4.78	.058
2.1	4.1	.056

D. PARAMETER SENSITIVITY

To help in determining the robustness of the system mathematical model using the selected non-dimensional parameters, a sensitivity study was performed. The "best fit" parameters were varied individually and then run through the "RMS.MX" program to determine the resultant effect on the fit between the actual and predicted performance curves. Results indicated that the model was not excessively sensitive to any of the individual parameters. Depth predictions were most sensitive to M_W, I_{YY}, F_1 and F_2. Pitch rate predictions were most sensitive to M_W, M_Q, M_D and F_2. It can be pointed out, however, that:

1. F_1 and F_2 are coefficients that take into effect the weight of the power supply tether. This tether was temporary and would not be used with subsequent AUV prototypes. These factors will be discarded at that time.
2. I_{YY} was reasonably calculated using the AUV physical characteristics. The values used were reasonably reliable and appeared to match the pitchrate responses well.
3. Sensitivities to M_W, Z_Q and M_D alone were slight and presented no foreseeable problems.

Of particular interest was the model sensitivity to the coefficient M_W. Appendix E illustrates these results. The effect can be summarized using Figure 2.1 as follows:

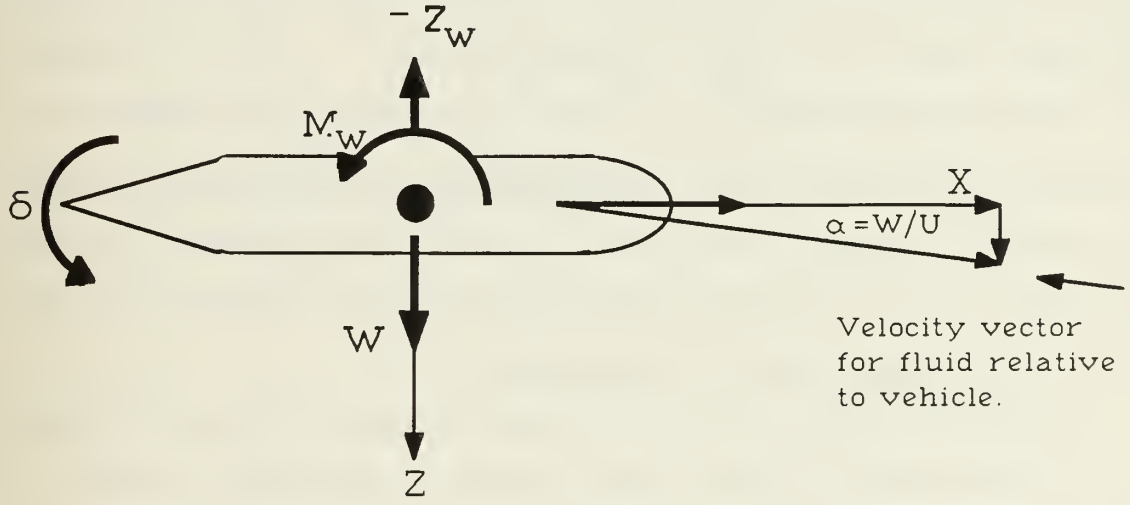

Figure 2.1 M_W Description

The coefficient M_W related to the influence that heave velocity, w, had on the pitch moment. When a vehicle moving with constant forward velocity, U, undergoes a heave velocity, w, the fluid particles no longer impinge directly on the nose of the vehicle but at some angle of

attack, α, to the vehicle centerline where $\alpha = w/U$. When the shape of the vehicle is like a wing, a lift force and moment, Z_w and M_w is established dependent on U and α. For a symmetric body, the moment, M_w, about the half length position may not be so large. It was found that the convenient value of zero appeared to match experimental data reasonably well. Increasing the heave-pitch coupling had the tendency to give a more damped character to the pitch rate response.

The most unusual thing about this is that the elimination of the pitch-heave coupling seemed to give the best prediction of the pitchrate response. While unusual, this was rationalized as correct by viewing the body as a wing symmetrical about its midpoint. More importantly, this result allowed the model to be later modified from a four state space ($\mathbf{x}' = [w\ q\ \theta\ z]$) to a three state space ($\mathbf{x}' = [q\ \theta\ z]$) as described in Chapter 3.

III. INITIAL DESIGN OF VERTICAL MOTION CONTROL

A. INTRODUCTION

In Chapter 2, Matrix-x was used to analyze the NPS AUV prototype equations of motion in the form:

$$S = \left|\begin{array}{c|c} A & B \\ \hline C & D \end{array}\right| \qquad (3.1)$$

which represented the simultaneous equations:

$$\dot{\mathbf{x}} = \mathbf{A}\mathbf{x} + \mathbf{B}\mathbf{u} \qquad (3.2)$$

$$\mathbf{y} = \mathbf{C}\mathbf{x} + \mathbf{D}\mathbf{u} \qquad (3.2a)$$

where X was the state variable:

$$\mathbf{x}' = [w \; q \; \Theta \; z] \qquad (3.3)$$

and $\mathbf{u}$ was the system input, and $\mathbf{y}$ the system output.

Using the dimensionless parameters determined in Chapter 2, Equations (3.2) and (3.2a) represented the equations of motion that described the motions of the NPS AUV Prototype. The equations' accuracy was verified by a favorable comparison between the actual and predicted vehicle motion. The objective of this chapter is to describe

the design of the closed loop control system for this system model.

B. OPEN LOOP CONTROL

The system model under open loop control is illustrated as shown in Figure 3.1 below:

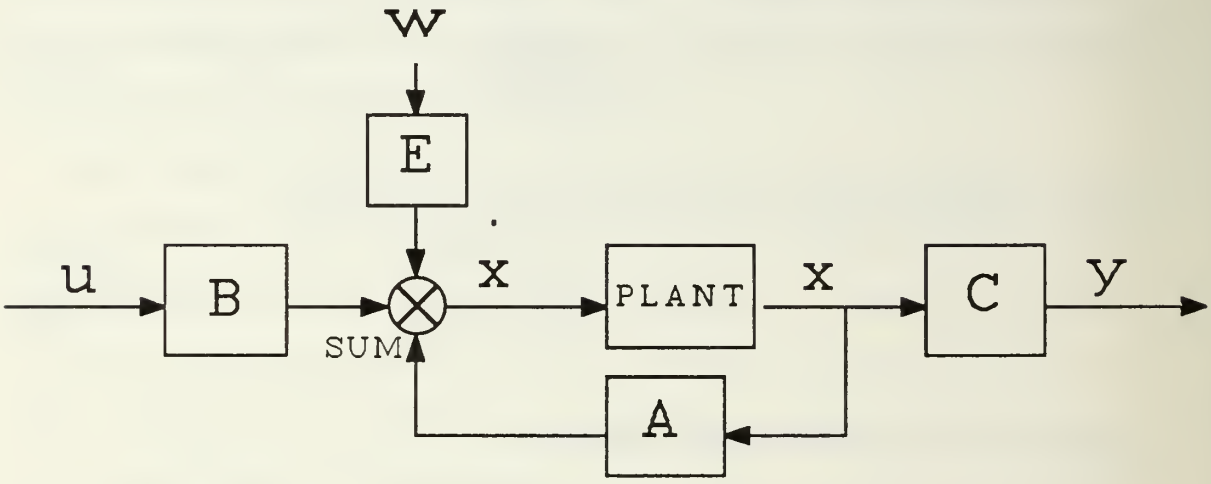

Figure 3.1 Open Loop Control

Figure 3.1. graphically describes Equations (3.2) and (3.2a) where the disturbance forces are contained within the external input, w. Equations (3.2) and (3.2a) are shown again below, with the included disturbance:

$$\dot{x} = Ax + Bu + Ew$$

$$y = Cx + Du$$

This was the open loop control used in the ten water trials of Reference 4, discussed in Chapter 2. Substituting values for the parameters of Tables 2.1 and 2.2 of Chapter 2 into the A, B, C and D Matrices of Equation (3.1) resulted in the following matrix representation of the OPEN LOOP control system, where the column vectors for B and E are combined, and **w** is represented as unity for convenience:

OPEN LOOP

$$\dot{\mathbf{x}} = \begin{vmatrix} \dot{w} \\ \dot{q} \\ \dot{\theta} \\ \dot{z} \end{vmatrix} = \begin{vmatrix} p_1 & p_2 & 0 & 0 \\ p_3 & p_4 & 0 & 0 \\ 0 & 1 & 0 & 0 \\ 1 & 0 & -U_X & 0 \end{vmatrix} \begin{vmatrix} w \\ q \\ \theta \\ z \end{vmatrix} + \begin{vmatrix} p_5 & p_6 \\ p_7 & p_8 \\ 0 & 0 \\ 0 & 0 \end{vmatrix} \begin{vmatrix} \delta \\ 1 \end{vmatrix} \qquad (3.3)$$

and

$$\mathbf{y} = \begin{vmatrix} w \\ q \\ \theta \\ z \end{vmatrix} = \begin{vmatrix} 1 & 0 & 0 & 0 \\ 0 & .72 & 0 & 0 \\ 0 & 0 & 1 & 0 \\ 0 & 0 & 0 & 3 \end{vmatrix} \begin{vmatrix} w \\ q \\ \theta \\ z \end{vmatrix} + \begin{vmatrix} 0 & 0 \\ 0 & 0 \\ 0 & 0 \\ 0 & 0 \end{vmatrix} \begin{vmatrix} \delta \\ 1 \end{vmatrix} \qquad (3.3a)$$

In the sensitivity calculations described in Chapter 2, it was determined that the effect of heave velocity and tether tension on vehicle depth control were negligible. Equations (3.3) and (3.3a) were then simplified by assuming heave velocity (w) and tether drag factor (p_8) negligible. The matrices then became:

$$\dot{x} = \begin{vmatrix} \dot{q} \\ \dot{\theta} \\ \dot{z} \end{vmatrix} = \begin{vmatrix} p_4 & 0 & 0 \\ 1 & 0 & 0 \\ 0 & -U_X & 0 \end{vmatrix} \begin{vmatrix} q \\ \theta \\ z \end{vmatrix} + \begin{vmatrix} p_7 \\ 0 \\ 0 \end{vmatrix} |\delta| \qquad (3.4)$$

and

$$y = \begin{vmatrix} q \\ \theta \\ z \end{vmatrix} = \begin{vmatrix} .72 & 0 & 0 \\ 0 & 1 & 0 \\ 0 & 0 & 3 \end{vmatrix} \begin{vmatrix} q \\ \theta \\ z \end{vmatrix} + \begin{vmatrix} 0 \\ 0 \\ 0 \end{vmatrix} |\delta| \qquad (3.4a)$$

Equations (3.4) and (3.4a) do not include the disturbance inputs for convenience, and, as needed, disturbances are introduced by the addition of a second column of parameters in the **B** matrix.

C. DERIVATION OF CLOSE LOOP CONTROL-- CONTINUOUS TIME WITH NO DISTURBANCES

Closed loop control was added by inserting the appropriate feedback gains into the system of Figure 3.1. This feedback allowed the controller to continuously shape the input u such that the output y was maintained at a desired value. In this case, u was the dive plane angle and y was the vehicle depth. This "closed loop" control system is illustrated in Figure 3.2. The objective was for the control system to maintain the value of u (dive plane angle) as necessary to:

1. Regulate the vehicle to the desired depth
2. Carry out depth change maneuvers.

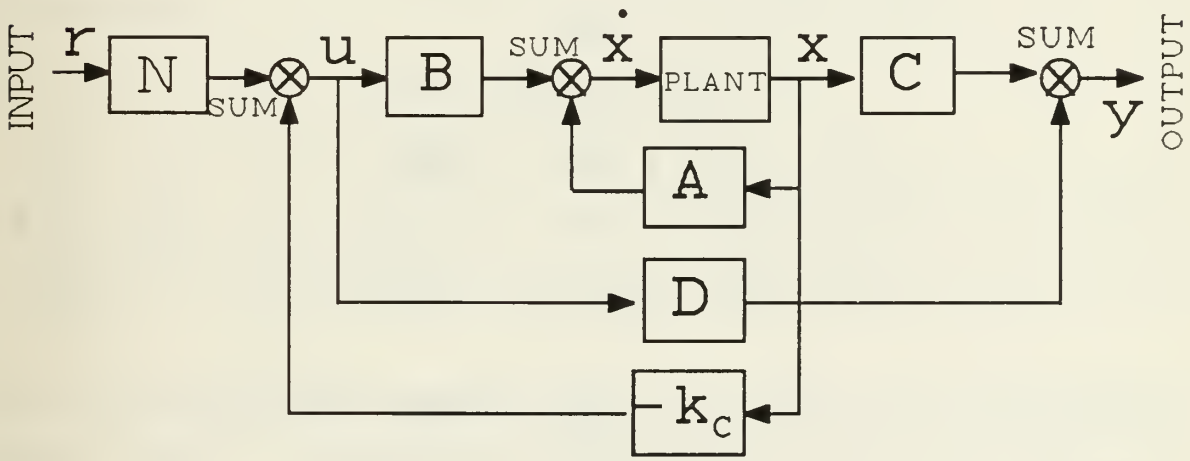

Figure 3.2. Closed Loop Control System

The design of the closed loop control system started with the following control law which is a linear combination of

the vehicle motion states and the reference commands:

$$u = -K_c x + Nr$$

where: x represents the state variables,

r is the reference signal, and is assumed to be constant

This control law, derived from applications of modern, multivariable control theory [Ref. 7] was substituted into the original model of Equation (3.2) to get:

$$\begin{aligned} x &= Ax + B(-Kx + Nr) \\ &= Ax - BKx + BNr \end{aligned}$$

or

$$x = (A - BK)x + (BN)r \qquad (3.5)$$

and

$$\begin{aligned} y &= Cx + D(-Kx + Nr) \\ &= Cx + DNr - DKx \end{aligned}$$

or

$$y = (C - DK)x + DNr \qquad (3.6)$$

Equations (3.4) and (3.5) were shaped into the format of Equation (3.1) for analysis by Matrix-x. The closed system matrix, SC, then became:

$$SC = \left| \begin{array}{cc} AC & BC \\ \hline CC & DC \end{array} \right| \qquad (3.7)$$

where: $AC = A - BK$, $BC = BN$

$CC = C$, $DC = D$

Closing the control loop as described above required the following matrix manipulations:

Starting with the closed loop version of Equation (3.5),

$$\dot{x} = ACx + BCu \qquad (3.8)$$

$$y = Cx + Du \qquad (3.8a)$$

and substituting the simplified closed loop matrices of Equations (3.4) and (3.4a) into Equations (3.8) and (3.8a) resulted in:

$$\dot{x} = \begin{vmatrix} \dot{q} \\ \dot{\theta} \\ \dot{z} \end{vmatrix} = \left\{ \begin{vmatrix} p_4 & 0 & 0 \\ 1 & 0 & 0 \\ 0 & -U_X & 0 \end{vmatrix} - \begin{vmatrix} p_7 \\ 0 \\ 0 \end{vmatrix} \begin{vmatrix} K_1 & K_2 & K_3 \end{vmatrix} \right\} \begin{vmatrix} q \\ \theta \\ z \end{vmatrix} + \left\{ \begin{vmatrix} p_7 \\ 0 \\ 0 \end{vmatrix} \begin{vmatrix} N_1 & N_2 & N_3 \end{vmatrix} \right\} r$$

and

$$y = \begin{vmatrix} .72 & 0 & 0 \\ 0 & 1 & 0 \\ 0 & 0 & 3 \end{vmatrix} \begin{vmatrix} q \\ \theta \\ z \end{vmatrix}$$

Note that the state feedback gains (K_1, K_2, K_3) may be computed using linear quadratic regulator or poleplace techniques, and the setpoint scale factor, N, is selected to achieve a zero error in the steady state condition.

D. DISCRETE TIME FORM FOR SAMPLED DATA SYSTEM

At this point, it is best to shift to the use of discrete time state equations. This is because modern, real time controllers are implemented using microprocessor based hardware and the actual gathering and analyzing of data in this study was done using digital computers sampling discrete data points to model the AUV motion.

Under the continuous time State Equation (3.2), vehicle motion was modelled as:

$$\dot{x} = Ax + Bu$$

Computer controlled vehicle motion is more appropriately described, however, using the discrete equation:

$$x_{K+1} = Gx_K + Hu_K$$

where K = 0,1,2,3,... represented the sequential individual data pieces processed by the digital computer. The values for G and H in terms of A and B are determined by

evaluating Equation (3.2) using the sampling period T utilized by the digital system, or:

$$\dot{\mathbf{x}} = \mathbf{Ax} + \mathbf{Bu}$$

which becomes, when integrated,

$$\mathbf{x}(t) = e^{\mathbf{A}t}\mathbf{x}(0) + e^{\mathbf{A}t}\int_0^t e^{-\mathbf{A}\tau}\,\mathbf{B}\mathbf{u}(\tau)d\tau$$

If T is selected to be short enough such that $\mathbf{u}(t)$ is constant over the sample period (as input from a standard zero order hold Digital to Analog Converter),

$$\mathbf{u}(\tau) = \mathbf{u}(KT)$$

$$\text{for } 0 < \tau < T \quad \text{and} \quad KT < t < (K+1)t$$

and since

$$\mathbf{x}((K+1)T) = e^{\mathbf{A}((K+1)T)}\,\mathbf{x}(0) + e^{\mathbf{A}((K+1)T)}\int_0^{(K+1)T} e^{-\mathbf{A}\tau}\mathbf{B}u(\tau)\,d(\tau)$$

and

$$\mathbf{x}(KT) = e^{\mathbf{A}KT}\,\mathbf{x}(0) + e^{\mathbf{A}KT}\int_0^{KT} e^{-\mathbf{A}\tau}\mathbf{B}\mathbf{u}(\tau)\,d\tau$$

then

$$\mathbf{x}((K+1)T) = e^{AT}\,\mathbf{x}(KT) + e^{A(K+1)T}\int_{KT}^{(K+1)T} e^{-A\tau}\mathbf{B}\mathbf{u}(\tau)d\tau$$

$$= e^{AT}\,\mathbf{x}(KT) + e^{AT}\int_{0}^{T} e^{-At}\,\mathbf{B}\mathbf{u}(KT)d\tau$$

or

$$\mathbf{x}((K+1)T) = e^{AT}\,\mathbf{x}(KT) + \int_{0}^{T} e^{A\lambda}\,\mathbf{B}\mathbf{u}(KT)d\lambda \qquad (3.9)$$

where $\lambda = T - t$

If $G(T)$ was defined as $e^{AT} = G$

and $H(T)$ was defined as $\left(\int_{0}^{t} e^{At}\,dt\right)B = H$

then Equation (3.9) became

$$\mathbf{x}_{(K+1)T} = G\mathbf{x}_{KT} + H\mathbf{u}_{KT}$$

From this point on, vehicle equations of motion will be written in the discrete format. State Equation matrices will continue to be labeled as **A**, **B**, **C** and **D** matrices, but will hereafter refer to the discrete case when the subscripts (K), (K+1),... appear. Specifically, the discrete format will be:

$$x_{K+1} = Ax_K + Bu_K$$

$$y_K = Cx_K + Du_K$$

for K = 0,1,2,3,...N

while the continuous format will remain:

$$\dot{x} = Ax + Bu$$

$$y = Cx + Du$$

This discrete format is then used to complete the derivation of the closed loop control system by finding an expression for the N matrix from Figure 3.2.

Since state conditions at time K+1 could be described as:

$$x_{K+1} = Ax_K + Bu_K$$

$$y_K = Cx_K + Du_K$$

FOR K = 0,1,...N

When this system was in steady state,

$$x_{K+1} = x_K = x_{SS}$$

or

$$Ix_{SS} = Ax_{SS} + Bu_{SS}$$

Since $u = -K_c x + Nr$ (control law)

then

$$Ix_{SS} = (A - BK)x_{SS} + BNr_{SS}$$

$$x_{SS} = [I-(A-BK)]^{-1}BNr_{SS}$$

$$y_{SS} = Cx_{SS}$$

or

$$N = \{C[I-AC]^{-1}B\}^{-1} \qquad (3.10)$$

Where A, B and C were the discretized forms of the open loop matrices from Equation (3.2).

E. CLOSED LOOP POLE PLACEMENT

The expression for N derived in the last section depends on **K**, the state feedback gains. Here, the values of **K** are determined based on pole placement methods [Ref. 7], using the Matrix-x program "POLE.MX" (see Appendix F). Poles were varied from .95 to .32 for and the effect on system response was observed. Detailed results are tabulated in ppendix G. See Appendix H for performance curves for sample pole combinations. It was found that poles of .92, .921 and .922 provided the best response without overworking the physical control mechanisms of the NPS AUV prototype. This is consistent with a desired time constant of approximately one to two seconds which would result in a vehicle that completes its depth change in four to eight seconds. (approximately four time constants), at data acquisition sample rate of 20 HZ.

Specifically, since: $Z = e^{-st}$

and

$t = .05$ seconds,

and if $s = \frac{1}{\tau}$ with $\tau = 1$ second,

then $Z = e^{-.05} = .95$

Where: Z was the discrete system pole location,

s was the reciprocal of the system time constant,

t was the sampling rate, and

τ was the system time constant.

Furthermore, if $\tau = 2$ seconds, then

$$Z = e^{(-2)(.05)} = .90$$

Therefore, a pole placement of .92, .921 and .922 for a 20 HZ sample rate was consistent with a desired rate of depth change of four to eight seconds.

F. PROTOTYPE VEHICLE PHYSICAL LIMITATIONS

The NPS AUV Prototype as described by Brunner [Ref. 4] had a ± .1 volt control signal limit on the dive plane actuator. Control analysis to this point did not account for this saturation limit so it became necessary to determine if the control scheme derived above was effective under this saturation limit. To resolve this, the SYSTEM BUILD section of Matrix-x was used to construct the system model derived in Chapter 2 and the closed loop control system designed in Sections B, C and D of this chapter. The resultant block diagram, see Appendix I, contained the closed system matrix derived in Section B with a limiter or saturator at its input to bound the values of dive plane

angle, δ, to $-.1 \leq \delta \leq .1$ (volts). Appendix J shows the system responses to step inputs using this limited input control. It became apparent that even under saturation conditions the vehicle response was effectively unchanged and the desired depth was still attained in the four to eight second time band.

G. EFFECT OF SENSOR BIAS ON PREDICTED PERFORMANCE

The pitch rate sensor aboard the NPS AUV prototype had inherent bias in the signals fed to the control system. It was therefore necessary to determined how this bias effected the accuracy of the control system in driving the vehicle to its desired depth. This was investigated by constructing block diagrams in the SYSTEM BUILD mode of Matrix-x which added biases of .025, .03, .04 and .05 to first the depth and then the pitch rate signal. The model was then subjected to a step input depth change command of +1 foot and the response observed. When the bias was added to the depth signal, the vehicle response was virtually uneffected for all values of bias tested. The model reached ordered depth in the same amount of time as the unbiased system. The effect of depth bias was therefore considered negligible. Appendix K shows the block diagram and response when both saturated input (discussed in Section E,

above) and biased pitchrate conditions are imposed simultaneously on the system.

When the bias was added to the pitch rate signal, the response time was uneffected but the final depth was greater than ordered depth and the difference between the two increased as the amount of bias increased. This was recognized as an unacceptable condition because it illustrated that the expected bias voltages could effect depth control by as much as 20% (for a bias of .05 volts). This effect was due to the fact that the controller used the pitch rate (directly measured by the vehicle's sensor) and integrated it to determine pitch angle of the vehicle. This operation was required by Equation (2.3) of the equations of motion described in Chapter 2 and shown again below:

$$\dot{w} = \frac{(Z_W)(U_X)(w)}{(M_{ZDW})} + \frac{(Z_Q)(U_X)(q)}{(M_{ZDW})} + \frac{(Z_D)(U_X^2)(d)}{(L)(M_{ZDW})} + \frac{(F_1)}{(M_{ZDW})} \qquad (2.1)$$

$$\dot{q} = \frac{(M_W)(U_X)(w)}{(L^2)(I_{YY})} + \frac{(M_Q)(U_X)(q)}{(L)(I_{YY})} + \frac{(M_D)(U_X^2)(\delta)}{(L^2)(I_{YY})} + \frac{(F_2)}{(M_{ZDW})} \qquad (2.2)$$

$$\dot{\theta} = q \qquad (2.3)$$

$$\dot{z} = w - (U_X)(\theta) \qquad (2.4)$$

Any constant (bias) errors picked up in the pitch rate signal was being amplified in the integration process. The result was an unacceptable error in the calculation of vehicle pitch angle. As shown in Equation (2.4) above, pitch angle was then used in the calculation of vehicle depth. In summary, any small constant error bias accompanying the measured pitch was being magnified by integration and then used to determine the vehicle depth. This accounted for the difference between the final depth of the unbiased and biased systems. It was therefore determined that another method was needed to generate pitch angle.

H. ADDITION OF A STATE OBSERVER

A state observer was designed that used measured pitch rate and depth to estimate the vehicle pitch angle. The basic observer is illustrated in Figure 3.3. The state observer design was based on the equation

$$\dot{\hat{x}} = A\hat{x} + Bu + k_0(y - C\hat{x}) \qquad (3.11)$$

Where: $\hat{x}$ was the state variable estimated by the observer k_0 was the observer feedback required for the observer to be able to follow and duplicate control system operation.

A, B and C were the original open loop control matrices of Equation (3.1)

Note that at this stage, disturbance, **w**, is ignored. Equation (3.11) is schematically depicted in Figure (3.3). Collecting terms and rearranging produced:

$$\dot{\hat{x}} = (A - k_0 C)\hat{x} + Bu + k_0 y$$

Which was then rearranged into the familiar State Space format:

$$\dot{\hat{x}} = [AO]\hat{x} + [BO]u \qquad (3.12)$$
$$y = [CO]\hat{x} + [DO]u$$

Where: **AO** was the observer **A** matrix,
BO was the observer **B** matrix and
CO was the observer **C** matrix.

It should be noted that the **AO** Matrix was determined to be the 3x3 matrix $(A - K_0C)$. The values for k_0 (observer feedback gains) were calculated using the Matrix-x POLEPLACE command. This calculated two values of gain for the two states (pitch rate and depth) that were to be used by the observer in estimating the third state (pitch angle). The poles chosen for the observer were .7, .71 and .72. These values were selected because they created

a faster response in the observer than in the controller itself. This condition was necessary to ensure the

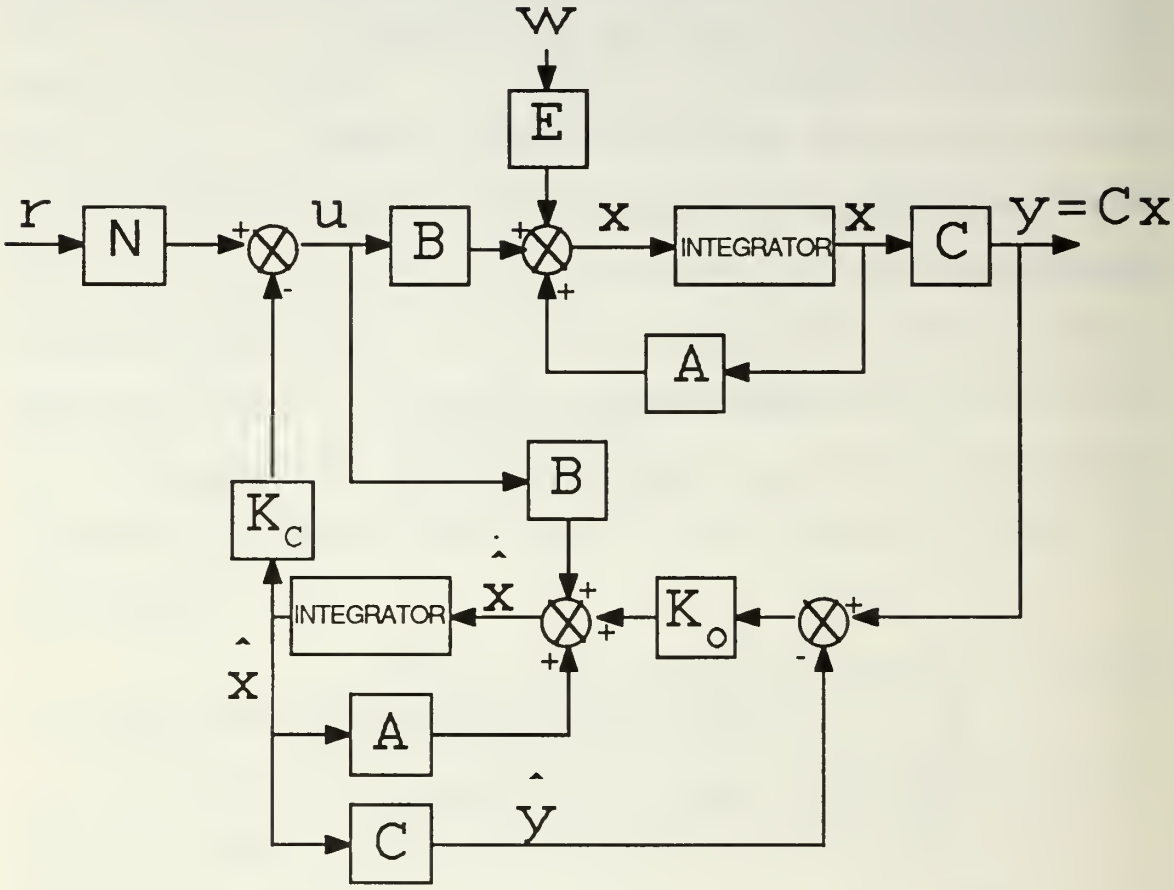

Figure 3.3. State Observer

observer would not slow down the overall simulation speed of the controller.

The BO Matrix was determined to be a 3x3 matrix whose first column was the original system B Matrix, and 2nd and 3rd columns were made up of the feedback gains determined in step 2.

The observer's CO Matrix was the same as the original system's C Matrix.

The observer's DO Matrix was a zero matrix.

The result was the following Closed Loop, State Observed System Matrix:

$$SCO = \left| \frac{[A-KC][Bk_1k_2]}{C \quad D} \right|$$

or

$$SCO = \left| \frac{AO \quad BO}{CO \quad DO} \right|$$

This system matrix was then analyzed by Matrix-x and produced the graphs of Appendix L, showing that the observed system using only two measured states and estimating the third, appeared to accurately approximate the actual three state system. This method of pitch angle generation therefore appeared superior to the integration method previously described. The state observer provides necessary information about the unmeasured pitch angle state, but does not, as yet, help to overcome the depth offset due to bias and disturbance, which is covered in the next chapter.

IV. EFFECT OF EXTERNAL DISTURBANCES AND THEIR COMPENSATION IN A DISTURBANCE OBSERVER/ESTIMATOR

A. INTRODUCTION

The designed closed loop control system (with state observer) of Chapter 3 was coded into Turbo Pascal and subsequently used to control the AUV prototype using an IBM personal computer [Ref. 8] in tow tank test runs. Observed depth control was unsatisfactory with the low feedback gains determined in Chapter 3. It was concluded that one possible cause of the low initial estimates of feedback gains and resultant unsatisfactory performance was that the equations of motion (Equations 2.1 through 2.4) and their respective dimensionless parameters determined in Chapter 2 may not adequately describe all hydrodynamic forces and moments effecting the motion of the AUV, such as surface and bottom effects, speed variations due to excessive control surface deflection, etc. An additional observer/estimator was therefore added to the controller described in Section C that would estimate these "disturbances" (indicated as $\mathbf{w}$ in Figure 3.3) and direct dive planes to compensate for them. Studies of the control

effects of unmodelled dynamics and their compensation is a subject of recent interest [Ref. 9].

B. DISTURBANCE OBSERVER CONCEPT

The design was initiated by considering new system equations for open loop control which included the disturbance (w_K) effects:

$$x_{K+1} = Ax_K + Bu_K + Ew_K \qquad (4.1)$$

and

$$y_K = Cx_K \qquad (4.1a)$$

This system is illustrated in Figure 4.1 below:

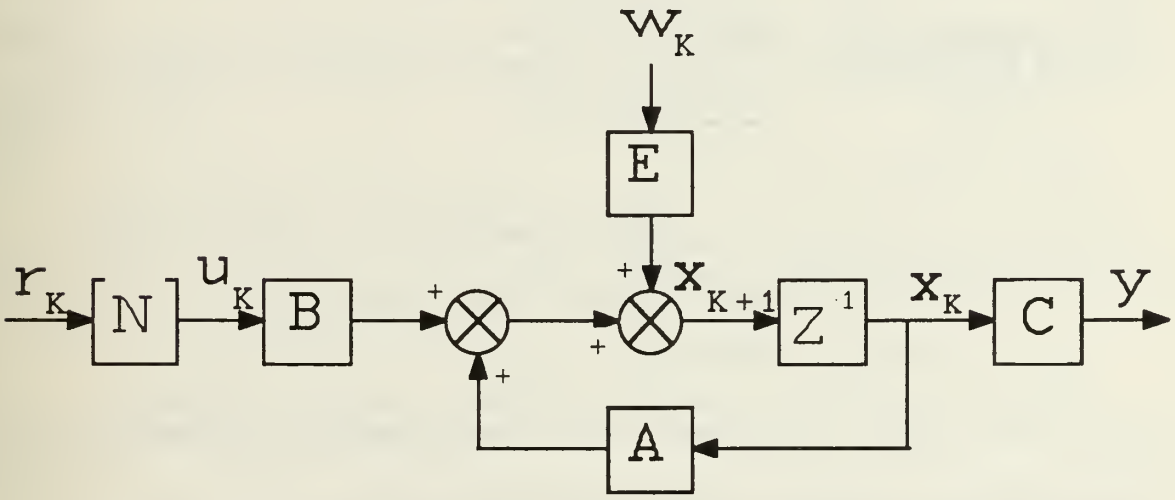

Figure 4.1. Basic Open Loop System With Disturbance

Note that r_K and y_K represent desired depth and actual depth respectively. The disturbance, w_K, was treated as an additional variable to be estimated in an observer. The

resulting system model (Figure 4.2) would therefore have two observers in it: one to observe and estimate the

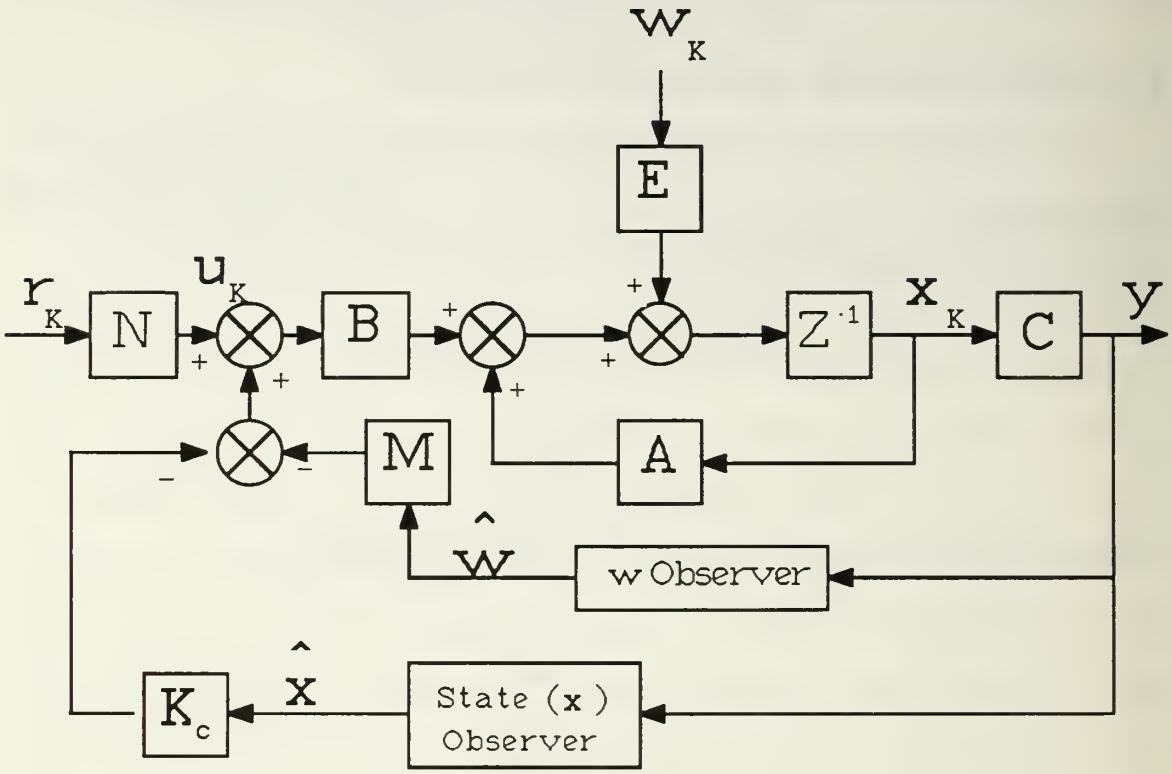

Figure 4.2. Closed Loop State Observed and Disturbance Compensated System (Basic Diagram)

required state variables, and the second to observe and ultimately compensate for the disturbances.

C. MODIFIED STATE OBSERVER

As described in Chapter 3, in order for an observer to accurately reproduce plant parameters, it must resemble the original open loop control system (Figure 3.1) as closely

as possible. The state observer model would therefore be as illustrated in Figure 4.3.

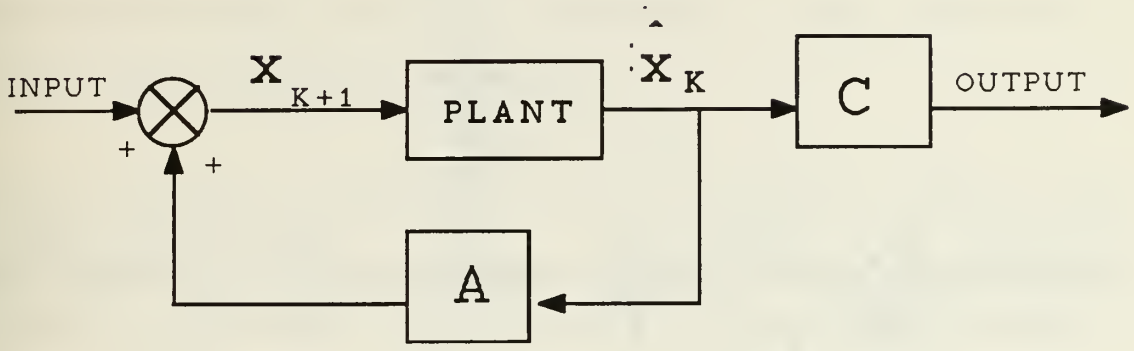

Figure 4.3. State Observer Model

In order for the state observer to best estimate all derived parameters, it needed to receive all possible inputs, specifically:

1. Dive plane command, u_K , sent to the original open loop system. (see Figure 4.1)
2. Best estimate of the disturbance, w_K, generated by the disturbance estimator.
3. A comparison of the state observer output and the original open loop system output, providing an error signal to be minimized.

With these inputs accounted for, the system model became as shown in Figure 4.4.

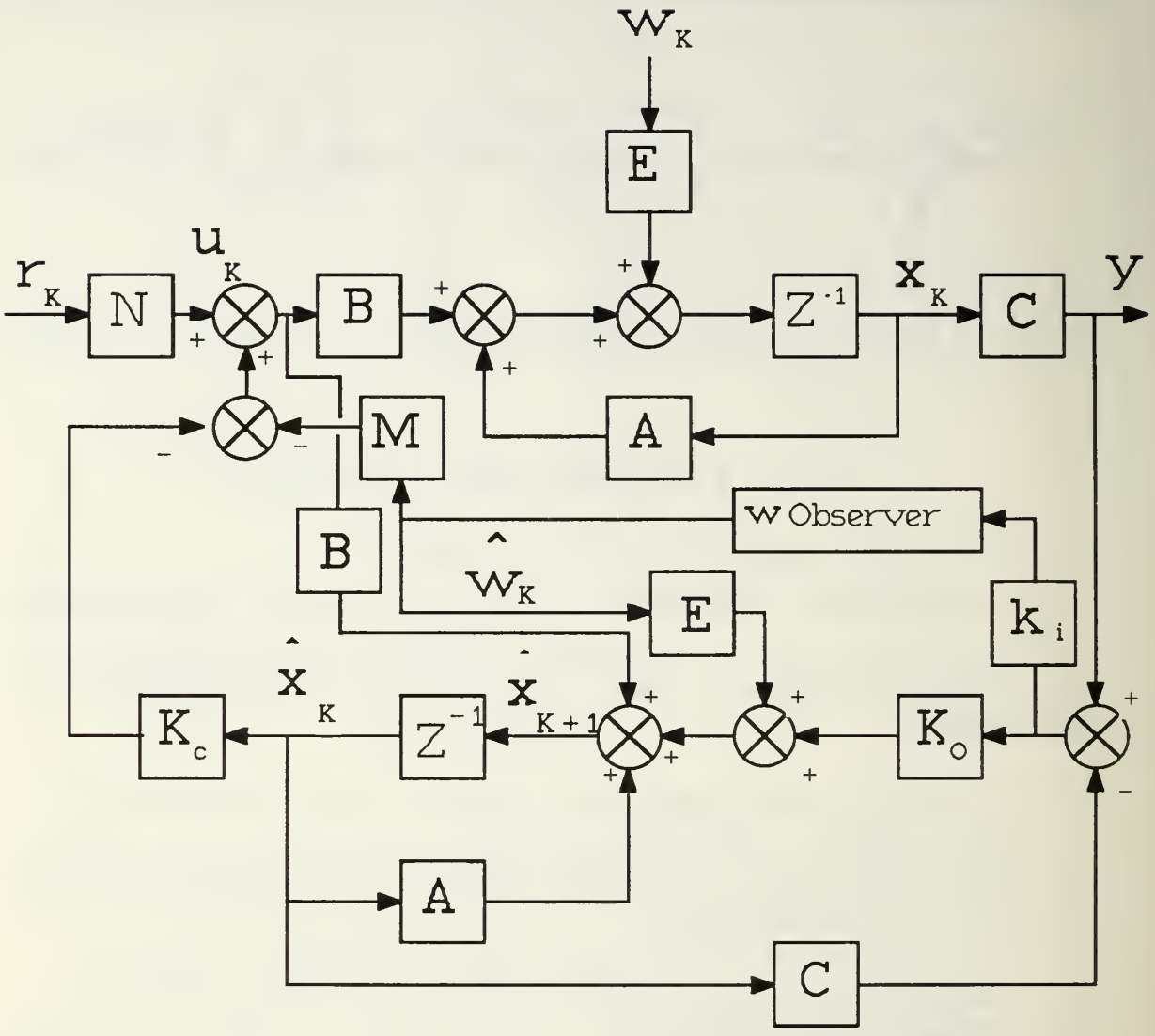

Figure 4.4 Observed System

D. DISTURBANCE OBSERVER

The disturbance observer/estimator was designed in a similar manner. For this model, the disturbance w_K was assumed to be of constant magnitude. Note that since w was to be modelled as a constant,

$$\hat{w}_{K+1} = \hat{w}_K$$

and, therefore, the value of gain **A** equaled 1. As with the state observer, the disturbance observer needed a comparison of the state observer and open loop system outputs - to provide an error signal to minimize. The final system model, including both state and disturbance observation, estimation and compensation is shown in Figure 4.5.

Inspection of Figure 4.5 verifies that the final vehicle design equation was, in fact, Equations (4.1) and (4.1a), shown again below:

$$x_{K+1} = Ax_K + Bu_K + Ew_K$$

and

$$y_K = Cx_K$$

Additionally it can be seen from Figure 4.5 that the Control Signal (u_K) Equation was:

$$u_K = -K_C \hat{x}_K - M\hat{w}_K + Nr \qquad (4.2)$$

and the design equations for both observers are:

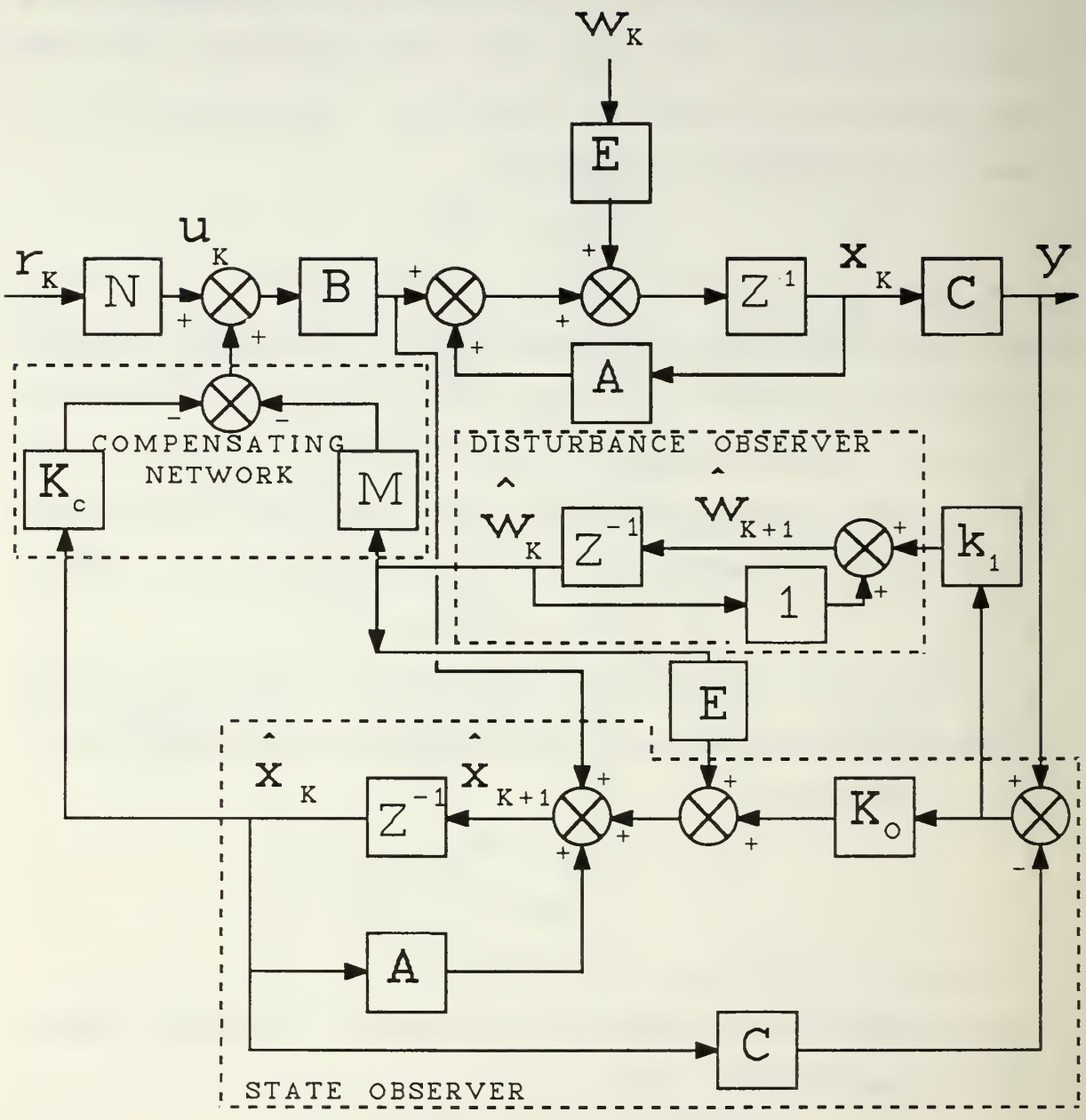

Figure 4.5. Final System Diagram

$$\hat{x}_{K+1} = A\hat{x}_K + Bu_K + K_o(y_K - C\hat{x}_K) + E\hat{w}_K \qquad (4.3)$$

(state observer)

$$\hat{w}_{K+1} = \hat{w}_K + K_1(y_K - C\hat{x}_K) \qquad (4.3a)$$

(disturbance observer)

Equations (4.3) and (4.3a) could be further written in matrix format to represent the performance of a single observer that estimated both state variables and disturbances. Specifically:

$$\begin{vmatrix} \hat{x} \\ \hat{w} \end{vmatrix}_{K+1} = \begin{vmatrix} A & E \\ 0 & 1 \end{vmatrix} \begin{vmatrix} \hat{x} \\ \hat{w} \end{vmatrix}_K + \begin{vmatrix} B \\ 0 \end{vmatrix} u_K + K_o \left\{ y_K - \begin{vmatrix} C & 0 \end{vmatrix} \begin{vmatrix} \hat{x} \\ \hat{w} \end{vmatrix}_K \right\} \qquad (4.4)$$

Equations (4.1), (4.1a), (4.2), and (4.4) completely described the operation of the entire vehicle and its control system. Equations (4.1) and (4.1a) represented the vehicle response, Equation (4.2) represented the control signal response, and Equation (4.4) represented the observer's response. These four equations needed to be coupled together to predict system response. Before that, however, some additional variables had to be identified.

The value for M in Equation (4.2) was determined by assuming that $\mathbf{r}=0$ and substituting $\mathbf{u_K}$ of Equation (4.2) into Equation (4.3), producing:

$$\mathbf{x}_{K+1} = \mathbf{A}\mathbf{x}_K + \mathbf{B}(-\mathbf{K}_C\mathbf{x}_K - \mathbf{M}\mathbf{w}_K) + \mathbf{E}\mathbf{w}_K$$

or, rearranging:

$$\mathbf{x}_{K+1} = (\mathbf{A} - \mathbf{B}\mathbf{K}_C)\mathbf{x}_K + (\mathbf{B}(-\mathbf{M}) + \mathbf{E})\mathbf{w}_K \qquad (4.5)$$

Since the objective was for the disturbance to have no effect on the steady state controlled depth, $(\mathbf{B}(-\mathbf{M}) + \mathbf{E})$ was set equal to zero and solved for M, resulting in $\mathbf{M} = (\mathbf{B}^{-1}\mathbf{E})$. The magnitude of the gain E was somewhat arbitrary at this point because it was amplifying a disturbance signal, w, of unknown magnitude. Therefore, considering the disturbance effects to be lumped at the input, setting B = E resulted in M = 1, for convenience. Other choices could be made for multi-output systems, for instance, to reduce the values of certain elements of the output vector.

The value for N in Equation (4.2) was determined by assuming that M=0 and substituting Equation (4.2) into Equation (4.3) to get:

$$\mathbf{x}_{K+1} = \mathbf{A}\mathbf{x}_K + \mathbf{B}(\mathbf{N}\mathbf{r}-\mathbf{K}_C\hat{\mathbf{x}}_K) + \mathbf{E}\mathbf{w}_K$$

then, assuming perfect observation $(\hat{\mathbf{x}} = \mathbf{x})$

$$\mathbf{x}_{K+1} = (\mathbf{A}-\mathbf{B}\mathbf{K}_C)\mathbf{x}_K + \mathbf{B}\mathbf{N}\mathbf{r} + \mathbf{E}\mathbf{w}_K$$

simplify by substituting $\mathbf{AC} = \mathbf{A}-\mathbf{B}\mathbf{K}_C$ (from Chapter 3) produced:

$$x_{K+1} = ACx_K + BNr + Ew_K$$

and assuming no disturbance, $w_K = 0$,

$$x_{K+1} = ACx_K + BNr$$

in steady state, $x_{K+1} = x_K = x_{SS}$ and $r_{SS} = y_{SS} = Cx_{SS}$

and solving for N produced:

$$N = \{C[I-AC]^{-1}B\}^{-1}$$

E. SYSTEM RESPONSE

The final objective, for analysis using Matrix-x, was to change Equations (4.2) through (4.4) into the format of Equation (3.1), or,

$$\text{SYSTEM MATRIX} = \begin{vmatrix} A & B \\ C & D \end{vmatrix}$$

where

$$\dot{x} = Ax + Bu$$

$$y = Cx + Du$$

This was done by substituting u_K of Equation (4.2) into Equations (4.1) and (4.4), and substituting y_K of Equation (4.1) into Equation (4.4). The resultant system matrix is:

$$SYS = \begin{vmatrix} A & B \\ C & D \end{vmatrix}$$

where:

$$A = \begin{vmatrix} A & -BK_C & -BM \\ k_O'C & & MBC \end{vmatrix} \quad \text{with} \quad MBC = \begin{vmatrix} A & E \\ 0 & 1 \end{vmatrix} - \begin{vmatrix} B \\ 0 \end{vmatrix} \times \begin{vmatrix} K_C & 1 \end{vmatrix}$$

$$B = \begin{vmatrix} \begin{vmatrix} B \\ 0 \end{vmatrix} * N & \begin{vmatrix} B \\ 0 \\ 0 \\ 0 \\ 0 \\ 0 \end{vmatrix} \end{vmatrix}$$

C is a 7 by 7 identity matrix, D is a 7 by 2 zero matrix

The system equation described above will simulate the response of all state variables (q, u and z) both actual and estimated, and the estimated disturbance, w_K.

The Matrix-x program and the system response to various combinations of input (desired depth, **r**) and disturbance, w_K, are provided in Appendix M. Note that values for the state observer feedback gains (k_0 Figure 4.6) are the first three elements of the 4 by 1 matrix produced by the Matrix-x 'Poleplace' command :
K_O = poleplace(AO', CO', OPOLES). The value of the disturbance observer feedback gain (K_1 in Figure 4.6) is the

last element of that same 4 by 1 matrix. The parameters OPOLES are the inputted values chosen for the observer poles.

The results of Appendix M illustrate several significant points. Where no disturbance is inserted (ACT DISTURBANCE = 0.0), actual and estimated parameters are identical and overlay to appear as one curve. This is because the observer model was designed to be identical to the vehicle model and initial conditions in both vehicle and observer were equal to zero. Therefore, estimated parameters that were generated in the observer system were identical to the vehicle parameters that were generated in the vehicle system. When a positive disturbance was inserted (ACT DISTURBANCE = 0.2), there was a time lag of approximately .5 seconds before the estimator outputs were equal to the actual outputs. A steady state dive command of -.2 volts was shown necessary to counter the disturbance. Similarly, a +.2 volt dive plane command was required to counter the -.2 volt disturbance in the third run.

V. HORIZONTAL EQUATIONS OF MOTION

A. INTRODUCTION

Chapters 2, 3 and 4 were involved with the verification of the vertical equations of motion and the control of the NPS AUV in the vertical plane. This chapter examines the horizontal equations of motion in a manner similar to that conducted in previous chapters. The greatest difference between the analysis of vertical and horizontal motion is the fact that in vertical motion, the vehicle is capable of sensing two reliable parameters--depth and pitch rate. It was shown that using these two inputs, a robust control system can be designed to satisfactorily control vehicle depth. In the horizontal plane, however, only one parameter is measured by onboard sensors--yaw rate. The major objective of this portion of the study therefore, became to design an adequate control system that can operate on only one measured input.

B. HORIZONTAL EQUATIONS OF MOTION

As was done for the vertical motion, the basic horizontal motion equations were adapted from the Six Degree of Freedom Equations of Motion developed in

Reference 5 and modified in Reference 3. The derivation is started with the yaw and sway equations shown below:

Equation (5.1) Yaw Equation of Motion

$$I_Z \dot{r} + (I_y - I_x)\, pg - I_{xy}(p^2 - q^2) - I_{yz}(pr + \dot{q}) + I_{xz}(qr - \dot{p}) + m[x_g(\dot{v} + ur - wp) - y_g(\dot{u} - vr + wq)] = \frac{\rho}{2} l^5 [N_{\dot{p}}' \dot{p} + N_{\dot{r}}' \dot{r} + N_{pq}' pq + N_{qr}' qr] + \frac{\rho}{2} l^4 [N_{\dot{v}}' \dot{v} + N_p' up + N_r' ur + N_{vq}' vq + N_{wp}' wp + N_{wr}' wr] + \frac{\rho}{2} l^3 [N_v' uv + N_{vw}' vw + N_{\delta r}' u^2 \delta r] \frac{\rho}{2} \int_{x_{tail}}^{x_{nose}} [C_{Dy}\, h(x)\, (v + xr)^2 + C_{Dz}\, b(x)\, (w - xq)^2] \frac{(v+xr)}{U_{cf}(x)}\, xdx + (x_G W - x_B B) \cos\Theta \sin\Phi + (y_G W - y_B B) \sin\Theta + \frac{\rho}{2} l^3 u^2 N_{prop}'$$

Equation (5.2) Sway Equation of Motion

$$m [\dot{v} + ur - wp + x_G(pq + \dot{r}) - y_G(p^2 + r^2) + z_G(qr - \dot{p})] = \frac{\rho}{2} l^4 [Y_{\dot{p}}' \dot{p} + Y_{\dot{r}}' \dot{r} + Y_{pq}' pq + Y_{qr}' qr] + \frac{\rho}{2} l^3 [Y_{\dot{v}}' \dot{v} + Y_p' up + Y_r' ur + Y_{vq}' vq + Y_{wp}' wp + Y_{wr}' wr] + \frac{\rho}{2} l^2 [Y_v' uv + Y_{vw}' vw + Y_{\delta r}' u^2 \delta r] - \frac{\rho}{2} \int_{x_{tail}}^{x_{nose}} [C_{Dy}\, h(x)\, (v + xr)^2 + C_{Dz}\, b(x)\, (w - xq)^2] \frac{(v+xr)}{U_{cf}(x)}\, xdx + (W - B) \cos\Theta \sin\Phi$$

The variables used to represent rotational and translational motion in the above Equations (5.1) and (5.2) are illustrated in Figure 5.1 below.

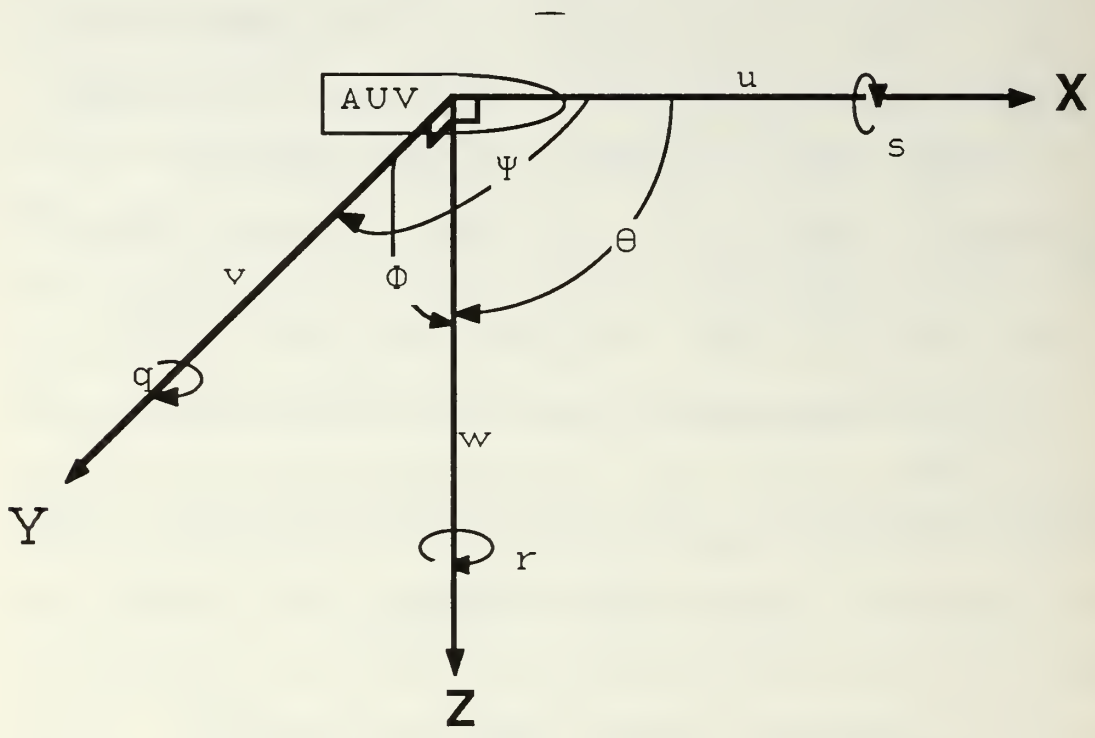

Figure 5.1. Body Centered Coordinate System

These two equations govern motion in the horizontal plane. They were simplified for analysis by making the following assumptions:

1. Constant velocity in the 'x' direction and zero 'x' direction acceleration,

2. The following hydrodynamic coefficients were neglected (assumed ≈ 0) : w, p, x_G, y_G, q, z_G, Y_p, $Y_{\dot{p}}$, $Y_{\dot{r}}$, $N_{\dot{v}}$, Y_{pq}, Y_{qr}, $\dot{q}$, $\dot{p}$, Θ, Φ, N_{prop}
3. Crossflow (integral) terms cancelled each other.

These assumptions appeared reasonable based on the following observations:

1. We considered only extremely small turns ($\Psi \approx 0$) in this analysis to ensure that vehicle performance was as linear as possible. The small rudder angles had negligible effect on the forward velocity and acceleration ; x = constant, $\dot{x} = 0$.
2. The vehicle stayed on the surface in this analysis. There was no vertical component of translational motion (heave, w), nor rotational motion (pitch, q). Corresponding accelerations were also negligible.
3. The slow speeds involved and the small rudder angles used caused no measurable roll, p, and the vehicle maintained a level position so $\Phi = 0$.
4. The NPS AUV was built such that the distance between the centers of buoyancy and mass was negligible; $x_G = y_G = z_G = 0$
5. Since p, $\dot{p}$, q, $\dot{q}$, r and $\dot{r}$ were neglected as discussed above, then Y_p, $Y_{\dot{p}}$, $Y_{\dot{r}}$, Y_{pq}, and Y_{qr} were also be neglected.
6. Due to the symmetrical shape of the NPS AUV, $N_{\dot{v}}$ was neglected.
7. The dual propellers of the NPS AUV operated together at the same RPM and direction. The vehicle was not designed to produce turning moment with its propellers so N_{prop} was neglected.

Applying the above assumptions simplifies Equations (5.1) and (5.2) to:

$$m\dot{v} = \frac{\rho}{2}\left(l^3 Y_{\dot{v}}\,\dot{v} + l^3 Y_r\, ur + l^2 Y_v\, uv + l^2 Y_{\delta r}\, u^2\, \delta r\right) - mur$$

and

$$I_Z\,\dot{r} = \frac{\rho}{2}\left(l^5 N_{\dot{r}}\,\dot{r} + l^4 N_r\, ur + l^3 N_v\, uv + l^3 N_{\delta r}\, u^2\, \delta r\right)$$

and solving for $\dot{v}$ and $\dot{r}$ produced:

$$\dot{v} = \frac{\rho l^2 u}{2m - \rho l^3 Y_{\dot{v}}}\left(lY_r + Y_v v + Y_{\delta r} u\,\delta r\right) - \frac{2mur}{2m - \rho l^3 Y_{\dot{v}}} \qquad (5.3)$$

and

$$\dot{r} = \frac{\rho l^3 u}{2I_z - \rho l^5 N_{\dot{r}}}\left(lN_r r + N_v v + N_{\delta r} u\delta r\right) \qquad (5.4)$$

To finish putting Equations (5.1) and (5.2) into state equation form, the following relationships were included:

$$\dot{\Psi} = r \qquad (5.5)$$

$$\dot{Y} = v - u\sin(\Psi) \qquad (5.6)$$

$$\dot{X} = u\cos(\Psi) \qquad (5.7)$$

Equations (5.3) through (5.6) were required to conduct the state space evaluation of horizontal motion as performed for the vertical motion in Chapters 2, 3 and 4. Equation (5.7) was required for the evaluation of the kinematic

performance of the vehicle. Equations (5.6) and (5.7) were further simplified to:

$$\dot{Y} = v - u\Psi \tag{5.8}$$

$$\dot{X} = u \tag{5.9}$$

It was assumed that all steering was done about a nominal path (i.e. $\Psi \approx 0$), and all angles were very small such that $\Psi \approx \sin(\Psi)$ and $\cos(\Psi) \approx 1$.

C. STATE SPACE CONFIGURATION

Putting Equations (5.3) through (5.6) into state space format resulted in:

$$\begin{vmatrix} \dot{v} \\ \dot{r} \\ \dot{\Psi} \\ \dot{Y} \end{vmatrix} = \begin{vmatrix} K1 & K2 & 0 & 0 \\ K3 & K4 & 0 & 0 \\ 0 & 1 & 0 & 0 \\ 1 & 0 & -u & 0 \end{vmatrix} \begin{vmatrix} v \\ r \\ \Psi \\ Y \end{vmatrix} + \begin{vmatrix} K5 \\ K6 \\ 0 \\ 0 \end{vmatrix} (\delta r)$$

$$Y = \begin{vmatrix} K7 & 0 & 0 & 0 \\ 0 & K8 & 0 & 0 \\ 0 & 0 & K9 & 0 \\ 0 & 0 & 0 & K10 \end{vmatrix} \begin{vmatrix} v \\ r \\ \Psi \\ Y \end{vmatrix}$$

Where:

$K1 = AY_v$ $\qquad$ $K2 = (AlY_r - \frac{2mr}{\rho l^2 A})$

$K3 = BN_v$ $\qquad$ $K4 = BlN_r$

$K5 = AuY_{\delta r}$ $\qquad$ $K6 = BuN_{\delta r}$

and $$A = \frac{\rho l^2 u}{2m - \rho l^3 Y_{\dot{v}}} \qquad B = \frac{\rho l^3 u}{2I_z - \rho l^5 N_{\dot{r}}}$$

and K7 through K10 were determined by the specific hardware used in controlling the vehicle. Note how this is consistent with the format:

$$\dot{\mathbf{x}} = \mathbf{A}\mathbf{x} + \mathbf{B}\mathbf{u}$$
$$\mathbf{y} = \mathbf{C}\mathbf{x} + \mathbf{D}\mathbf{u}$$

that was used in Chapters 2 and 3. In this case, $\mathbf{y}$ is the transfer distance and $\mathbf{D}$ is the zero matrix.

D. COMPUTER SIMULATION OF HORIZONTAL MOTION

First estimate numerical values for parameters in the above derived equations of motion were obtained from Reference 2, which provides hydrodynamic coefficients for the Swimmer Delivery Vehicle from which the NPS AUV was designed. Although the values were not expected to be exactly the same as those for the AUV, they were considered close enough to provide a working model from which to evaluate Equations (5.3) through (5.6). The following values were used:

$Y_r = 2.97 \times 10^{-2}$ $Y_v = -9.31 \times 10^{-2}$
$N_{\dot{r}} = -3.4 \times 10^{-3}$ $Y_{\delta r} = 2.73 \times 10^{-2}$
$Y_{\dot{v}} = -5.55 \times 10^{-2}$ $N_r = -1.64 \times 10^{-2}$
$N_v = -7.42 \times 10^{-3}$ $N_{\delta r} = -1.29 \times 10^{-2}$

The following dimensions and parameters were also used:

$\rho = 62.4 \frac{lb}{ft^3}$ $\quad l = 2.5$ ft $\quad m = .609$ slugs

$I_Z = .213$ ft-lb-sec^2 $\quad u = 1.8 \frac{ft}{sec}$

Substituting the above values into Equations (5.3) and (5.4) produced:

1. $\dot{v} = .902416r - 1.18119v + .62346dr$ (5.10)
2. $\dot{r} = -1.36119r - .24634v - .7709dr$ (5.11)
3. $\dot{\Psi} = r$ (5.12)
4. $\dot{Y} = v - 1.8\Psi$ (5.13)

Equations (5.10) through (5.13) were then used to simulate the AUV response to various rudder inputs. The equations were fed into the MATRIX-X System Build Mode to create the model represented by the block diagram of Appendix N. The MATRIX-X programs "AUVTURNPLOT" and "AUVMULTIPLOT" of Appendix O were then written to plot the path traversed and the resultant vehicle heading, angular velocity, X and Y distances, and rudder angle responses to different rudder commands. These plots are shown in Appendix P.

VI. TOW TANK TESTING OF VERTICAL MOTION CONTROLLER

A. INTRODUCTION

This chapter deals with the equipment utilized, the procedures followed and the results obtained in testing the controller designed in Chapters 2 through 4.

Vehicle testing was performed in the Naval Postgraduate School 40 foot long tow tank located in the basement of Halligan Hall. This tank has a cross section of four feet by four feet and was filled with fresh water. Testing and calibration of all system components utilized basic laboratory equipment such as multimeters, monometers, oscilloscopes and a personal computer. Data was recorded on the same PC that contained the designed controller and also provided depth commands to the vehicle, as described by Reina in Reference 8. Several of the runs were recorded on video tape and have been retained by NPGS.

B. CALIBRATION

The only vehicle onboard equipment that needed occasional recalibration was the depth pressure cell. This sensor was critical because it was the only sensor used for feedback control. This was conducted several times during the course of about three months of testing, when the

vehicle depth indication began to visibly drift from the actual depth as observed by operators through the glass walls of the tow tank. It should be noted that high accuracy was not necessary for this instrument as long as readings were consistent. Calibration was performed following the procedures described by Brunner [Ref. 4]. The cell was warmed up by applying power for 30 minutes. All zeros were adjusted with the cell sensing lines vented to atmosphere. A 30 inch manometer, constructed in the laboratory specifically for this purpose, was then connected to the high pressure port. Water level in the manometer was then adjusted at several intervals from zero inches to 30 inches and the output of the cell was adjusted to conform with the ratio of .256 volts per inch depth established in Reference 4. With these occasional calibrations, the depth cell appeared to work satisfactorily throughout the test period.

The pressure cell built onboard the vehicle for the original purpose of measuring vehicle speed did not perform satisfactorily. Vehicle speed was therefore determined by timing the vehicle while travelling a measured length of the tow tank.

Vehicle pitchrate was provided from the on board pitchrate gyro described in Reference 4. No calibration beyond that which was performed in Reference 4 was

required for this component, which was of secondary importance in the feedback system.

C. TEST PROCEDURES AND DATA ACQUISITION

A typical test run was initiated with one operator physically holding the vehicle at a specified depth at one end of the tow tank. After the controller was started from the PC and the depth command inserted, the operator released the vehicle. All control data was transmitted to the vehicle from the PC via a radio transmitter. Depth and pitchrate data were sent from the vehicle to the PC via the attached tether. All electrical power was also supplied to the vehicle through the same tether. The tether was designed to create minimum drag on the vehicle as it moved through the water and was also bouyed by using small floats. The hydrodynamic effect of the tether, although small, was noticeable and had to be accounted for, as discussed later.

Approximately 40 test runs were conducted throughout a period of about three months, with the following objectives in mind:

1. Initial runs were dedicated mainly to adjusting electrical gains in the controller, enabling it to operate satisfactorily with a newly installed radio transmitter.
2. Differences between the theoretical hydrodynamic model of Chapter 2 and actual observed vehicle motion

were expected. Subsequent runs were, therefore, conducted to determine how these differences would manifest themselves in the observed vehicle performance.
3. Final runs were performed for the purpose of evaluating how changes in control feedback gains and observer characteristics affected vehicle performance, and finally to fine tune these values to produce the most stable, yet rapid depth excursion possible.

D. TEST RESULTS

The vehicle controller that was developed in Chapters 2 through 4 is illustrated in Figure 6.1 It should be noted that Figure 6.1 is a condensed version of Figure 4.5.

Figure 6.1 illustrates the major components of the observed, compensated, closed loop controlled system. Specifically:

1. **N** Gain--scales the input signal (desired depth) to a value ensuring zero steady state error.
2. **Saturator**--incorporates the physical limitation of ± .4 radians of dive plane movement into the theoretical model.
3. **System**--the theoretically derived mathematical model of the AUV vehicle
4. **Estimator**--uses vehicle depth as measured by onboard sensors and estimates vehicle pitchrate, pitch angle and depth. The accuracy of these estimates is only as good as the mathematical model of the vehicle from which the estimator is designed.
5. **Controller Gains**--gains applied to the error signals (i.e., difference between desired and estimated conditions) detected by the controller. These gains determine just how much the dive planes will move to correct for the errors found by the controller.

In Chapter 3, the theoretical closed loop controlled system (the **System** block of Figure 6.1) was finally represented by Equations 3.7 and 3.8, which are, in discrete form:

$$\mathbf{x}_{K+1} = \mathbf{A}_{sys}\mathbf{x}_K + \mathbf{B}_{sys}\mathbf{u}_K$$

and

$$\mathbf{y}_K = \mathbf{C}_{sys}\mathbf{x}_K + \mathbf{D}_{sys}\mathbf{x}_K$$

or, in Matrix-x format:

$$SYS = \left| \begin{array}{cc} A_{sys} & B_{sys} \\ C_{sys} & D_{sys} \end{array} \right| \qquad (6.1)$$

Similarly, the **Estimator** was determined to be represented by:

$$EST = \left| \begin{array}{cc} A_{EST} & B_{EST} \\ C_{EST} & D_{EST} \end{array} \right| \qquad (6.2)$$

Determination of numerical values for the elements of the matrices of Equations (6.1) and (6.2) was performed as follows:

1. The Initial System Matrix

Initially, the hydrodynamic coefficients used were those developed in Section C of Chapter 2 for a vehicle speed of 2.1 feet/sec, specifically:

$$Z_W = -1.5 \qquad Z_Q = 0 \qquad M_W = 0$$

$M_Q = -.15 \quad Z_D = 0 \quad M_D = .253$

$M_{ZDW} = 1.005 \quad I_{YY} = .072$

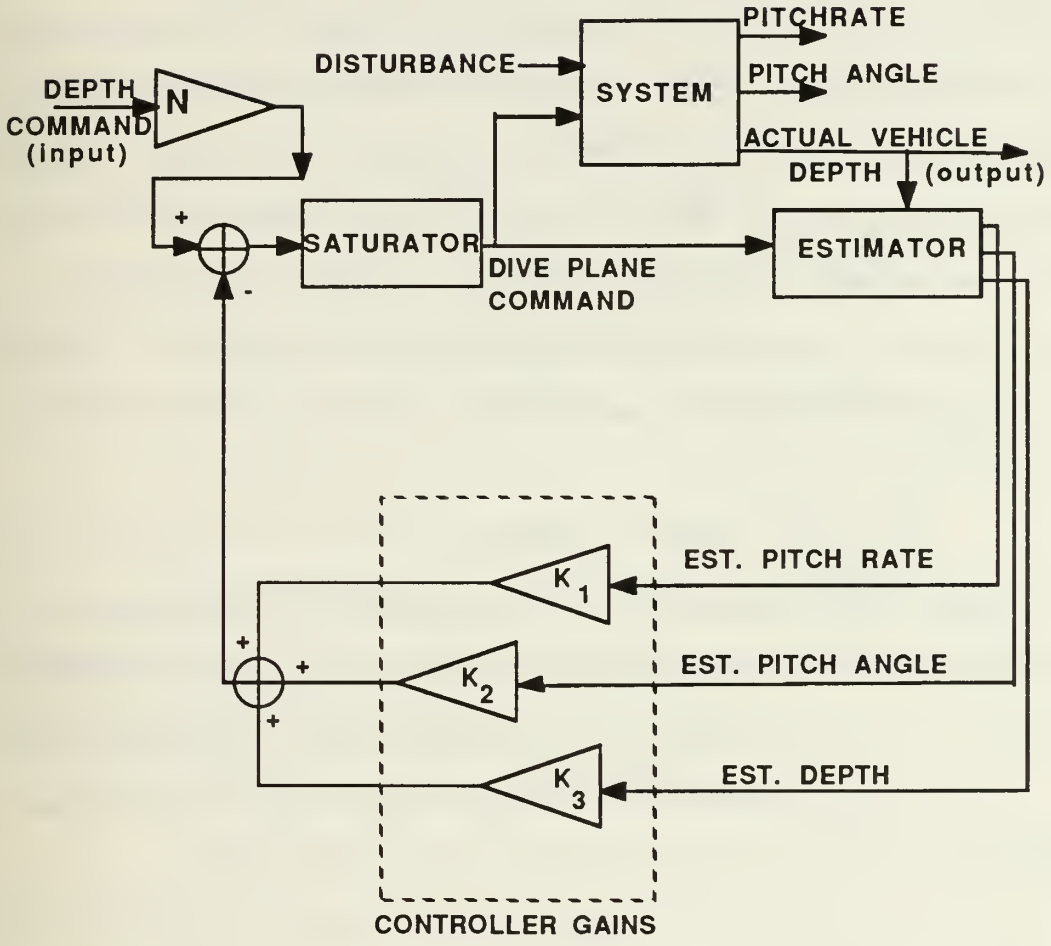

Figure 6.1 Theoretical System/Controller Design

In the open loop test runs of Reference 4, control commands were sent to the AUV via the attached tether. One equipment modification made subsequent to those open

loop runs was the incorporation of a radio transmitter so commands could be sent to the AUV by the control computer, instead of through manual operation of the joystick [Ref. 4]. In the initial test runs subsequent to that modification, it was necessary to ensure that signals sent via the radio link were not altered during transmission due to the different transmission medium. It was found that one parameter, M_D, needed to be modified at the source (computer) end of the transmission to ensure that the same control signal was received by the AUV. The value of M_D that properly accounted for this modification was:

$$M_D = .1289.$$

These values were then substituted into Equation 2.6 which produced the open loop control state space system discretized at 0.2 seconds to represent the 5 HZ sampling rate. The following specific A_{sys}, B_{sys}, C_{sys}, and D_{sys} resulted:

$$A_{sys} = \begin{vmatrix} .6873 & 0 & 0 \\ .1668 & 1 & 0 \\ -.0372 & -.42 & 1 \end{vmatrix} \qquad B_{sys} = \begin{vmatrix} .2419 \\ .0257 \\ -.0037 \end{vmatrix}$$

$$C_{sys} = \begin{vmatrix} 72 & 0 & 0 \\ 0 & 1 & 0 \\ 0 & 0 & 3.08 \end{vmatrix} \qquad D_{sys} = \begin{vmatrix} 0 \\ 0 \\ 0 \end{vmatrix}$$

The procedures described in Chapter 3 were then used to close the control loop. The control poles of the closed loop system were determined using the Linear Quadratic Regulator (LQR) method to be:

$$\text{Controller Poles} = [.5709,\ .8173 \pm j.1426] \qquad (6.3)$$

with the following state variable gains:

$$k_1 = 1.0429 \quad k_2 = 2.5732 \quad k_3 = -.7562 \qquad (6.4)$$

In using the LQR method, a state weighting matrix of I (3x3) and a control weight of 0.1 was used.

The value for the N gain (see Figure 6.1) was determined to be -.24552 using the derivation for Equation 3.10 presented in Section D of Chapter 3.

2. The Initial Estimator Matrix

Following the procedures of Chapter 3 Section H, the closed loop observer (or estimator) matrices were determined to be:

$$A_{EST} = \begin{vmatrix} .6873 & 0 & .919 \\ .1668 & 1 & 2.001 \\ -.0372 & -.42 & -.757 \end{vmatrix} \qquad B_{EST} = \begin{vmatrix} .242 & -.298 \\ .026 & -.653 \\ -.004 & .571 \end{vmatrix}$$

$$C_{EST} = \begin{vmatrix} 1 & 0 & 0 \\ 0 & 1 & 0 \\ 0 & 0 & 1 \end{vmatrix} \qquad D_{EST} = \begin{vmatrix} 0 & 0 \\ 0 & 0 \\ 0 & 0 \end{vmatrix}$$

This estimator design was based on pole placement of: Estimator Poles = [.3 , .31 , .32] in which its open loop matrix was that given by $\mathbf{A_{sys}}$ and the output array was the last row of the $\mathbf{C_{sys}}$ given in the previous section. The resultant observer gains were $\mathbf{k_o}$ = [-.298,-.653,.571]

3. Final System and Estimator Matrices

Initial test runs were conducted using the feedback gains originally derived in Chapter 3. Results of these initial runs revealed insufficient vehicle stability through the rapid depth changes. It appeared that the mathematical model of AUV motion, upon which the controller design was based, did not reflect actual vehicle performance closely enough. Specifically, the feedback gains appeared to be too low, the unmodelled disturbances had to be accounted for, and the original B_{sys} matrix needed to be refined.

Test runs were conducted for the purpose of observing how an increase in the feedback gains effected the stability of the vehicle. Runs were performed until a satisfactory value for feedback gains was determined. The selected values are those given in Equation (6.4).

As discussed in Chapter 4, it was determined that disturbances not modelled in the equations of motion were

another apparent cause of instability. The major contributors to this disturbance were suspected to be ballast unbalance (the vehicle was slightly heavy aft), tether weight and drag, surface and bottom effects, and vehicle acceleration. The model needed to be modified to account for these disturbances. Originally, the intention was to incorporate the disturbance estimator developed in Chapter 4. However, analysis of that technique indicated that the stability of the controller produced from that design was sensitive to vehicle and estimator mismatch.

The B_{sys} matrix was adjusted to more accurately reflect vehicle characteristics by conducting closed loop runs and computer simulations and observing how variations of B_{sys} effected performance.

In summary, the final successful runs (to be described later) were obtained by:

1. Increasing the feedback gains to the values shown in Equation 6.4,
2. Incorporation of disturbance compensation, and,
3. Refining the values of the B_{sys} matrix to better represent the hydrodynamic characteristics of the vehicle.

The final system and estimator matrices thus became:

$$A_{sys} = \begin{vmatrix} .6873 & 0 & 0 \\ .1668 & 1 & 0 \\ -.0372 & -.42 & 1 \end{vmatrix} \quad B_{sys} = \begin{vmatrix} .363 & .363 \\ .039 & .039 \\ -.006 & -.006 \end{vmatrix}$$

$$C_{sys} = \begin{vmatrix} 72 & 0 & 0 \\ 0 & 1 & 0 \\ 0 & 0 & 3.08 \end{vmatrix} \quad D_{sys} = \begin{vmatrix} 0 & 0 \\ 0 & 0 \\ 0 & 0 \end{vmatrix}$$

and

$$A_{EST} = \begin{vmatrix} .6873 & 0 & .919 \\ .1668 & 1 & 2.011 \\ -.0372 & -.42 & -.757 \end{vmatrix} \quad B_{EST} = \begin{vmatrix} .363 & -.298 \\ .039 & -.653 \\ -.006 & .571 \end{vmatrix}$$

$$C_{EST} = \begin{vmatrix} 1 & 0 & 0 \\ 0 & 1 & 0 \\ 0 & 0 & 1 \end{vmatrix} \quad D_{EST} = \begin{vmatrix} 0 & 0 \\ 0 & 0 \\ 0 & 0 \end{vmatrix}$$

E. TEST VS. THEORY FOR SELECTED CASES

The Matrix-x system "Depthin" (Appendix Q) loaded with the matrices just developed was then created for the purpose of verifying that the theoretical system/controller was an accurate model of the actual AUV performance.

This was accomplished by inputting into the computer model the same depth commands that were used in the final AUV tow tank tests, and then comparing the simulated and actual responses. Vehicle data from the tow tank tests TEST81 and TEST82 were used where a depth change from approximately 1.5 to 7 volts was commanded. This corresponded to an actual rapid depth change of about two feet. Performance plots of the computer simulation are in Appendix R. These results are summarized as follows:

1. Initial Comparison--Figure 6.2

Computer simulated and actual vehicle responses to the same depth command are shown in Figure 6.2. In this computer simulation, no disturbance was accounted for ($w=0$). The figure shows a steady state error of approximately .08 volts, which was consistent with the feedback gains used (given in Equation (6.4)).

2. Elimination of Steady State Error--Figure 6.3

It was anticipated that the steady state error of Figure 6.2 was the result of not accounting for the unmodelled disturbances discussed above. The steady state error was subsequently matched by inserting a disturbance of .08 volts into the model. The results of adding the disturbance is shown in Figure 6.3.

Actual and theoretical responses were more consistent in Figure 6.3. This agreement illustrates that

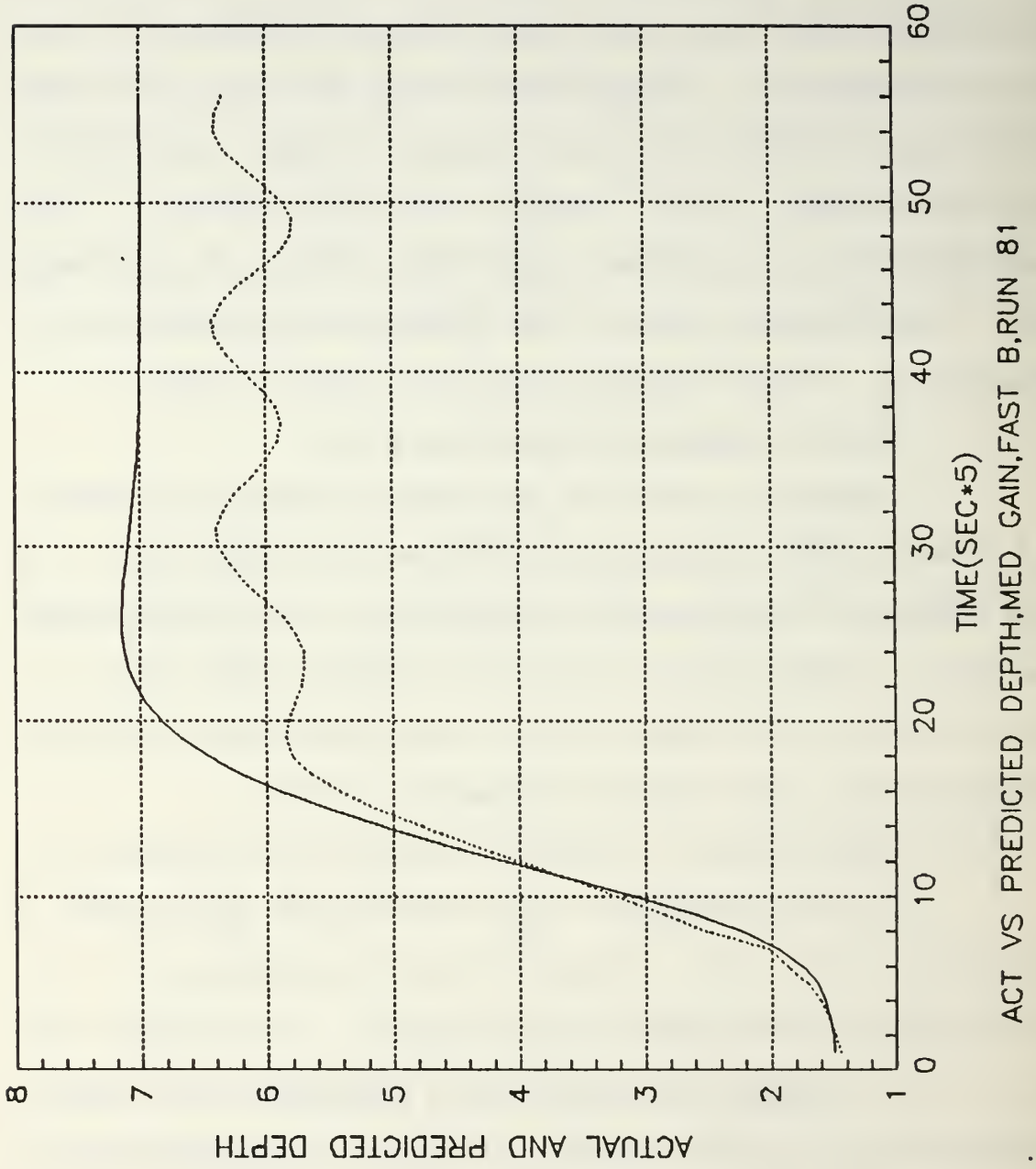

Figure 6.2 Initial Simulation/Vehicle Comparison

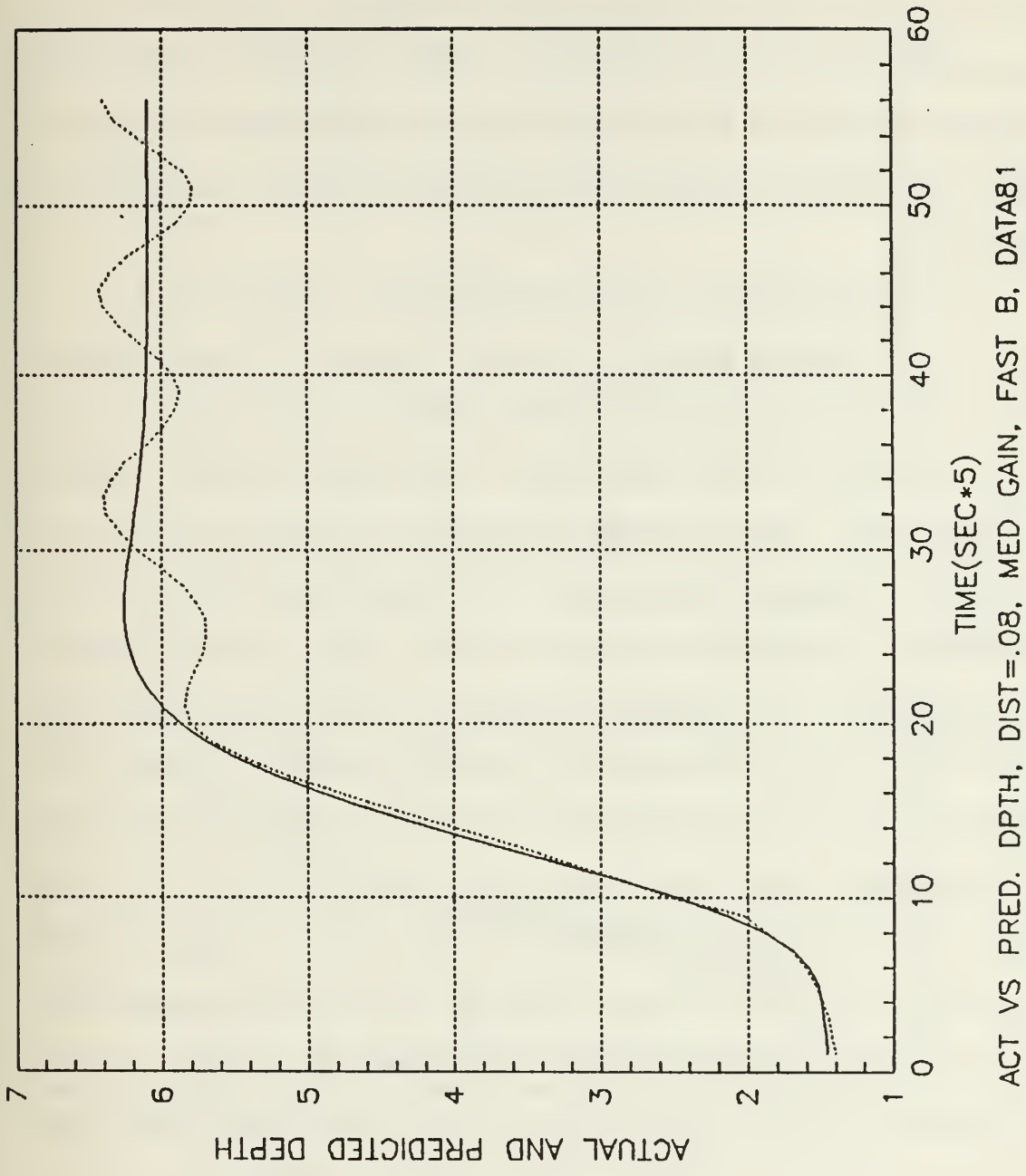

Figure 6.3 Elimination of Steady State Error

the .08 disturbance is really present in the vehicle. There was, however, still an apparent discrepancy between actual and predicted vehicle stability. The computer simulated response appeared to be much more stable than the actual vehicle response, as shown by the oscillatory segment of Figure 6.3.

3. Simulating Vehicle Stability--Figure 6.4

As stated before, system stability relied heavily upon how accurately the mathematical model (upon which the controller was designed) reflected actual vehicle performance. After studying several of the tow tank test results, it became apparent that vehicle stability was particularly sensitive to values in the B_{sys} matrix used by the controller. It therefore appeared reasonable that even small errors in formulating the B_{sys} matrix might be a potential source of dissimilarity between the actual vehicle and computer simulated responses. In an effort to match actual and computer simulated stability, the B_{sys} matrix was altered until the two results were more consistent. Figure 6.4 shows the results of multiplying the B_{sys} matrix by a factor of 2.2, producing the following system matrices:

$$A_{sys} = \begin{vmatrix} .6873 & 0 & 0 \\ .1668 & 1 & 0 \\ -.0372 & -.42 & 1 \end{vmatrix} \qquad B_{sys} = \begin{vmatrix} .798 & .363 \\ .085 & .039 \\ -.012 & -.006 \end{vmatrix}$$

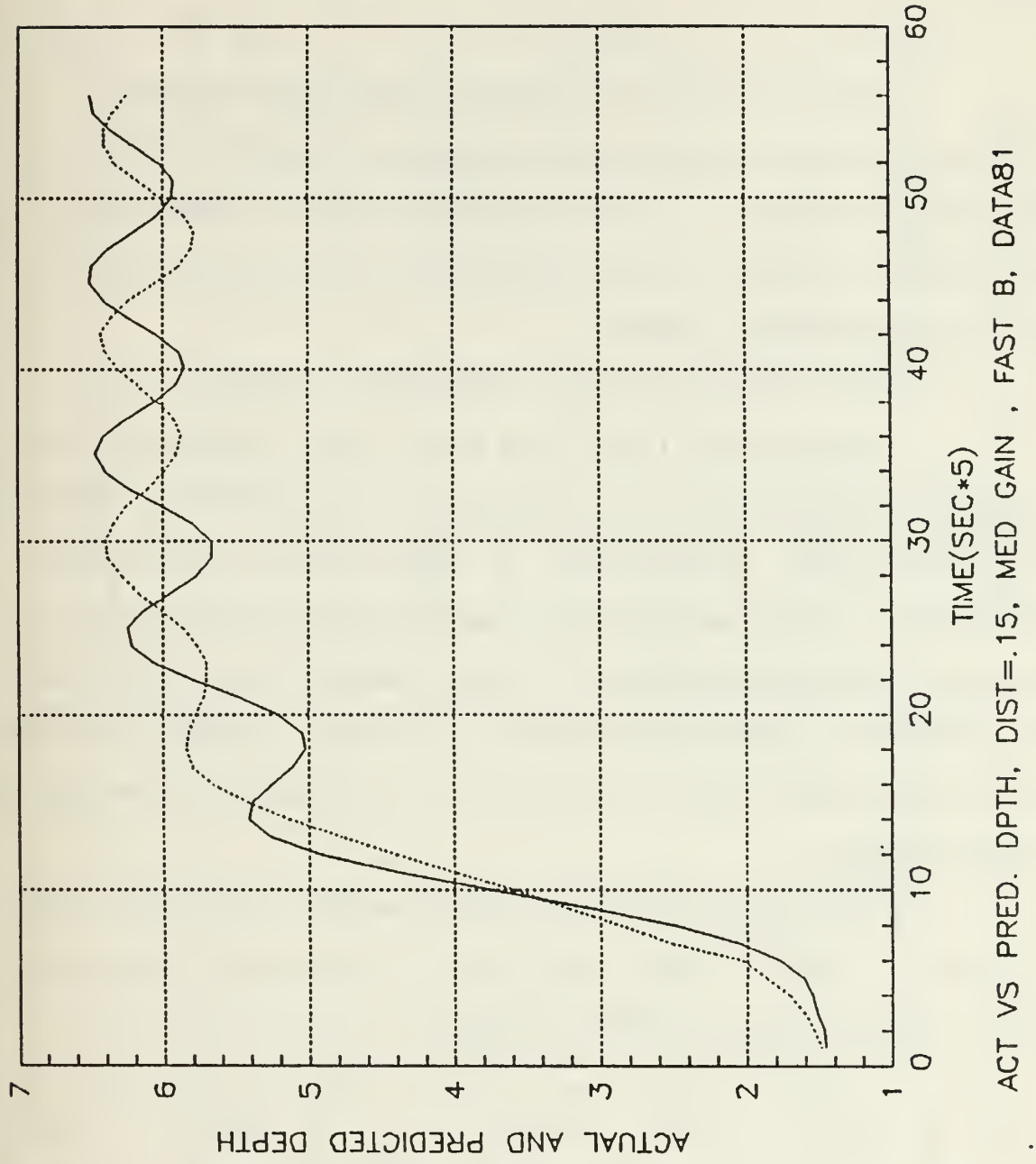

Figure 6.4 Simulating Actual Vehicle Stability

$$C_{sys} = \begin{vmatrix} 72 & 0 & 0 \\ 0 & 1 & 0 \\ 0 & 0 & 3.08 \end{vmatrix} \qquad D_{sys} = \begin{vmatrix} 0 & 0 \\ 0 & 0 \\ 0 & 0 \end{vmatrix}$$

This adjustment produced a simulated response with oscillations of period and magnitude roughly equal to the actual response. It is, therefore, fairly certain that the vehicle response is more sensitive to dive plane action than was originally thought.

4. Fine Tuning System Stability--Figure 6.5

Analysis of the final test runs suggested that system stability depended strongly on the speed with which the estimator responded to dive plane commands. Therefore, a final adjustment made to the controller for the purpose of enhancing entire system stability was to increase the values of the first column of the B_{EST} matrix, which determined how fast the estimator responds to dive plane angle changes.

The final controller gains were therefore: k_C = [1.0429, 2.5732, -.7562] and the final observer gains were: k_O = [.5442, .0578, -.0084]

$$A_{EST} = \begin{vmatrix} .6873 & 0 & .919 \\ .1668 & 1 & 2.011 \\ -.0372 & -.42 & -.757 \end{vmatrix} \qquad B_{EST} = \begin{vmatrix} .544 & -.298 \\ .058 & -.653 \\ -.008 & .571 \end{vmatrix}$$

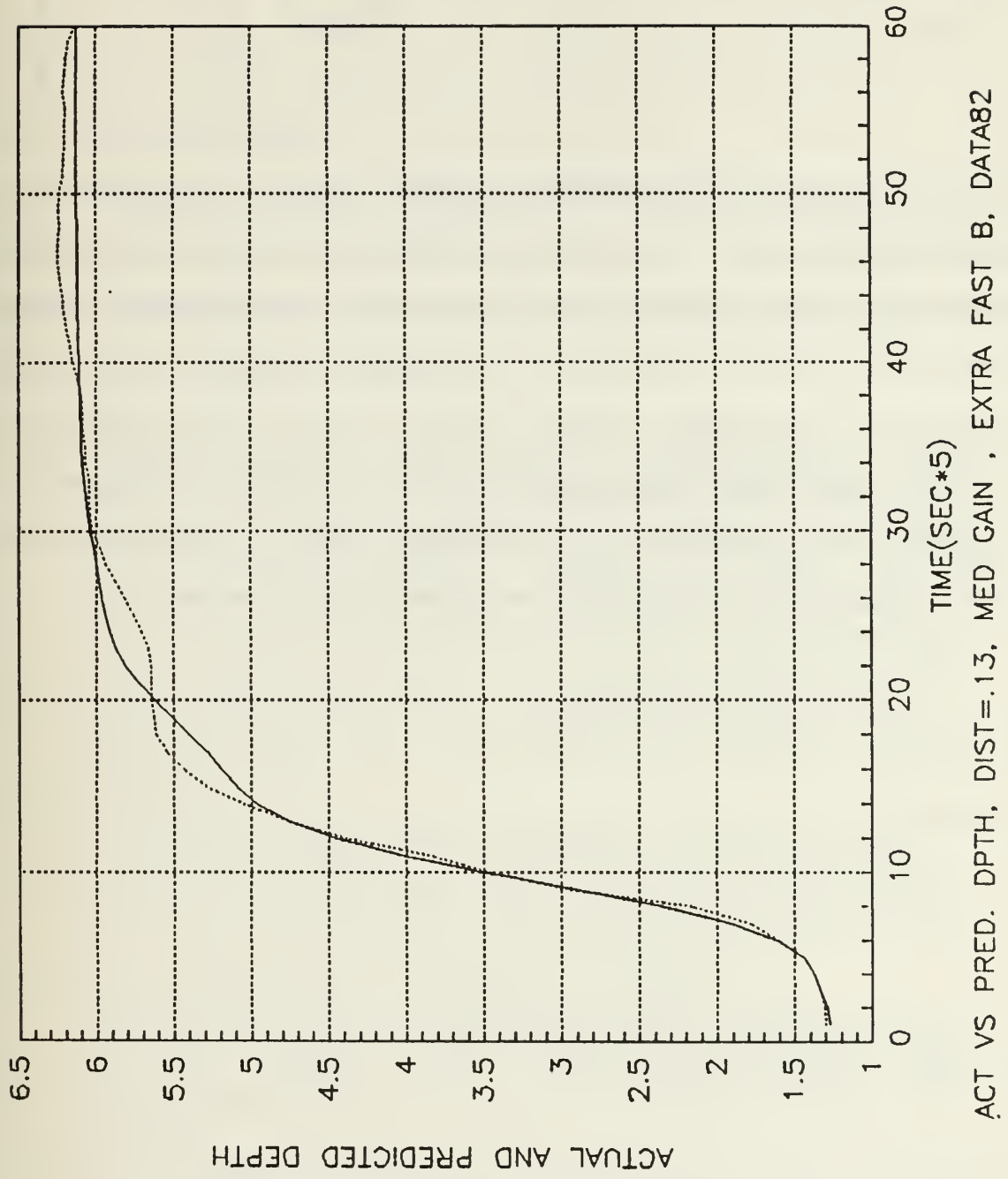

Figure 6.5 Fine Tuning System Stability

$$C_{EST} = \begin{vmatrix} 1 & 0 & 0 \\ 0 & 1 & 0 \\ 0 & 0 & 1 \end{vmatrix} \qquad D_{EST} = \begin{vmatrix} 0 & 0 \\ 0 & 0 \\ 0 & 0 \end{vmatrix}$$

Figure 6.5 shows the actual vehicle response after this adjustment was made. The computer simulated response is also plotted on Figure 6.5. Comparison of the two plots serves to illustrate the close similarity between actual and theoretical vehicle motion, once all conditions are properly matched and accounted for. These results serve to reflect the accuracy of the overall system model and the effectiveness of the controller designed in this study.

VII. CONCLUSIONS AND RECOMMENDATIONS

A. CONCLUSIONS

This study shows that an effective closed loop controller can be designed for rapid depth changes of an AUV, using a model based compensator and depth output only. Specifically, it shows that:

1. Using vehicle depth as the only external input, state observers can provide all remaining controller data. This is particularly useful in cases where vehicle size or cost limits the ability to install the highly accurate sensors needed to produce reliable pitchrate data. Errors in the generation of pitchrate data severely effect predicted vehicle depth. Since most gyro's are susceptible to bias error, eliminating the need for pitchrate/angle gyro's eliminates this potential source of depth error.
2. Vehicle equations of motion can be initially estimated by matching computer simulations with open loop vehicle tow tank tests, but will be more accurately determined by using a model based compensator and observing vehicle closed loop responses.
3. To some extent, unmodelled hydrodynamic disturbances can be compensated for by using proper controller design, thereby relaxing the need for highly detailed development of hydrodynamic equations of motion.
4. When these equations are manipulated using modern state space controls techniques, adequate closed loop control is possible.
5. Similar techniques may be applied towards the development of horizontal motion control.

The controller developed in this study, while stable, was sensitive to changes in vehicle parameters. It therefore appears that an adaptive type controller would provide the most robust design for a controller that needs to maintain an accurate prediction of vehicle response under varying conditions.

It is possible to compensate unmodelled disturbances by assuming all disturbances to be a single, additional system state variable of unknown magnitude. This disturbance variable can then be estimated by incorporating a separate disturbance observer/ estimator. The effect of this disturbance can then be compensated for in a model based compensator. Although this method of disturbance compensation worked well in computer simulation, it was determined to be sensitive to parameter mismatch. This would reduce the robustness of the controller when confronted with the varying, uncontrolled conditions found outside of the laboratory. Again, use of adaptive control would be expected to regain robustness.

B. RECOMMENDATIONS

Continuing follow-up research is recommended as described below:

1. Use data generated in the final closed loop runs to investigate methods for refining the establishment of

vehicle hydrodynamic parameters. Investigate adaptive methods for controller tuning as parameters change.

2. Conduct a direct comparison of the disturbance compensation performed in this study with the more traditional integral of error control techniques, focusing on robustness.
3. Perform further comparison to illustrate the advantage in controller robustness gained by using the model based compensator design approach versus the more conventional proportional-integral-derivative controller design.
4. Investigate new robust methods for control of depth change maneuvering in the face of unmodelled disturbances and parameter uncertainty.

APPENDIX A

Matrix-x Program "MOD.MX"

```
  L=28/12;
  UX=SPEED;
//
  ZW=   P(1); // HEAVE DAMPING
  ZQ=   P(2); // CROSS COUPLING (PITCH)
  MW=   P(3); // CROSS COUPLING (HEAVE)
  MQ=   P(4); // PITCH DAMPING
  ZD=   P(5); // MOMENT EFFECT
  MD=   P(6); // MOMENT EFFECT MD=2*ZD
  MZDW= P(7); // MASS + ADDED MASS
  IYY=  P(8); // INERTIA + ADDED INERTIA
//
  A11=ZW*UX/MZDW/L;A12=ZQ*UX/MZDW;B11=-ZD*UX*UX/L/MZDW;
  B12=F(1)/MZDW; B22=F(2)/IYY;
  A21=MW*UX/L/L/IYY;A22=MQ*UX/L/IYY;B21=MD*UX*UX/L/L/IYY;
  AA=[A11 A12 0 0;A21 A22 0 0;0 1 0 0;1 0 -UX 0];
  NS=4;BB=[B11 B12;B21 B22;0 0;0 0];
  CC=[1 0 0 0;0 0.72 0 0;0 0 1 0;0 0 0 3];DD=[0 0;0 0;0 0;0 0];
  S=[AA BB;CC DD];
  V=EIG(AA);
  SD=DISCRETIZE(S,NS,0.05);
  YHAT=FILP(SD,U,X0);
// QBIAS IS ADDED TO RESPONSE OF PITCH RATE OF MAGNITUDE DELTA
  QBIAS=DELTAQ*ONES(250,1);
  ZBIAS=DELTAZ*ONES(250,1);
  YHAT(:,2)=YHAT(:,2)+QBIAS;
  YHAT(:,4)=YHAT(:,4)+ZBIAS;
  PLOT([YHAT(:,1) YHAT(:,3)],'LOWER LEFT/...
  XLABEL/TIME/YLABEL/HEAVE VEL,PITCH ANG/TITLE/   UV01093 DATA  ...
  F=0,0    XO=0,-.1,0,0/');
  PLOT([Y2 YHAT(:,2)],'UPPER RIGHT/XLABEL/TIME/YLABEL/PITCH RATE/...
  TITLE/ZD=0 MD=.27 MZDW=1.005 IYY=.072      /');
  PLOT([Y3 YHAT(:,4)],'LOWER RIGHT/XLABEL/TIME/...
  YLABEL/DEPTH/TITLE/DELZ=4.5 DELQ=.05 UX=1.8/');
  PLOT (U(:,1),'UPPER LEFT/XLABEL/TIME/YLABEL/DIVE PLANE ANGLE/...
  TITLE/      ZW=-1.5 ZQ=0 MW=0 MQ=-.15/');
  RETURN
```

Figure A1. Matrix-x Program "MOD.MX"

APPENDIX B
Test Run Performance Curves

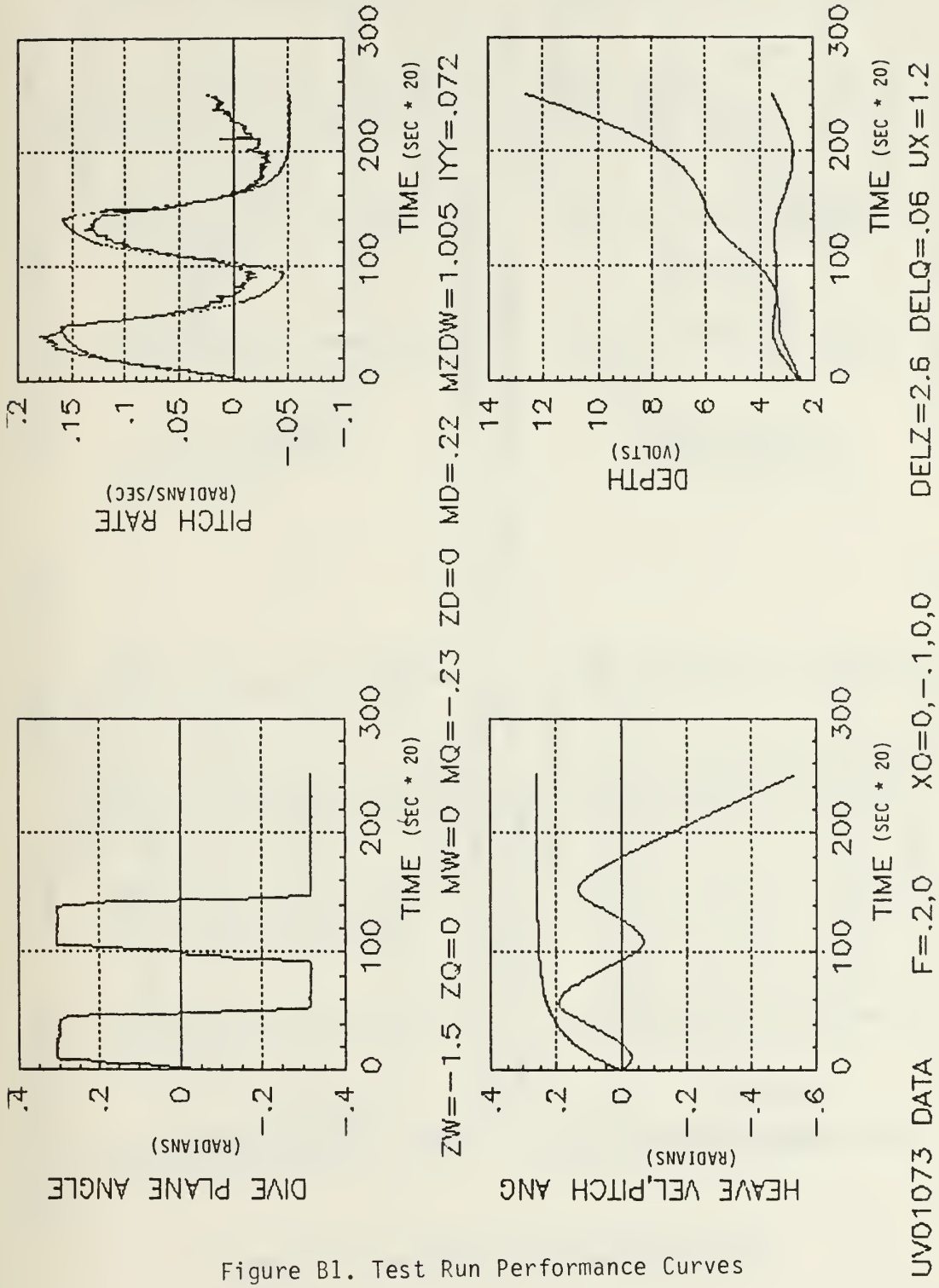

Figure B1. Test Run Performance Curves

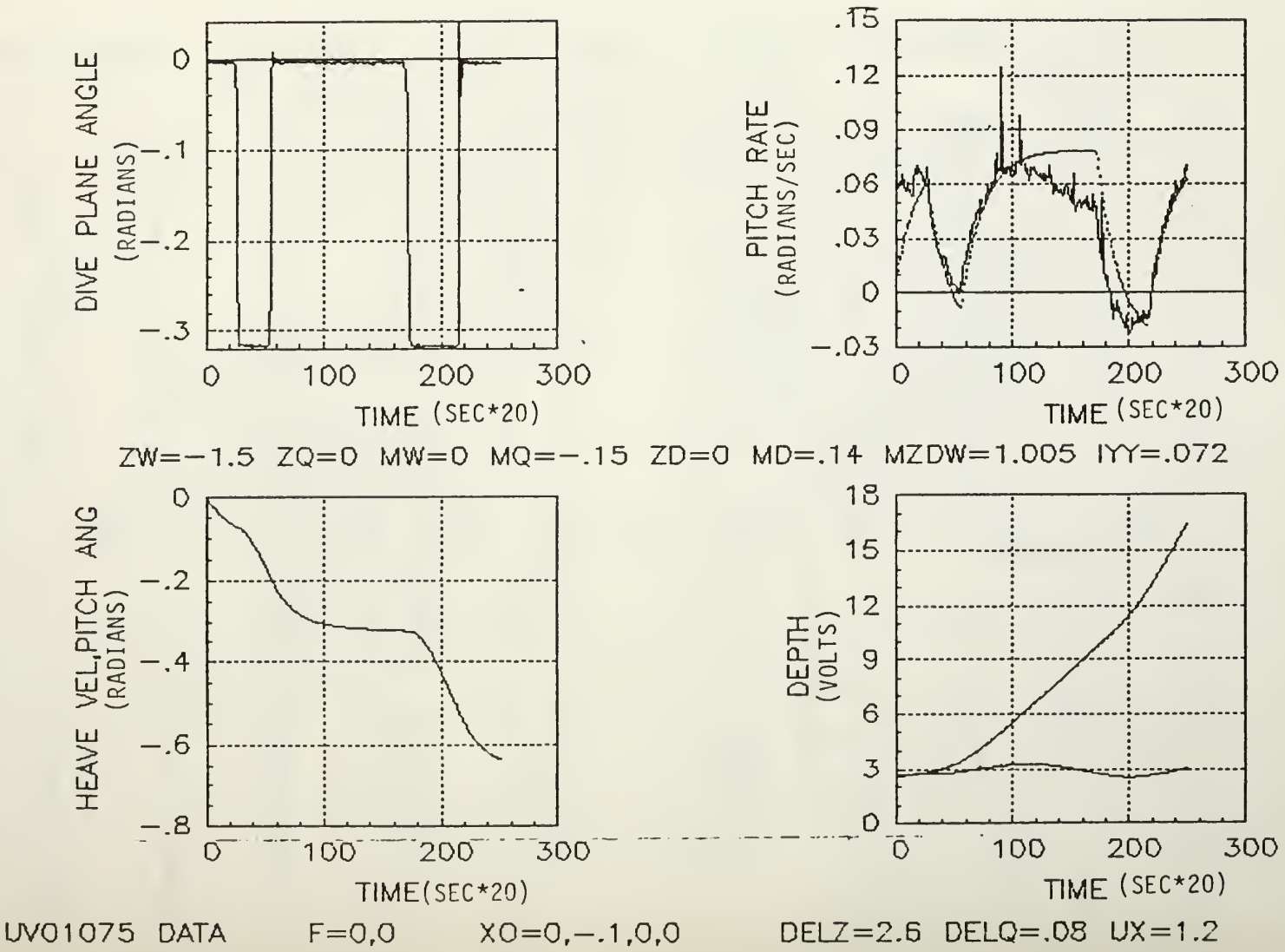

Figure B2. Test Run Performance Curves

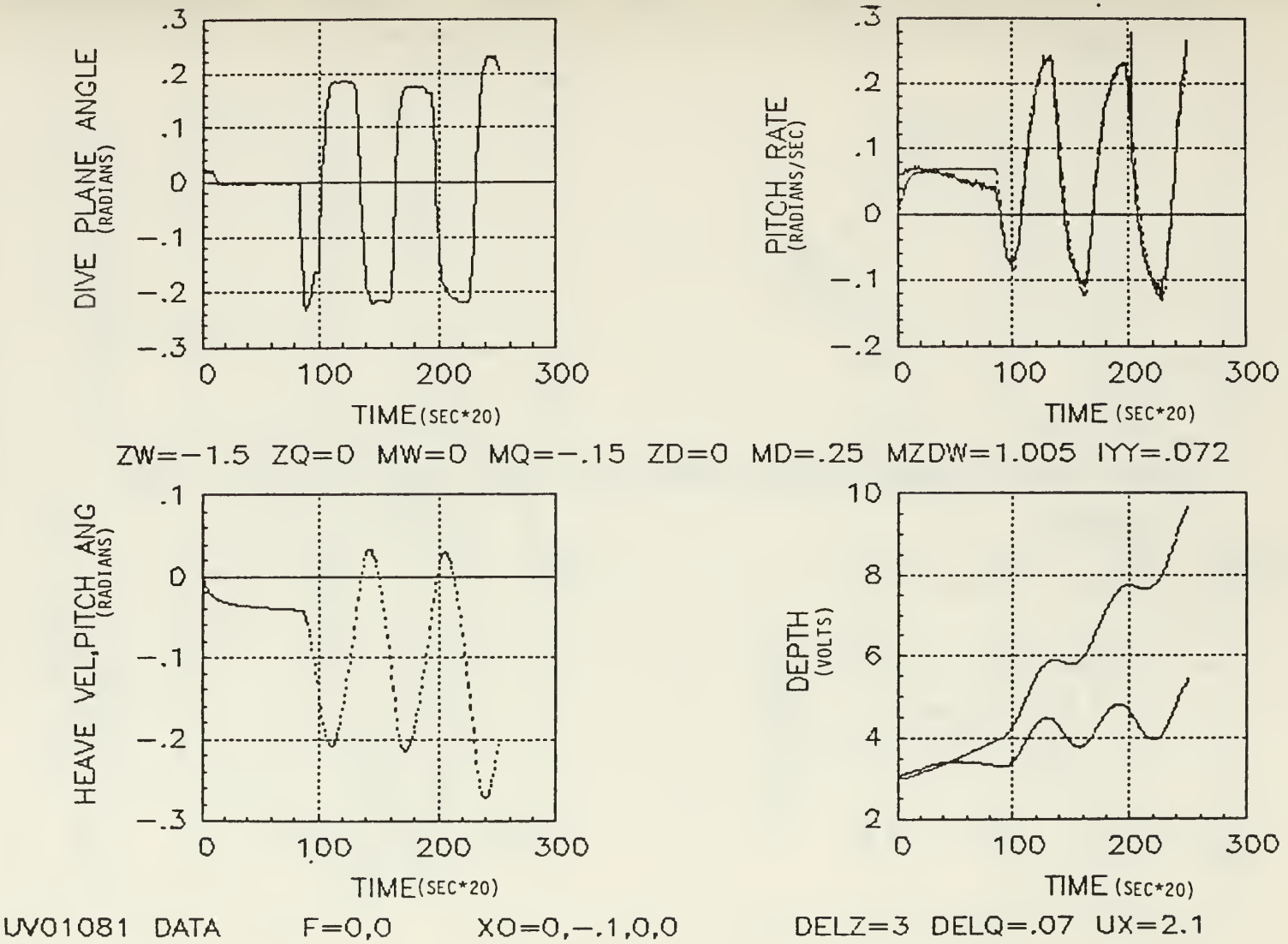

Figure B3. Test Run Performance Curves

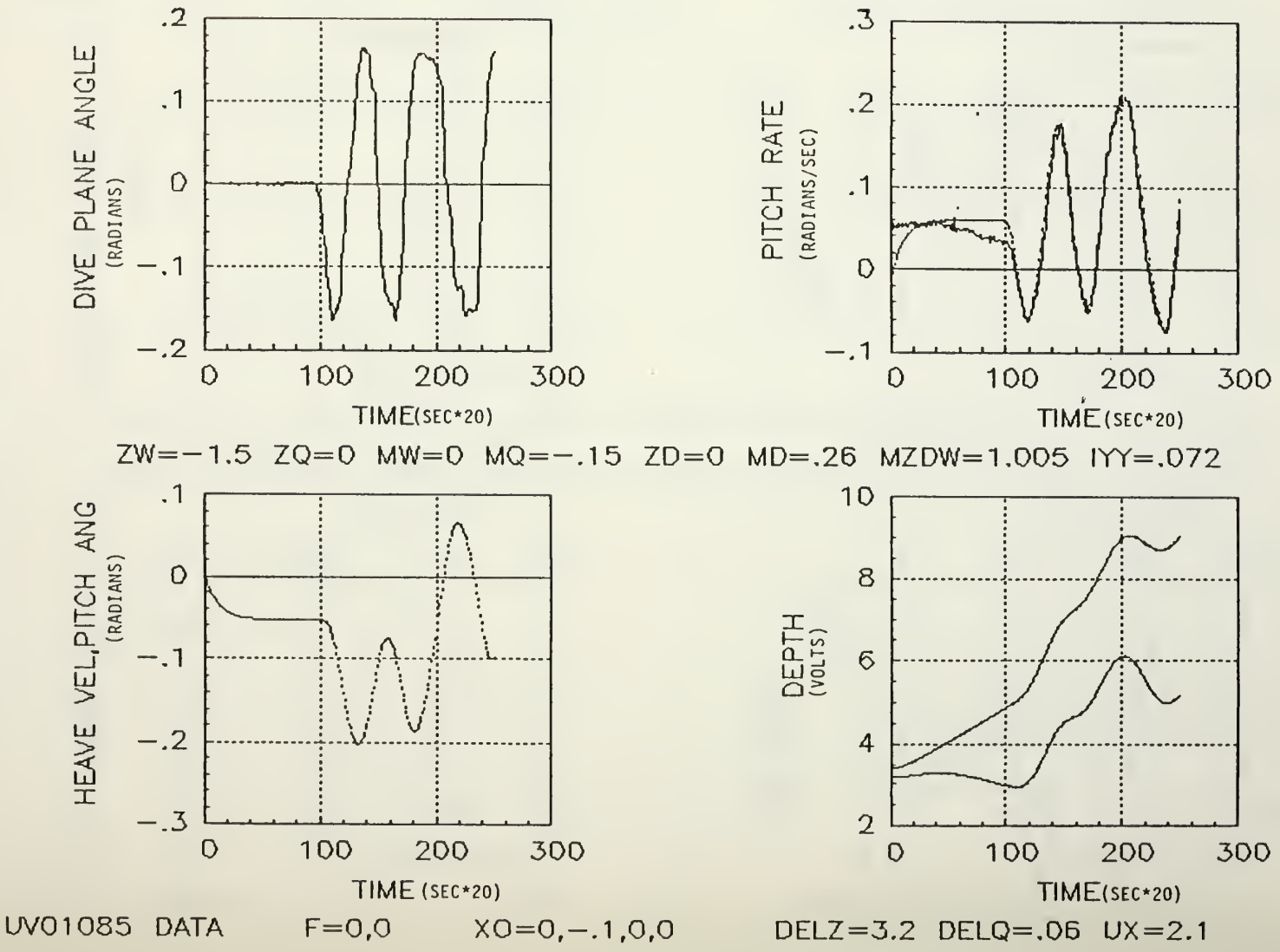

Figure B4. Test Run Performance Curves

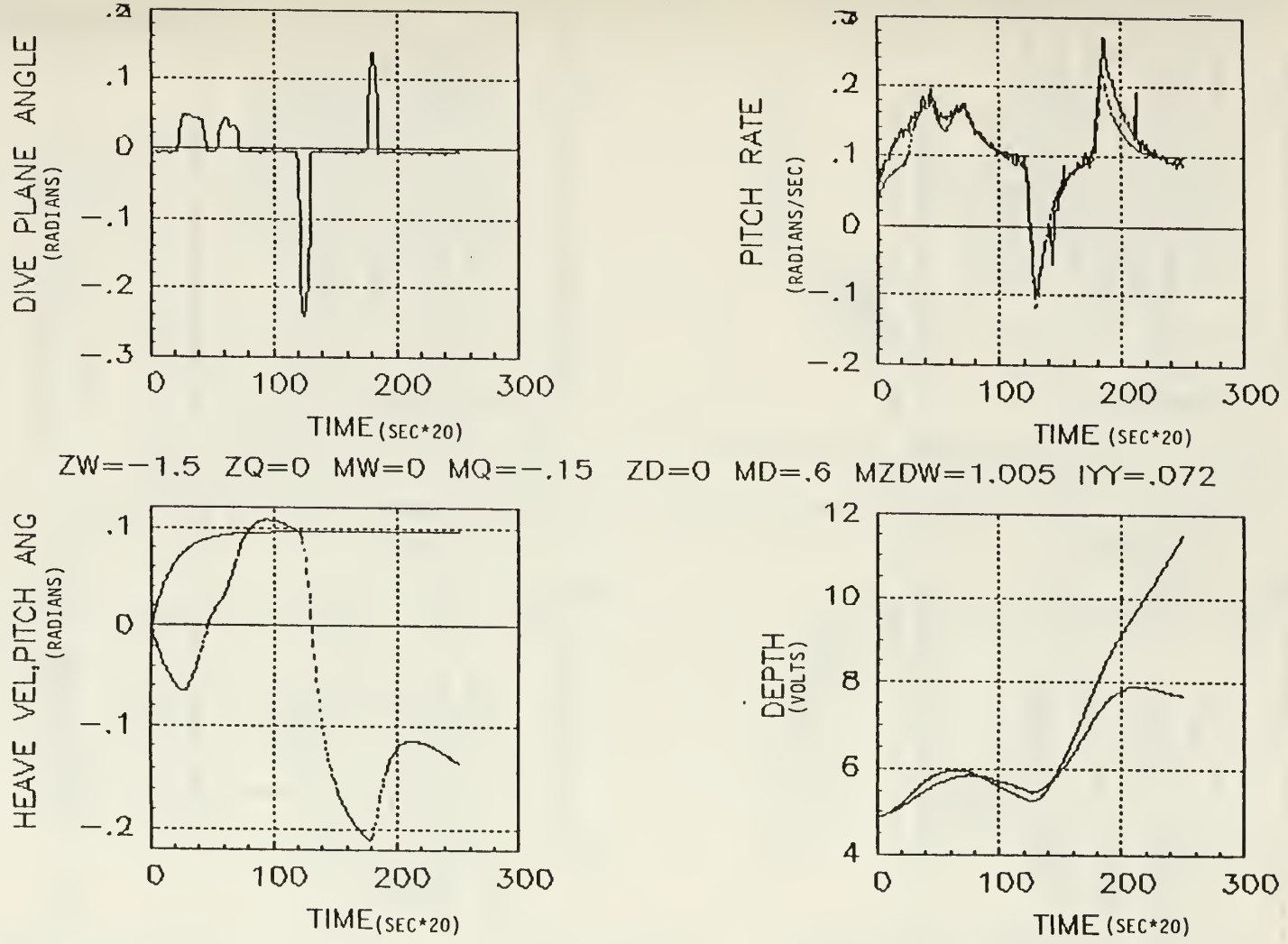

Figure B5. Test Run Performance Curves

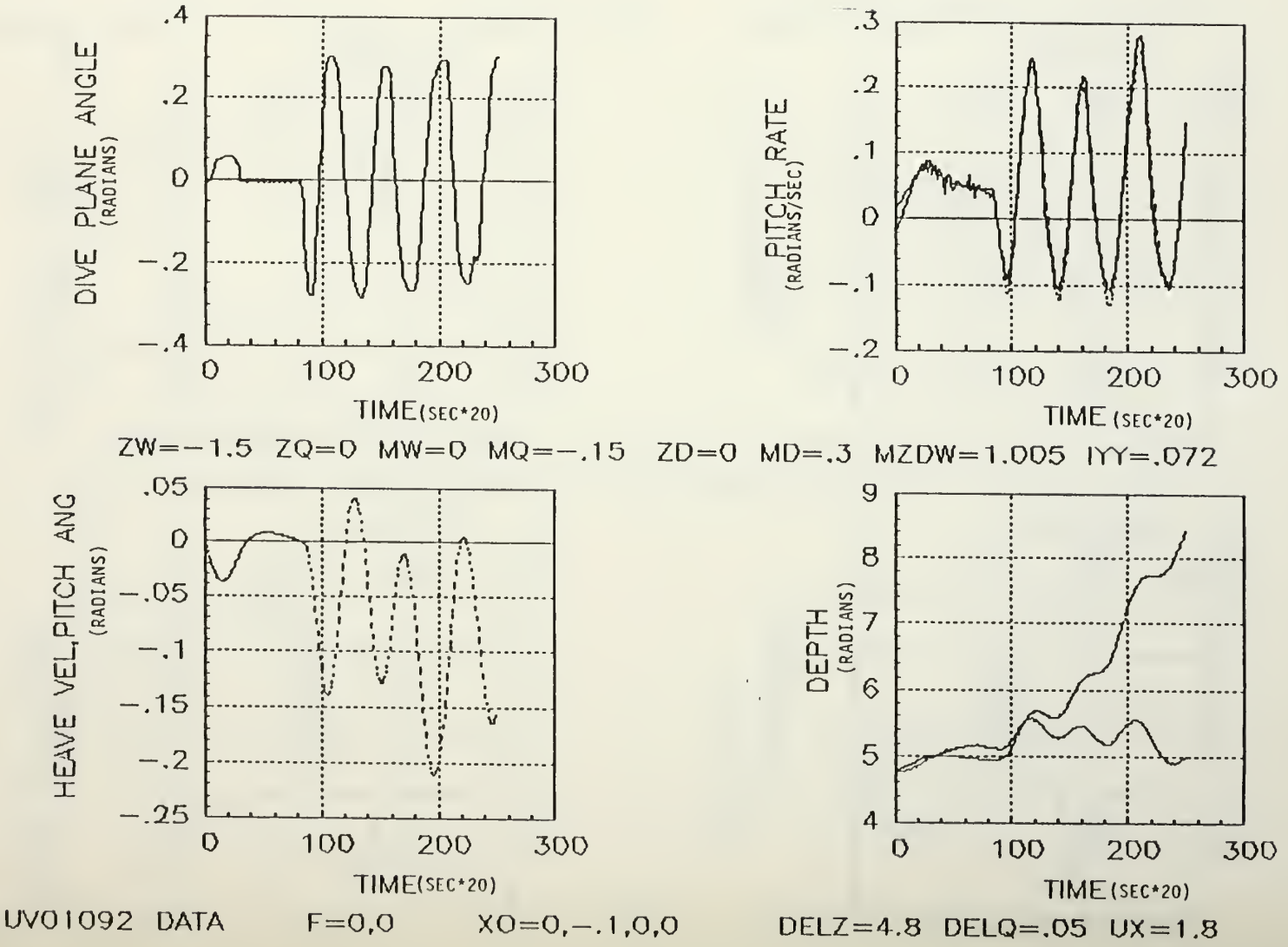

Figure B6. Test Run Performance Curves

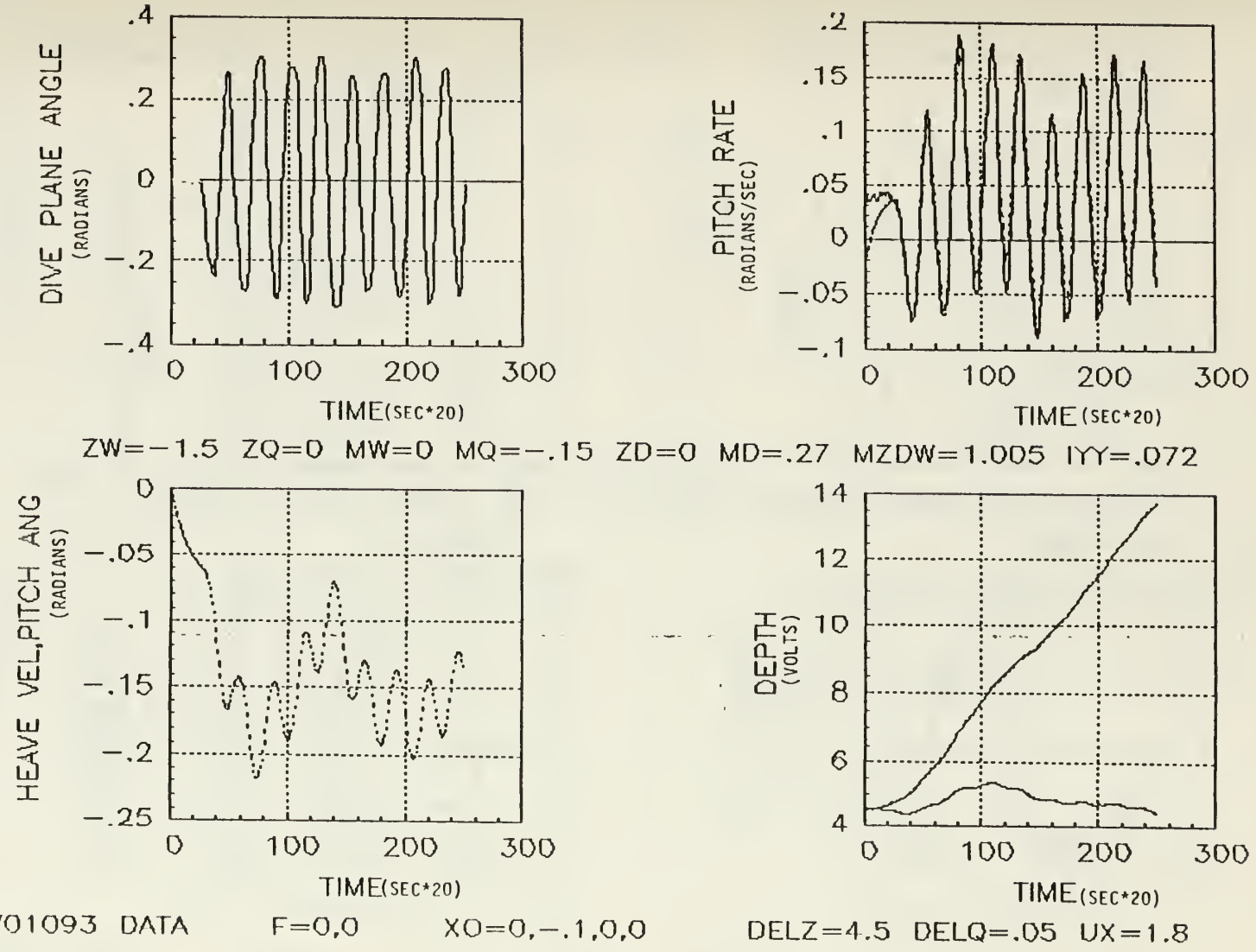

Figure B7. Test Run Performance Curves

Figure B8. Test Run Perfoemance Curves

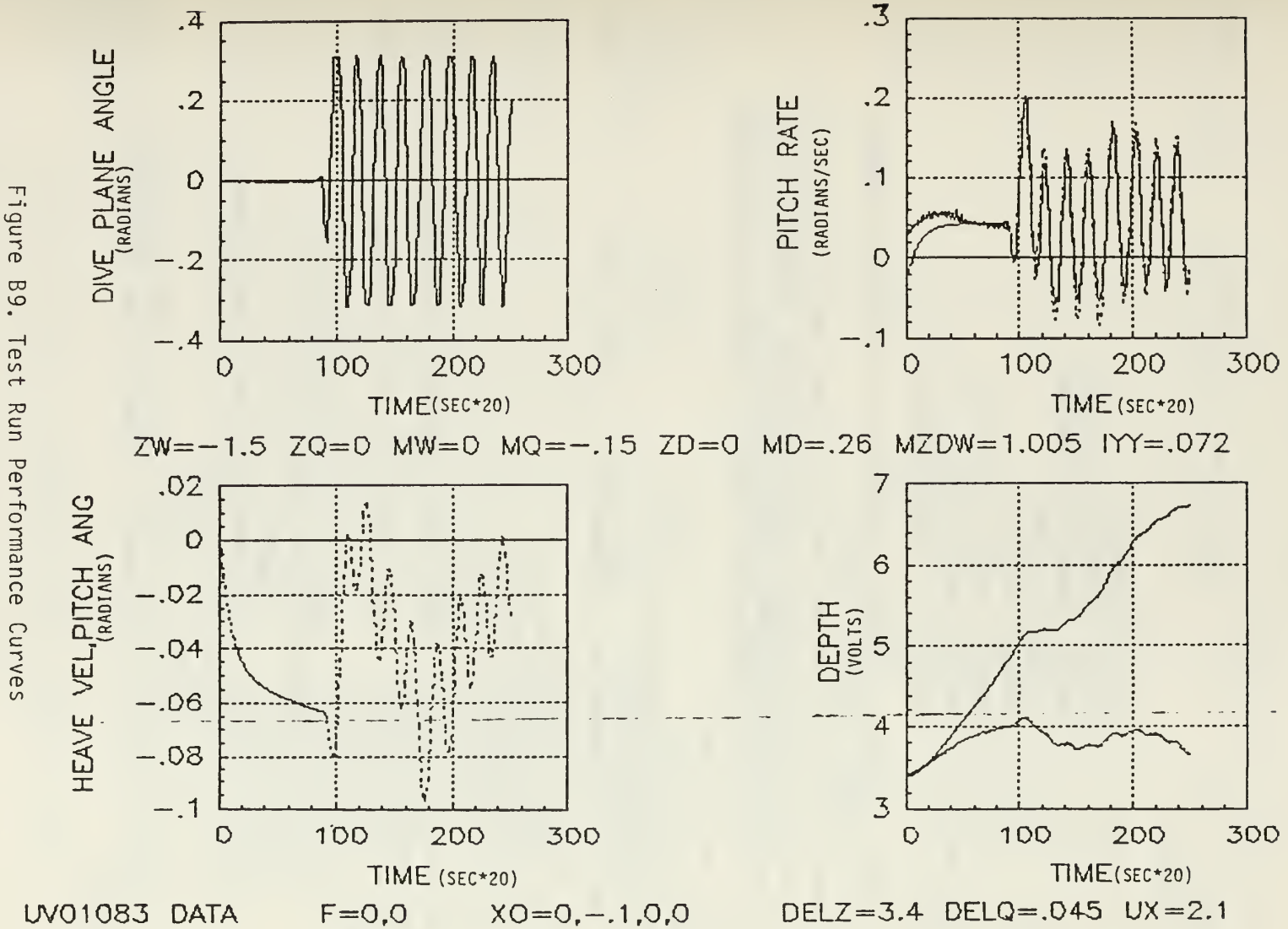

Figure B9. Test Run Performance Curves

APPENDIX C
Matrix-x Program "RMS.MX"

```
L=28/12;
UX=SPEED;
//
ZW=   P(1); // HEAVE DAMPING
ZQ=   P(2); // CROSS COUPLING (PITCH)
MW=   P(3); // CROSS COUPLING (HEAVE)
MQ=   P(4); // PITCH DAMPING
ZD=   P(5); // MOMENT EFFECT
MD=   P(6); // MOMENT EFFECT MD=2*ZD
MZDW= P(7); // MASS + ADDED MASS
IYY=  P(8); // INERTIA + ADDED INERTIA
//
A11=ZW*UX/MZDW/L;A12=ZQ*UX/MZDW;B11=-ZD*UX*UX/L/MZDW;
B12=F(1)/MZDW; B22=F(2)/IYY;
A21=MW*UX/L/L/IYY;A22=MQ*UX/L/IYY;B21=MD*UX*UX/L/L/IYY;
AA=[A11 A12 0 0;A21 A22 0 0;0 1 0 0;1 0 -UX 0];
NS=4;BB=[B11 B12;B21 B22;0 0;0 0];
CC=[1 0 0 0;0 0.72 0 0;0 0 1 0;0 0 0 3];DD=[0 0;0 0;0 0;0 0];
S=[AA BB;CC DD];
V=EIG(AA);
SD=DISCRETIZE(S,NS,0.05);
YHAT=FILP(SD,U,X0);
// QBIAS IS ADDED TO RESPONSE OF PITCH RATE
//OF MAGNITUDE DELTA
QBIAS=DELTAQ*ONES(250,1);
ZBIAS=DELTAZ*ONES(250,1);
YHAT(:,2)=YHAT(:,2)+QBIAS;
YHAT(:,4)=YHAT(:,4)+ZBIAS;
QRMS1=Y2-YHAT(:,2);QRMS2=QRMS1.*QRMS1;QRMS3=SUM(QRMS2)/250;
QRMS4=SQRT(QRMS3)
ZRMS1=Y3-YHAT(:,4);ZRMS2=ZRMS1.*ZRMS1;ZRMS3=SUM(ZRMS2)/250;
ZRMS4=SQRT(ZRMS3)
//  PLOT([YHAT(:,1) YHAT(:,3)],'LOWER LEFT/...
//  XLABEL/TIME/YLABEL/HEAVE VEL,PITCH ANG/...
//  TITLE/QRMS=       ZRMS=      /');
//  PLOT([Y2 YHAT(:,2)],'UPPER/XLABEL/TIME/YLABEL/...
//  PITCH RATE/TITLE/P=-1.5,0,0,-.15,0,.255,1.005,.072...
//    F=.11,0   XO=0,-.1,0,0/');
//  PLOT([Y3 YHAT(:,4)],'LOWER RIGHT/XLABEL/TIME/...
//  YLABEL/DEPTH/TITLE/DELZ=4.1 DELQ=.056 UX=2.1/');
RETURN
```

APPENDIX D

Results of Data Processing Through "RMS.MX"

Parameter	Nominal	Average	Individual Speeds(f/s) 1.2	1.8	2.1
Z_W	-1.5	-1.5	-1.5	-1.5	-1.5
Z_Q	0	0	0	0	0
M_W	0	0	0	0	0
M_Q	-.15	-.158	-.19	-.15	-.15
Z_D	0	0	0	0	0
M_D	.6	.235	.18	.38	.253
M_{ZDW}	1.005	1.005	1.005	1.005	1.005
I_{YY}	.072	.072	.072	.072	.072

CALCULATED ROOT MEAN SQUARE ERRORS
(Pitchrate RMS error/Depth RMS error)

RUN NUMBER (REF 4)	USING NOMINAL VALUES	USING AVERAGE VALUES	USING SPEED DEPENDENT VALUES
UV01073	.2543/6.0108	.0606/1.4908	.0263/2.4294
UV01075	.1453/22.9625	.0308/9.9636	.0162/9.2043
UV01078	.3072/54.8087	.0975/20.0351	.0539/14.7368
UV01081	.1431/5.0330	.0202/2.6903	.0190/2.1660
UV01083	.0876/2.9393	.0148/2.3165	.0156/1.6546
UV01085	.0916/5.3888	.0183/2.7911	.0168/2.2795
UV01091	.0207/1.2281	.0439/.8325	.0320/.4218
UV01092	.0976/2.5115	.0263/2.1355	.0291/1.5961
UV01093	.0792/10.0583	.0213/5.0563	.0266/6.3896
UV01096	.0604/.7969	.0309/1.340	.0236/.6822
AVERAGE ERROR FOR ALL RUNS	.1287/11.1738	.0304/4.7161	.0233/3.9130

APPENDIX E
Model Sensitivity to M_w

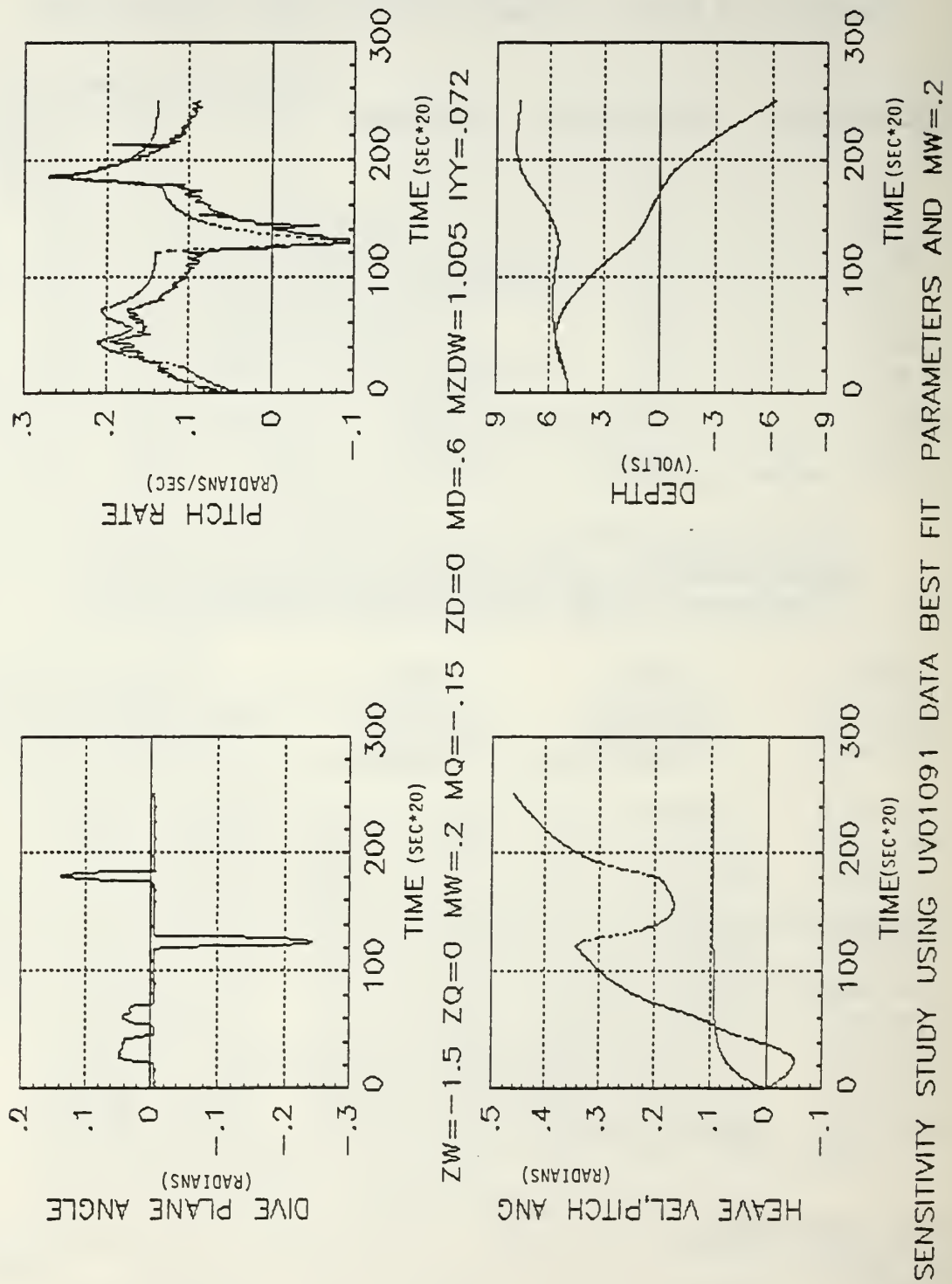

Figure E1. Model Sensitivity to M_W

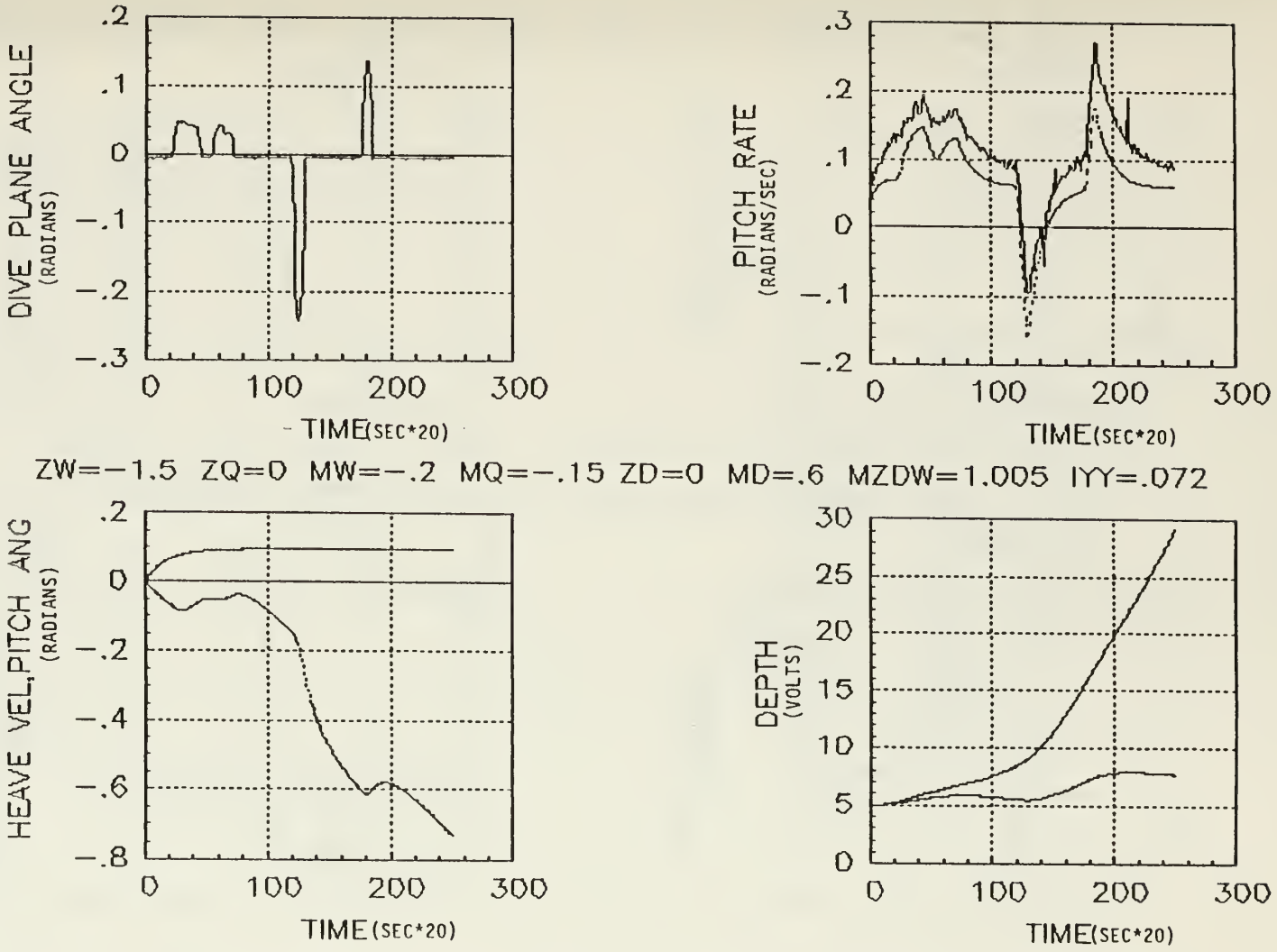

Figure E2. Model Sensitivity to M_w

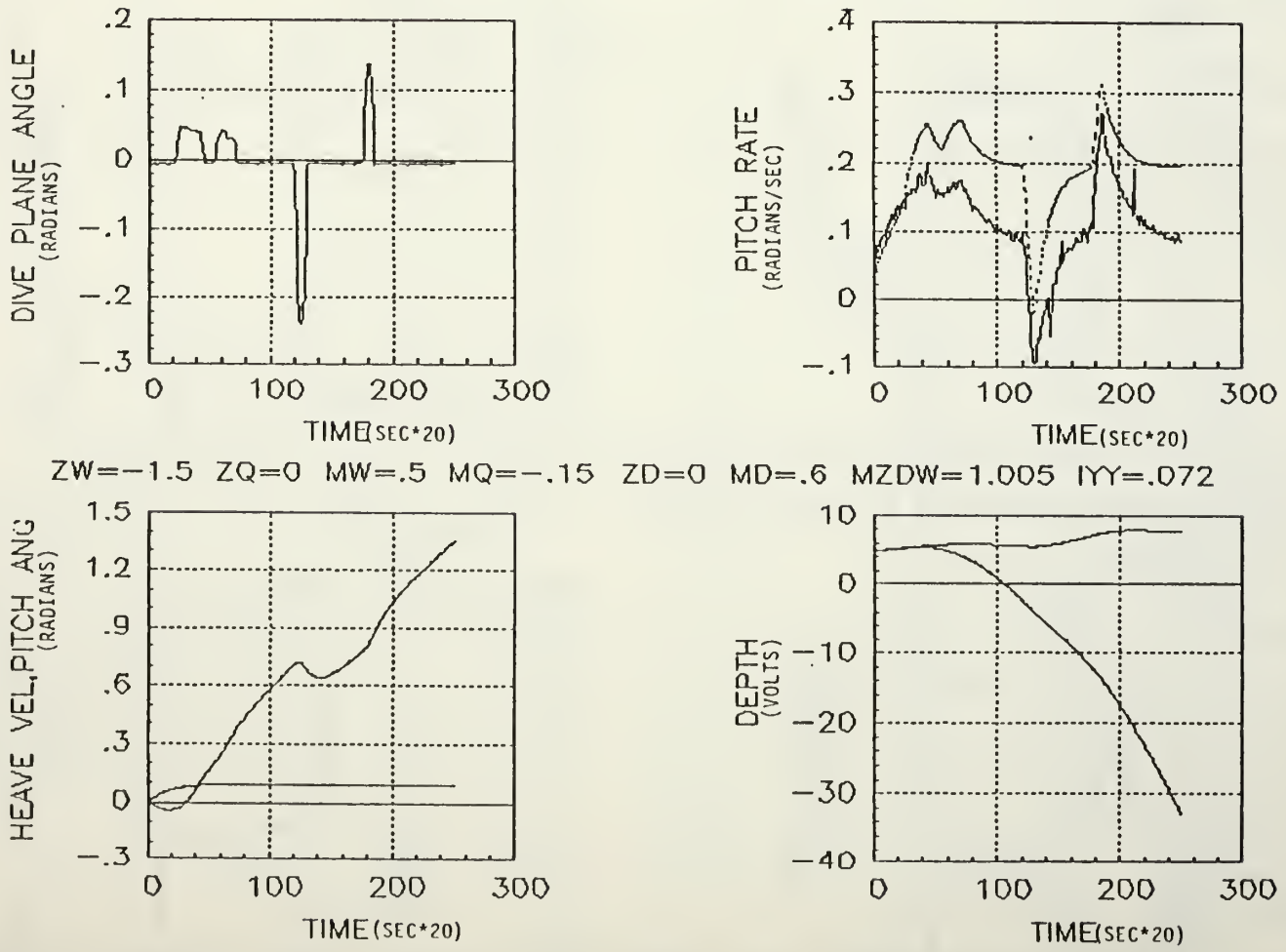

Figure E3. Model Sensitivity to M_W

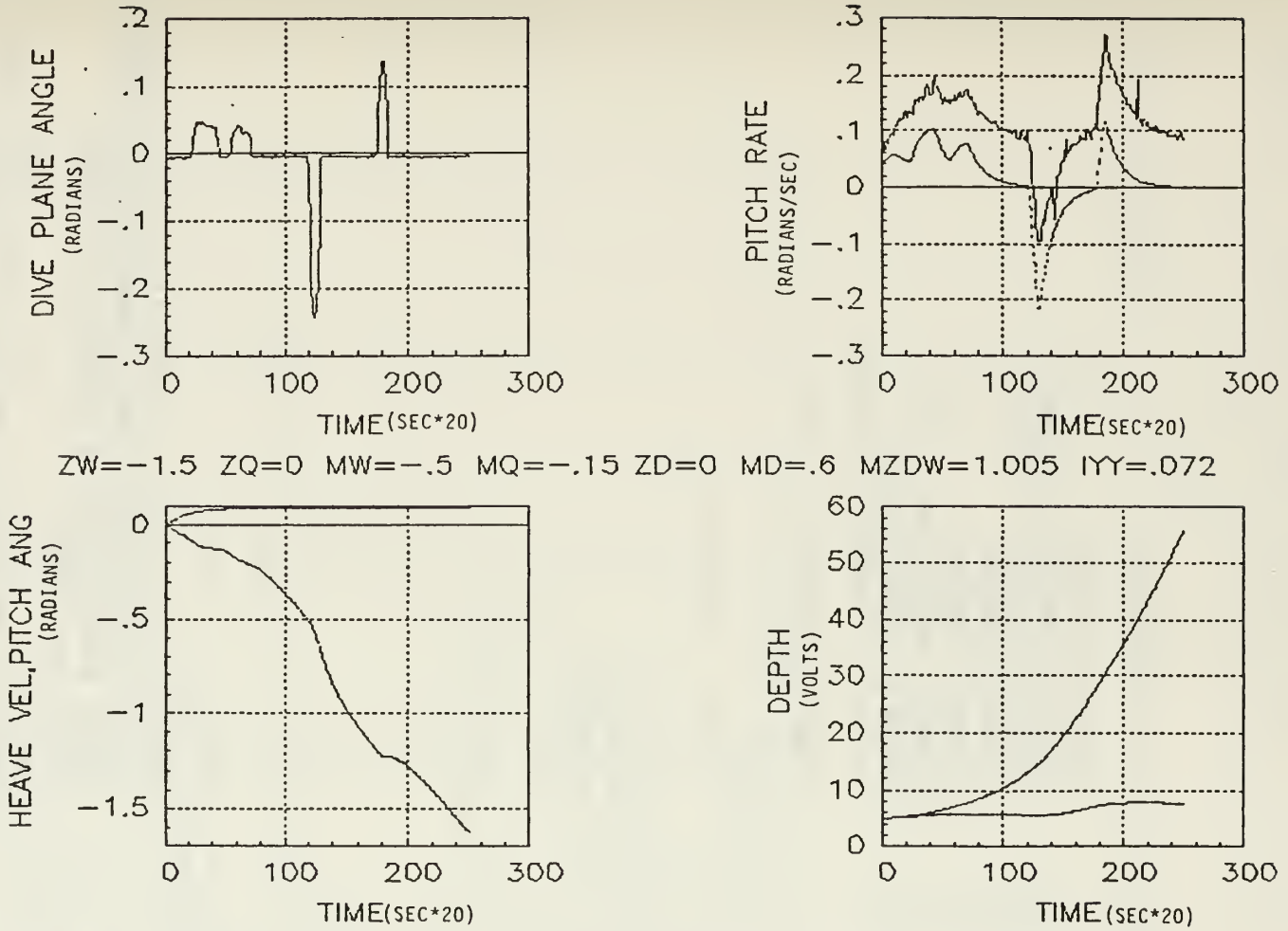

Figure E4. Model Sensitivity to $M_{\dot{w}}$

APPENDIX F
Matrix-x Program "POLE.MX"

```
L=28/12;
UX=SPEED;

ZW=    P(1); // HEAVE DAMPING
ZQ=    P(2); // CROSS COUPLING (PITCH)
MW=    P(3); // CROSS COUPLING (HEAVE)
MQ=    P(4); // PITCH DAMPING
ZD=    P(5); // MOMENT EFFECT
MD=    P(6); // MOMENT EFFECT MD=2*ZD
MZDW=  P(7); // MASS + ADDED MASS
IYY=   P(8); // INERTIA + ADDED INERTIA

A22=MQ*UX/L/IYY;B21=MD*UX*UX/L/L/IYY;
A=[A22 0 0;1 0 0;0 -UX 0];
NS=3;B=[B21;0;0];
C=[0.72 0 0;0 1 0;0 0 3];D=[0;0;0];
S=[A B;C D];
SD=DISCRETIZE(S,3,.2);
[A B C D]=SPLIT(SD,3);
K=POLEPLACE(A,B,POLES)
CZ=[C(3,1) C(3,2) C(3,3)];
AC=A-B*K;
I=[1 0 0 ;0 1 0;0 0 1];
AN=INV((CZ)*INV(I-AC)*B);
BC=B*AN;
CC=C;
DC=D*AN;
V=EIG(AC);
SC=[AC BC;CC DC];
CU=[[(-1)*K(1)] [(-1)* K(2)] [(-1)*K(3)]];
DCU=AN;
SU=[AC BC;CU DCU];
[T,Y]=DSTEP(SC,3,150);
PLOT (Y(:,1),'UPPER RIGHT/XLABEL/TIME/YLABEL/PITCH RATE/');
PLOT (Y(:,2),'LOWER LEFT/XLABEL/TIME/YLABEL/PITCH ANGLE/');
PLOT (Y(:,3),'LOWER RIGHT/XLABEL/TIME/YLABEL/DEPTH/...
TITLE/POLES = .88, .881 .882/');
[Q,U]=DSTEP(SU,3,150);
PLOT (U,'UPPER LEFT/XLABEL/TIME/YLABEL/DIVE PLANE ANGLE/');
```

APPENDIX G

TABLE G1. DETAILED RESULETS OF PLOE OPTIMIZATION STUDY USING 'POLE.MX' WITH A 20 HZ SAMPLING RATE

POLES			FEEDBACK GAINS ("K", volts)		
.92	.921	.922	.6315	1.5299	-.4598
.92	.82	.922	1.0224	2.8162	-1.0476
.92	.72	.922	1.4094	4.0898	-1.6296
.92	.62	.922	1.7964	5.3633	-2.2116
.92	.52	.922	2.1834	6.6369	-2.7936
.92	.42	.922	2.5704	7.9105	-3.3756
.92	.32	.922	2.9574	9.1840	-3.9576
.92	.921	.82	1.0261	2.8368	-1.0610
.92	.921	.72	1.4129	4.1181	-1.6505
.92	.921	.62	1.7997	5.3994	-2.2400
.92	.921	.52	2.2252	6.8088	-2.8884
.92	.921	.42	2.5733	7.9619	-3.4189
.92	.921	.32	2.9601	9.2432	-4.0084
.82	.921	.922	1.0187	2.7957	-1.0345
.72	.921	.922	1.4059	4.0616	-1.6092
.62	.921	.922	1.7931	5.5374	-2.1840
.52	.921	.922	2.1803	6.5932	-2.7587
.42	.921	.922	2.5676	7.8590	-3.3334
.32	.921	.922	2.9548	9.1249	-3.9081
.92	.82	.821	1.3825	4.8976	-2.4041
.92	.72	.721	2.1056	9.7834	-5.8290
.92	.62	.621	2.7783	16.2128	-10.7461
.92	.52	.521	3.4109	24.1858	-17.1556
.92	.42	.421	4.0032	33.7025	-25.0574
.92	.32	.321	4.5552	44.7628	-34.4515
.82	.821	.922	1.3856	4.8428	-2.3440
.72	.721	.922	2.0993	9.7027	-5.6832

TABLE G1(con't). DETAILED RESULETS OF PLOE OPTIMIZATION STUDY USING 'POLE.MX' WITH A 20 HZ SAMPLING RATE

POLES			FEEDBACK GAINS ("K", volts)		
.62	.621	.922	2.7728	16.1097	-10.4775
.52	.521	.922	3.4059	24.0637	-16.7267
.42	.421	.922	3.9987	33.5647	-24.4310
.32	.321	.922	4.5512	44.6127	-33.5902
.82	.921	,822	1.3854	4.8497	-2.3608
.72	.921	.722	2.0990	9.7148	-5.7355
.62	.921	.622	2.7723	16.1252	-10.5838
.52	.921	.522	3.4053	24.0810	-16.9058
.42	.921	.422	3.9981	33.5821	-24.7015
.32	.921	.322	4.5506	44.6286	-33.9708
.82	.821	.822	1.7336	7.5841	-5.3492
.72	.721	.722	2.7233	17.7672	-20.2557
.62	.621	.622	3.6093	31.5723	-50.7755
.52	.521	.522	4.4002	48.4923	-102.5049
.42	.421	.422	5.1045	68.0202	-181.0398
.32	.321	.322	5.7308	89.6490	-291.9767
.95	.951	.952	.2778	.5946	-.1097
.94	.941	.942	.3969	.8592	-.1915
.93	.931	.932	.5148	1.1711	-.3063
.91	.911	.912	.7470	1.9351	-.6574
.90	.901	.902	.8613	2.3861	-.9049
.89	.891	.892	.9744	2.8825	-1.2078
.88	.881	.882	1.0864	3.4237	-1.5716

APPENDIX H
Selected Pole Placement Performance

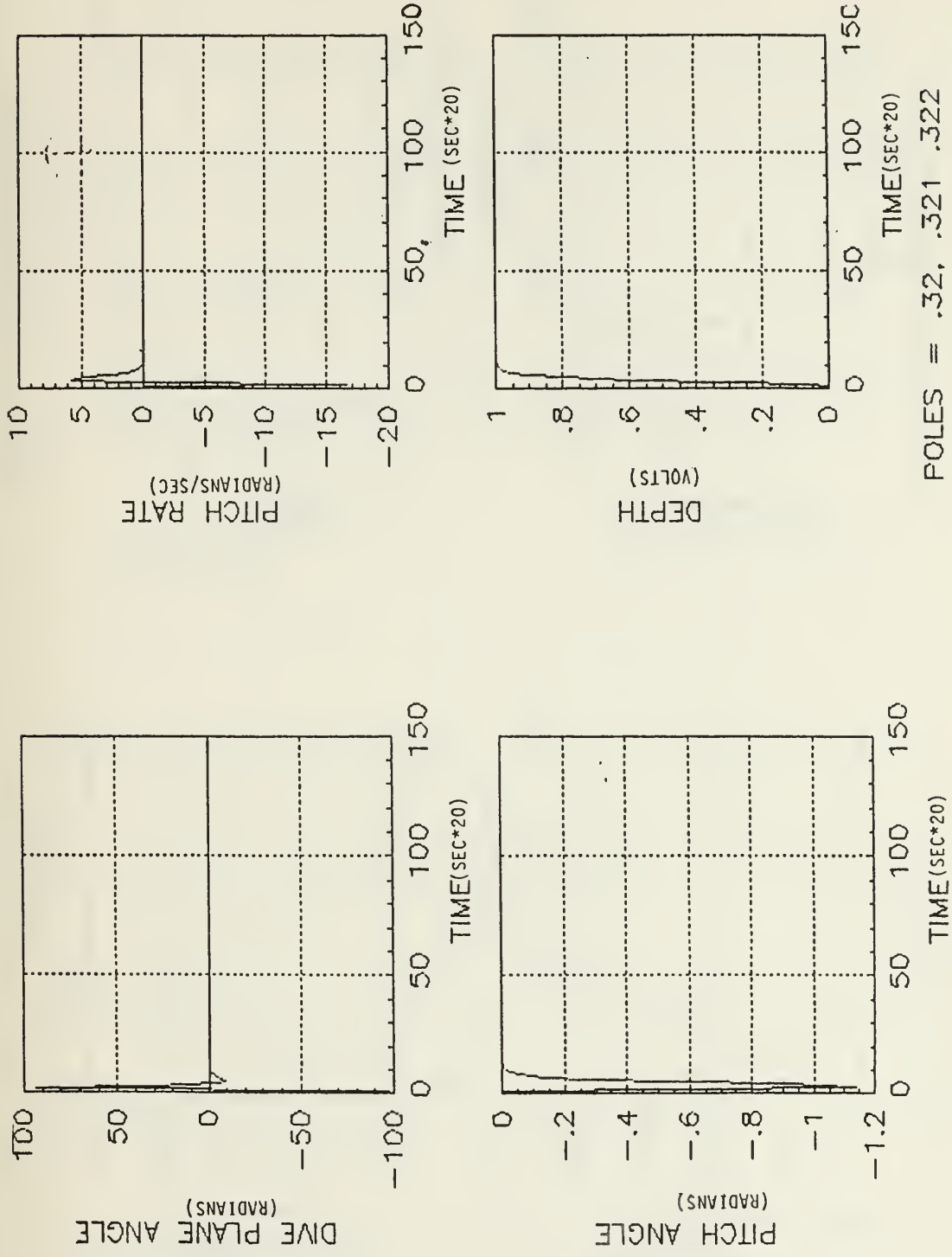

Figure H1. Selected Pole Placement Performance

Figure H2. Selected Pole Placement Performance

Figure H3. Selected Pole Placement Performance

APPENDIX I
Saturated Closed Loop System

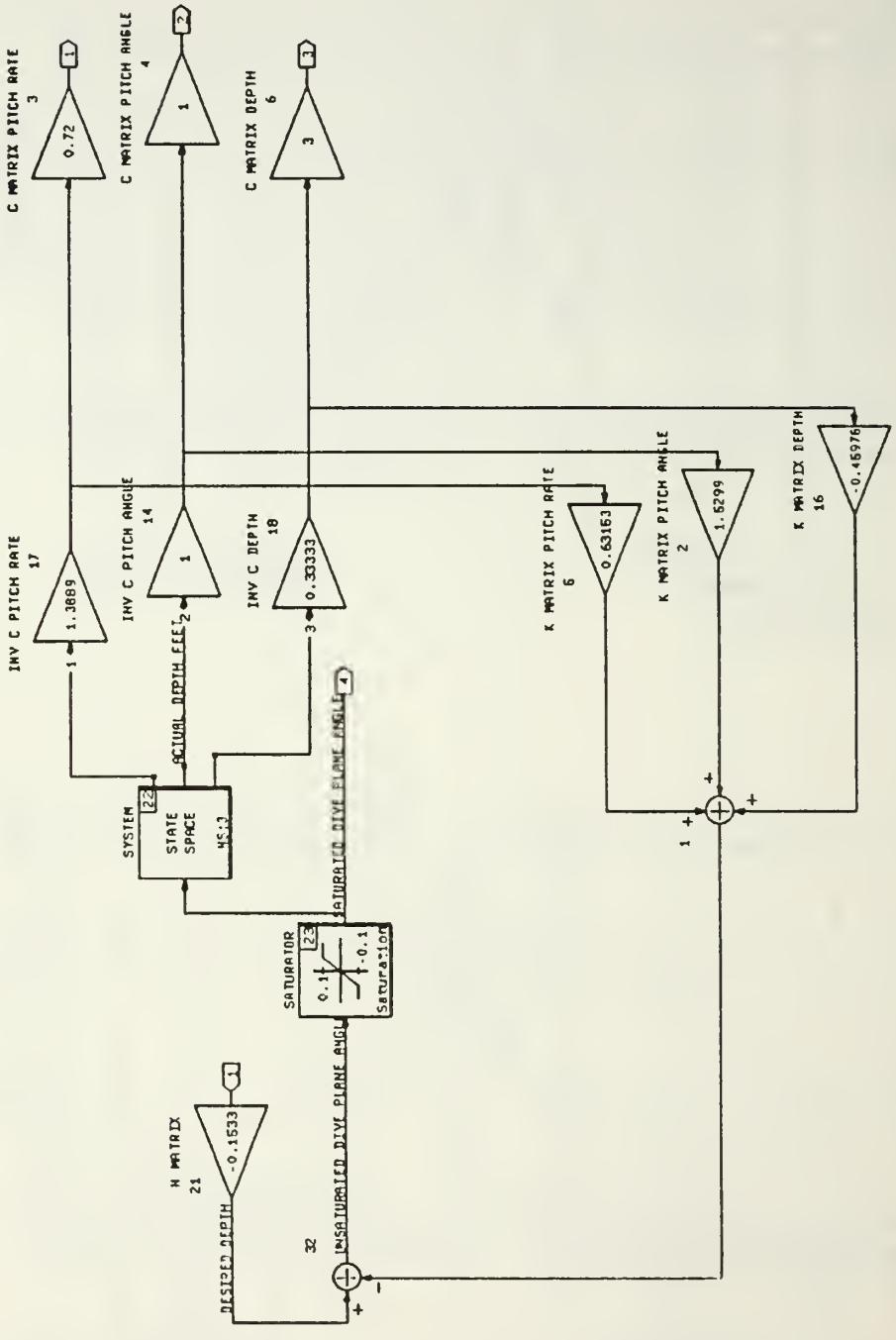

Figure I1. Saturated Closed Loop System

APPENDIX J
Saturated System Response

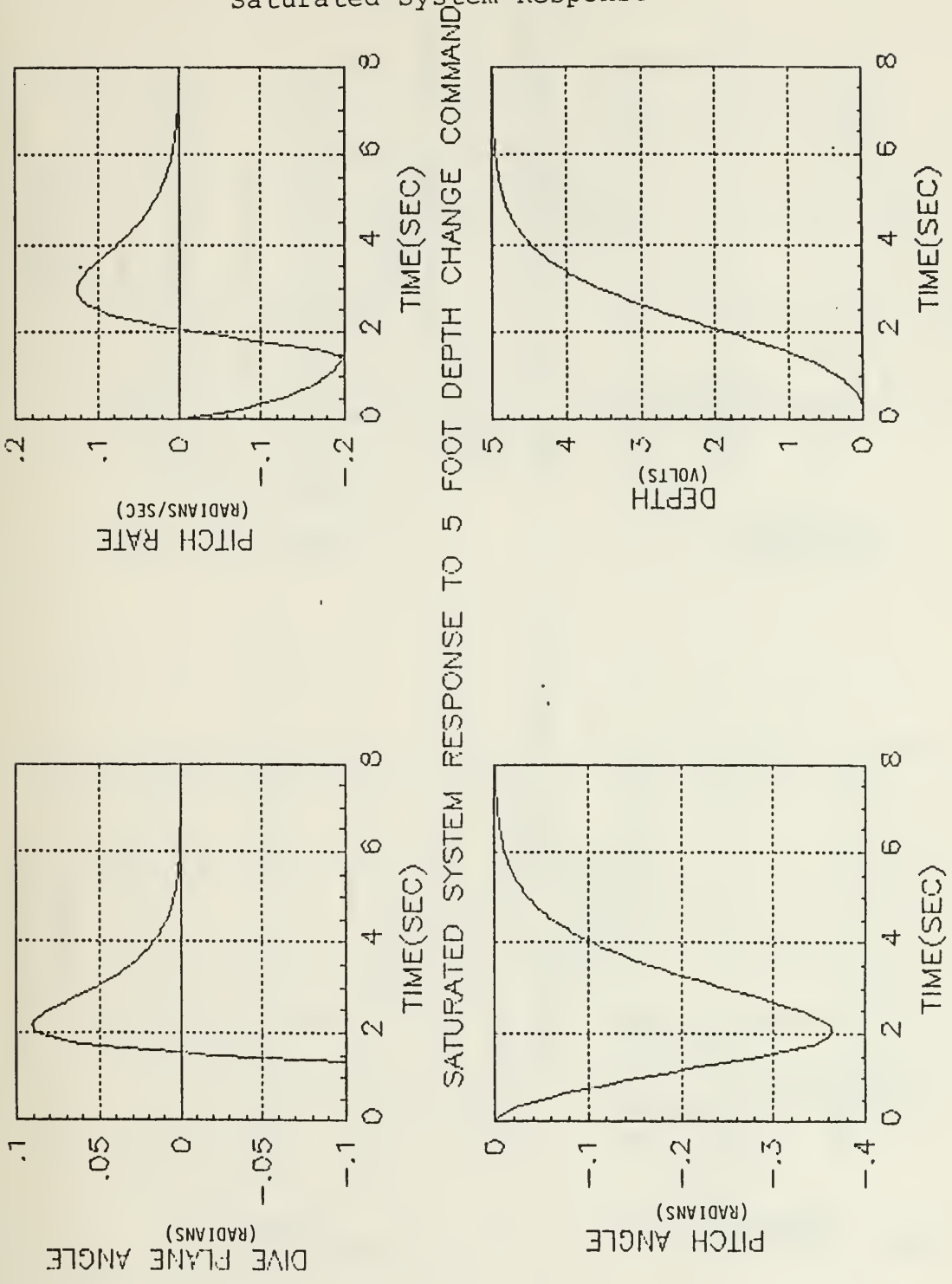

Figure J1. Saturated System Response

Figure J2. Saturated System Response

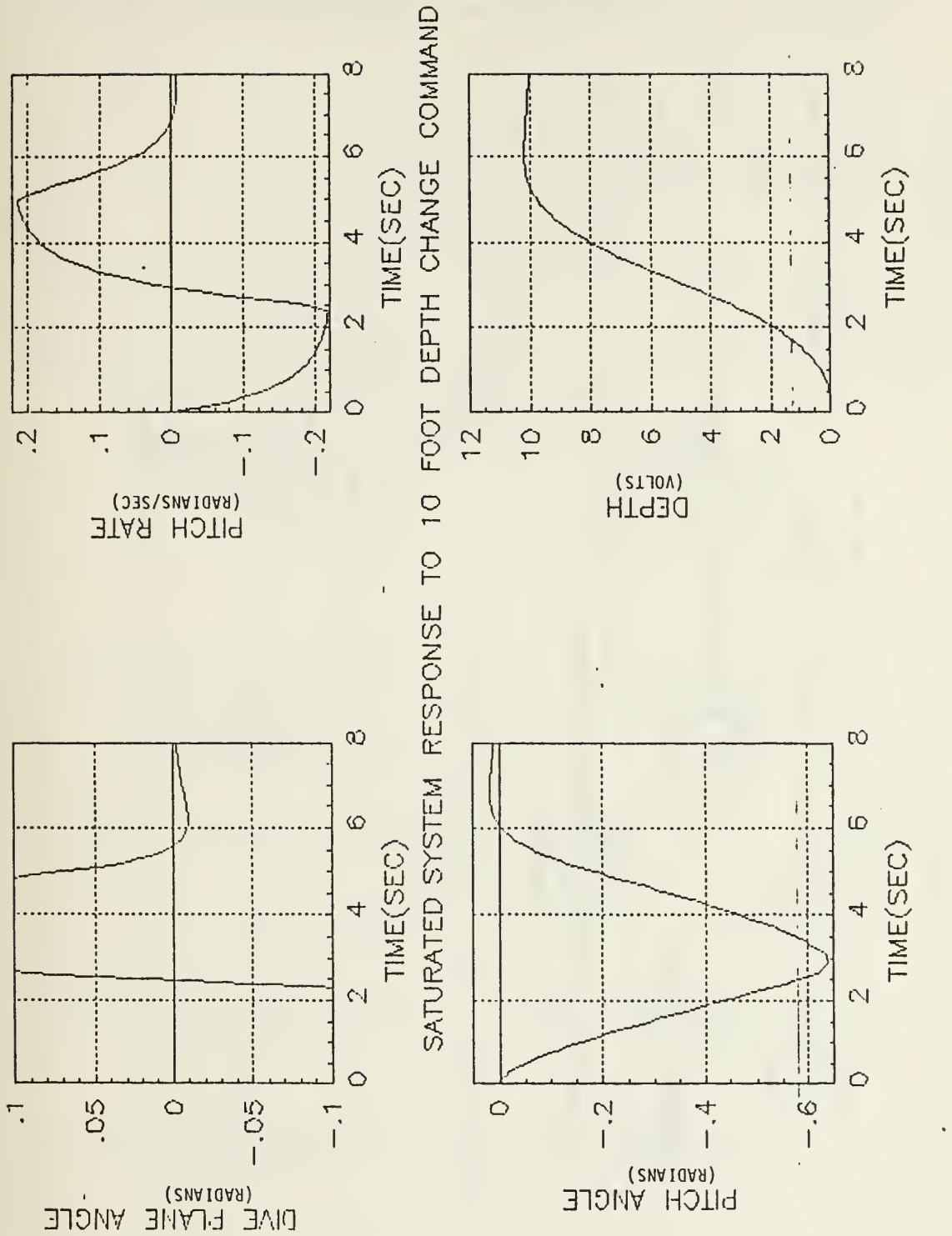

Figure J3. Saturated System Response

APPENDIX K

Saterated and Biased System Block Diagram and Response

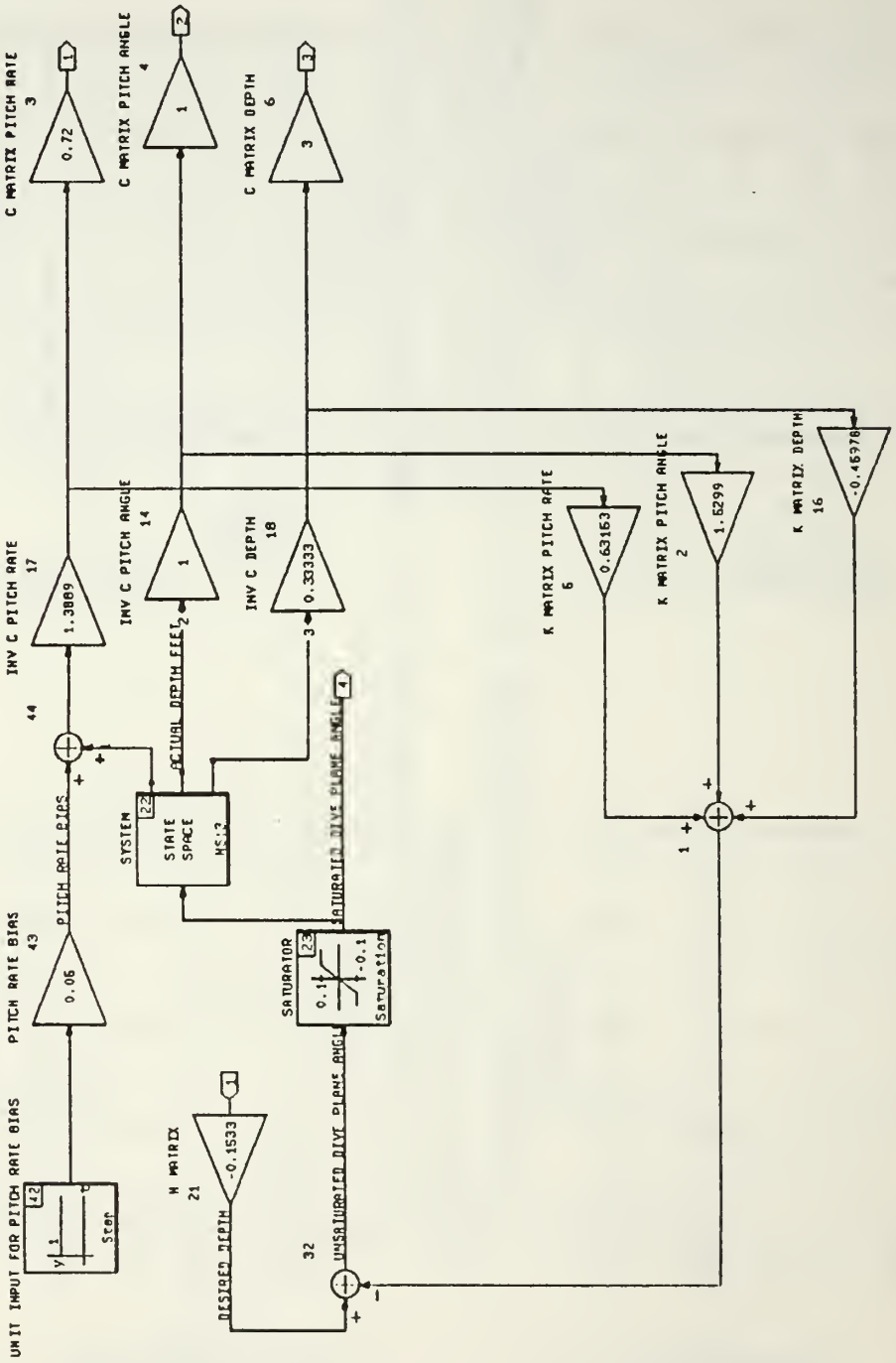

Figure K1. Saturated and Biased System

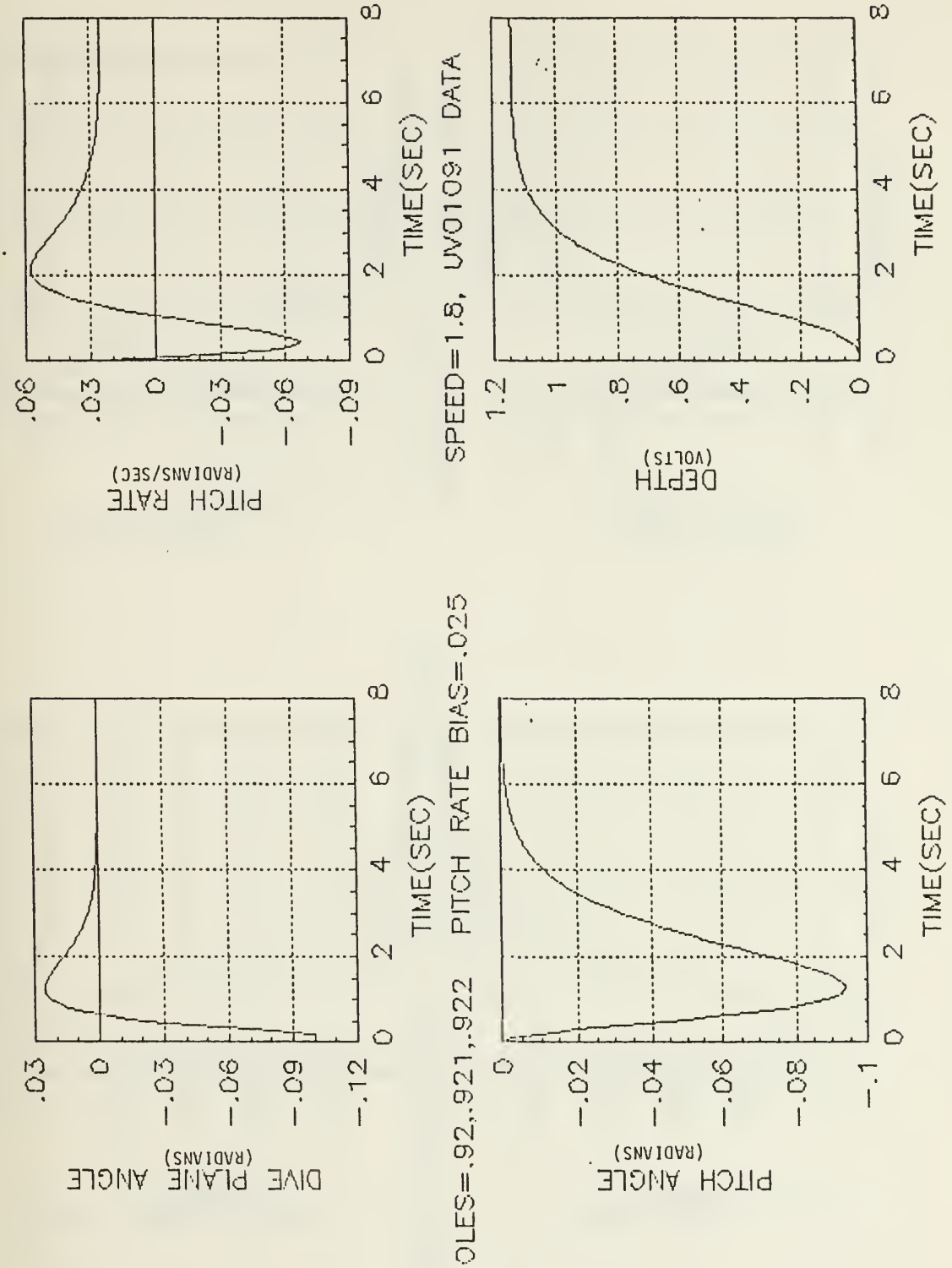

Figure K2. Saturated and Biased System Response

Figure K3. Saturated and Biased System Response

Figure K4. Saturated and Biases System Response

Figure K5. Saturated and Biased System Response

Figure K6. Saturated and Biased System Response

Figure K7. Saturated and Biased System Response

APPENDIX L
Observed System Block Diagram

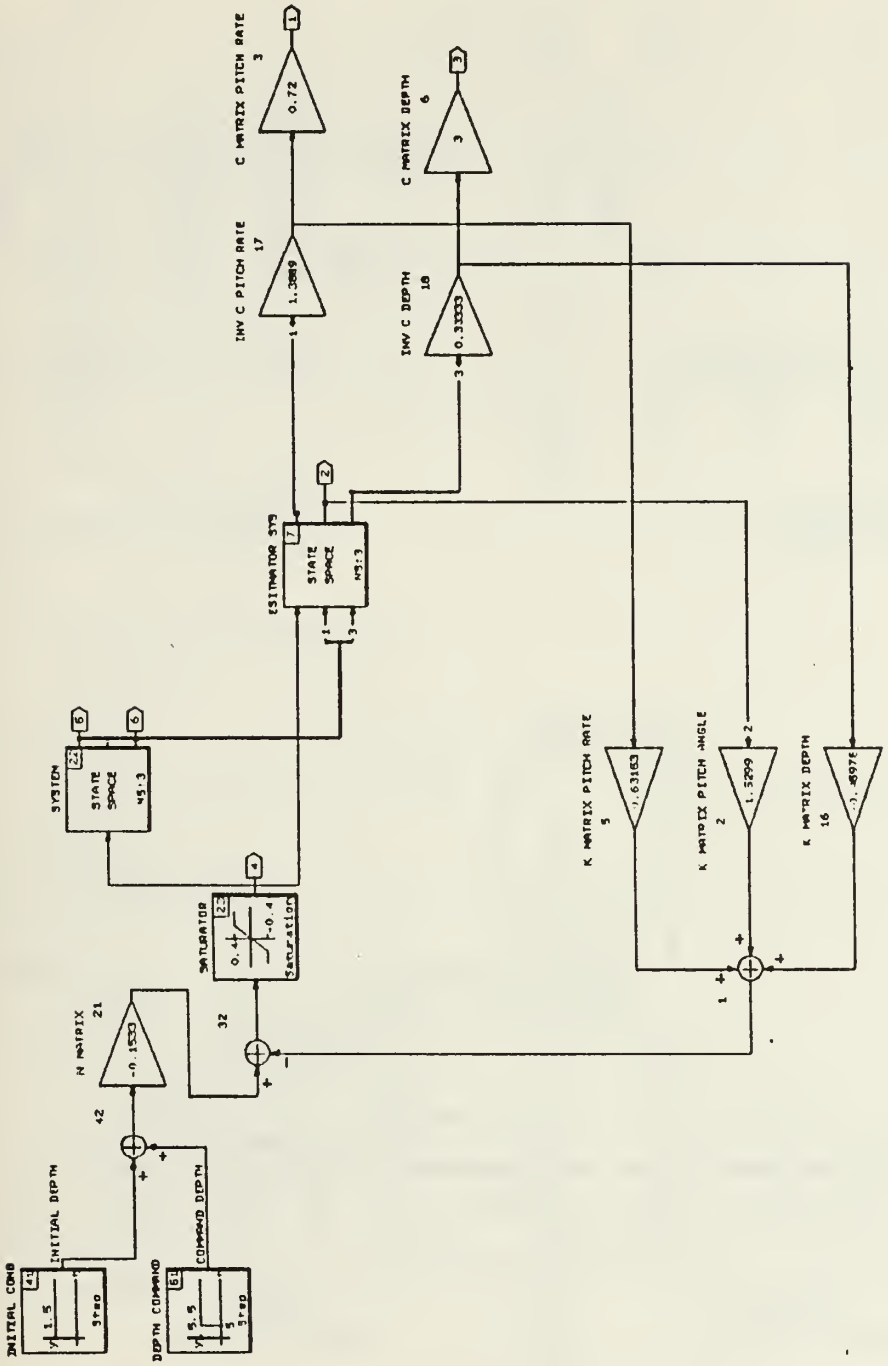

Figure L1. Observed System Block Diagram

Figure L2. Observed System Response

APPENDIX M
Matrix-x Program "DISTPOLE.MX"

```
L=28/12;
UX=SPEED;

ZW=    P(1); // HEAVE DAMPING
ZQ=    P(2); // CROSS COUPLING (PITCH)
MW=    P(3); // CROSS COUPLING (HEAVE)
MQ=    P(4); // PITCH DAMPING
ZD=    P(5); // MOMENT EFFECT
MD=    P(6); // MOMENT EFFECT MD=2*ZD
MZDW=  P(7); // MASS + ADDED MASS
IYY=   P(8); // INERTIA + ADDED INERTIA

A22=MQ*UX/L/IYY;B21=MD*UX*UX/L/L/IYY;
A=[A22 0 0;1 0 0;0 -UX 0];
NS=3;B=[B21;0;0];
C=[0.72 0 0;0 1 0;0 0 3];D=[0;0;0];
S=[A B;C D];
SD=DISCRETIZE(S,3,.2);
[A B C D]=SPLIT(SD,3);
B=B*1.5;
POLES=[.5709;.8173+JAY*.1426];
K=POLEPLACE(A,B,POLES);
CZ=[C(3,1) C(3,2) C(3,3)];
AC=A-B*K;
I=[1 0 0 ;0 1 0;0 0 1];
AN=INV((CZ)*INV(I-AC)*B);BC=B*AN;
AO=[(A) (B);[0 0 0 1]];BO=[(B);[0]];
CO=[0 0 3 0];DO=[0];
SO=[AO BO;CO DO];
OPOLES=[.3 .31 .32 .33];KO=POLEPLACE(AO',CO',OPOLES);
AOC=AO-KO'*CO;
IO=[1 0 0 0;0 1 0 0;0 0 1 0;0 0 0 1];
MBC=AOC-BO*[K 1];
KOC=KO'*[C(3,1) C(3,2) C(3,3)];
BKC=B*K;BOC=BO*AN;
SYS1=[A -BKC -B BC B];
SYS2=[SYS1;KOC MBC BOC [0;0;0;0]];
SYS3=[SYS2;EYE(7) 0.0*ONES(7,2)];
Z=7;W=4;
IN=[Z*ONES(30,1) W*ONES(30,1)];[Y]=FILP(SYS3,IN);
CU=[0 0 0 -1*K(1) -1*K(2) -1*K(3) -1];DU=[AN 0];
SYS4=[SYS2;CU DU];[U]=FILP(SYS4,IN);
Y(:,3)=3*Y(:,3);Y(:,6)=3*Y(:,6);
PR=[Y(:,1) Y(:,4)];PA=[Y(:,2) Y(:,5)];
DTH=[Y(:,3) Y(:,6)];DF=[Y(:,7) U];
PLOT (PR,'UPPER RIGHT/XLABEL/TIME(SEC*20)/YLABEL/ACT & EST PITCH RATE/...
 TITLE/CPOLES=.6,.61,.62/');
PLOT (PA,'LOWER LEFT/XLABEL/TIME(SEC*20)/YLABEL/ACT & EST PITCH ANGLE/TITLE...
 /OPOLES=.3,.31,.32,.33/');
PLOT (DTH,'LOWER RIGHT/XLABEL/TIME(SEC*20)/YLABEL/ACT & EST DEPTH/...
TITLE/COMMAND DEPTH=1/');
PLOT (DF,'UPPER LEFT/XLABEL/TIME(SEC*20)/YLABEL/DIVE COM & EST W/TITLE...
 /ACT DISTURBANCE=-0.2/');
```

Figure M1.

Figure M2. Compensated System Response

Figure M3. Compensated System Response

Figure M4. Compensated System Response

APPENDIX N
AUV Horizontal Motion System Block Diagram

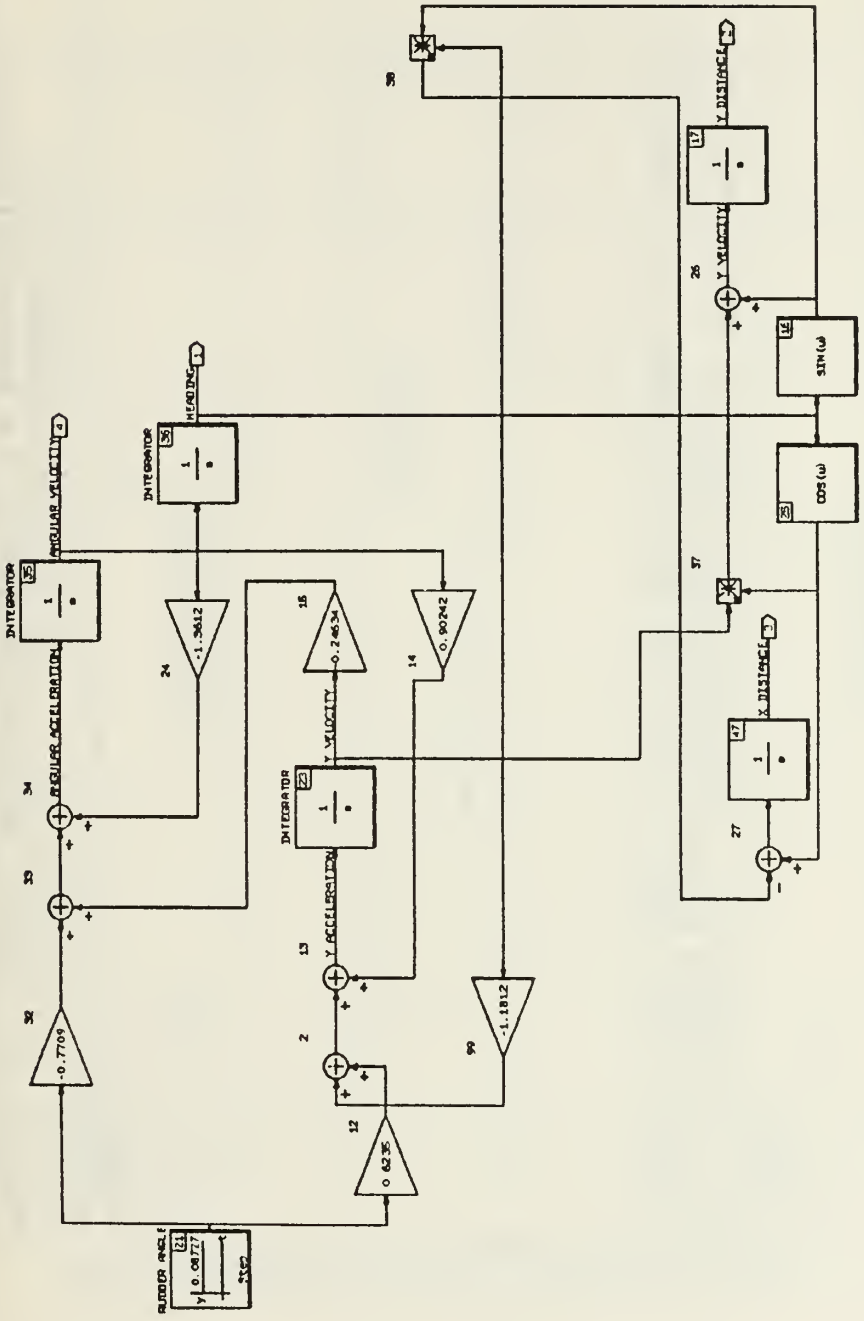

Figure N1. AUV Horizontal Motion System Block Diagram

APPENDIX O
Matrix-x Programs "AUVTURNPLOT" and "AUVMULTIPLOT"

"AUVTURNPLOT"

```
T=[0:0.4:20]';
U=1.8;
Y=SIM(T);
PLOT (Y(:,2),Y(:,3),'XLABEL/TRANSFER DISTANCE (NON-DIMENSIONAL)...
/YLABEL/ADVANCE DISTANCE (NON-DIMENSIONAL)/...
TITLE/AUV TURN PATH: 2.1 FPS, 30 DEG LFT RUDDER, 20 TIME UNITS/')
```

"AUVMULTIPLOT"

```
T=[0:1.5:105];
T=T';
U=ONES(T);
Y=SIM(T,U,.1,.1);
Y1=[Y(:,1) Y(:,2) Y(:,3) Y(:,4) 360/2/3.1415926*Y(:,5)];
PLOT (T,Y1,'TITLE/5 DEG LEFT RUDDER AT 3.6 FPS/COLOR(3)=4/...
XLABEL/TIME(SEC)/YLABEL/HEADING,ANG VEL,X DIST,Y DIST,RUDDER ANG/');
```

APPENDIX P
AUV Horizontal System Response

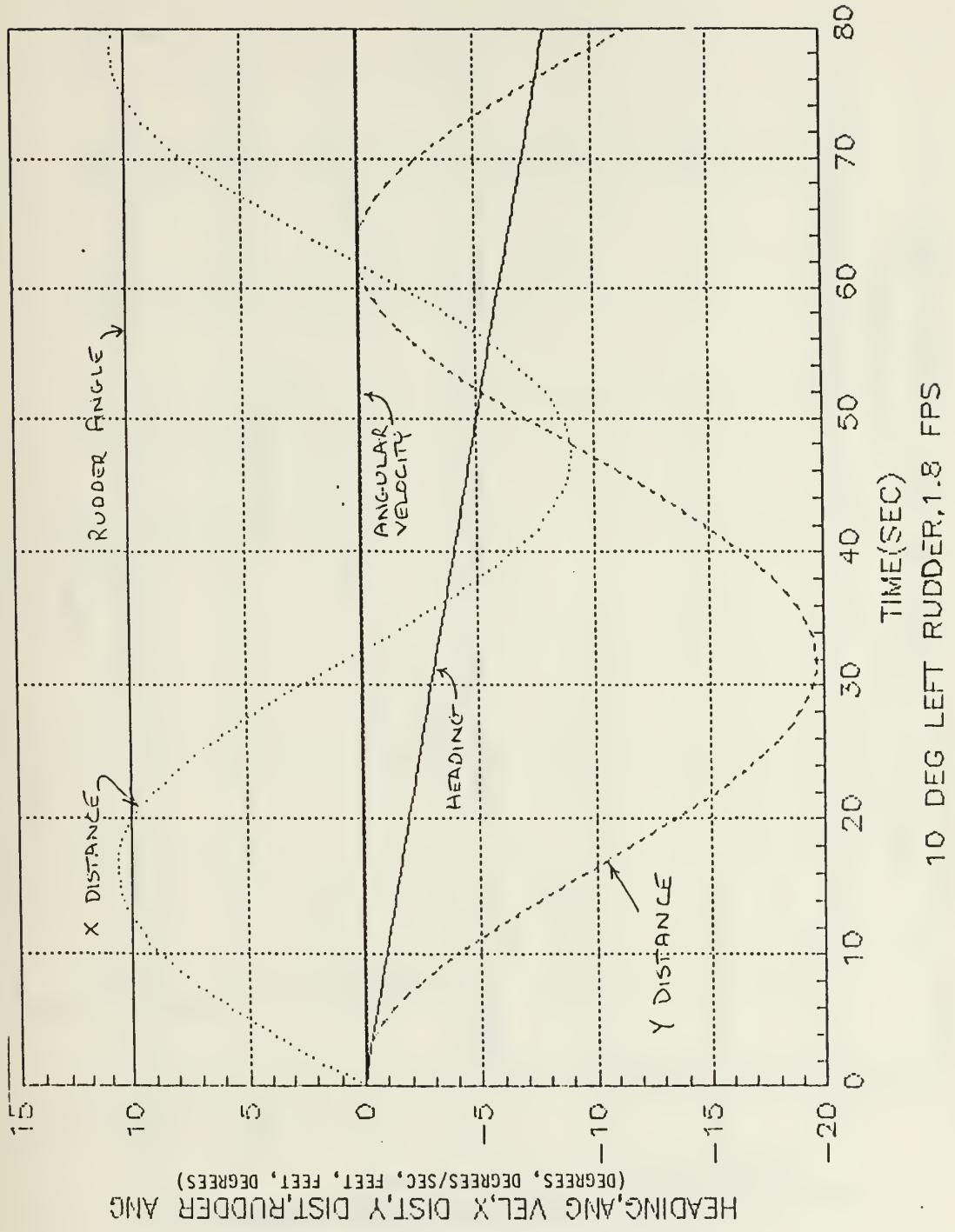

Figure P1. AUV Horizontal System Response

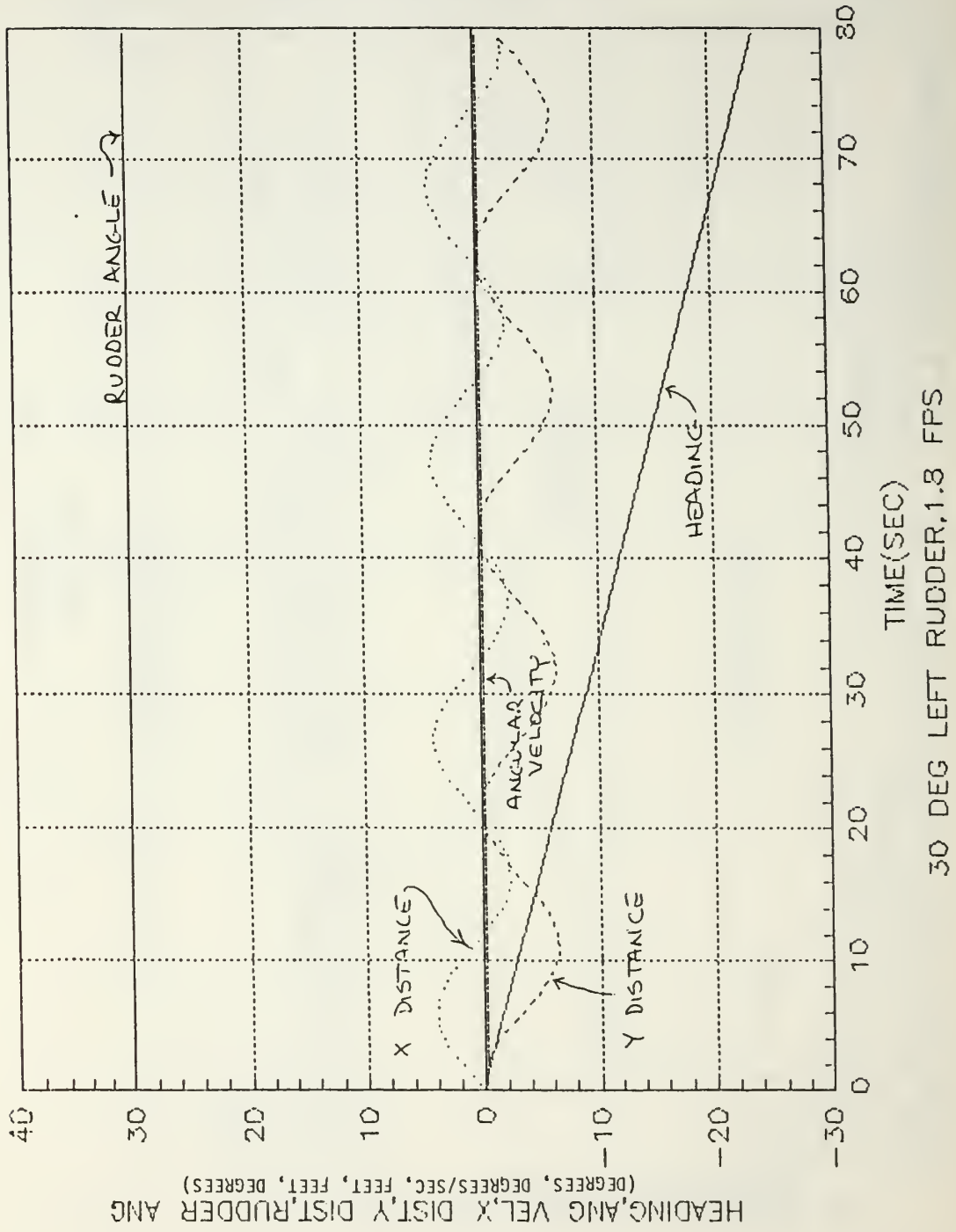

Figure P2. AUV Horizontal System Response

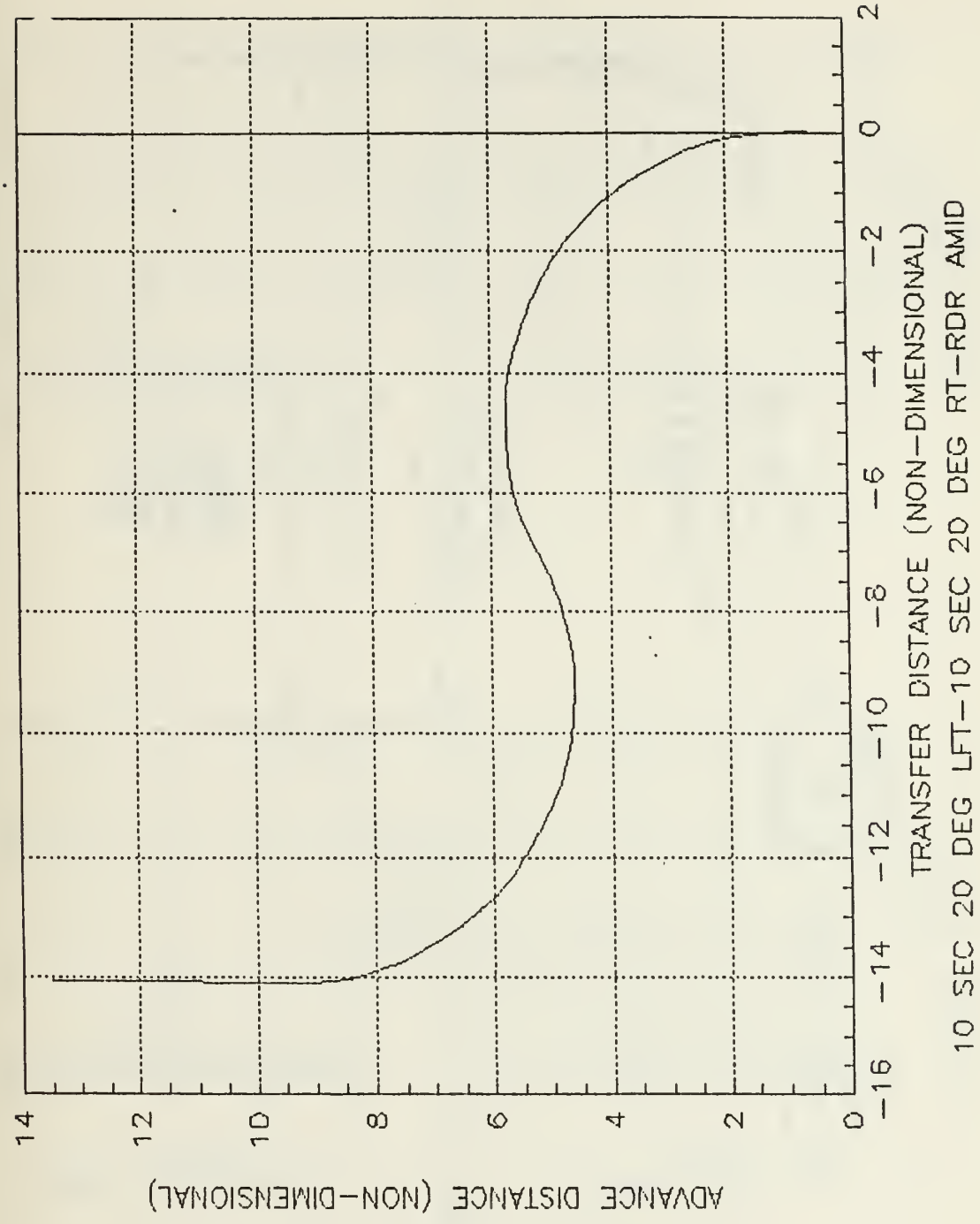

Figure P3. AUV Horizontal System Response

APPENDIX Q

Matrix-x Program "DEPTHIN.MX" Block Diagram

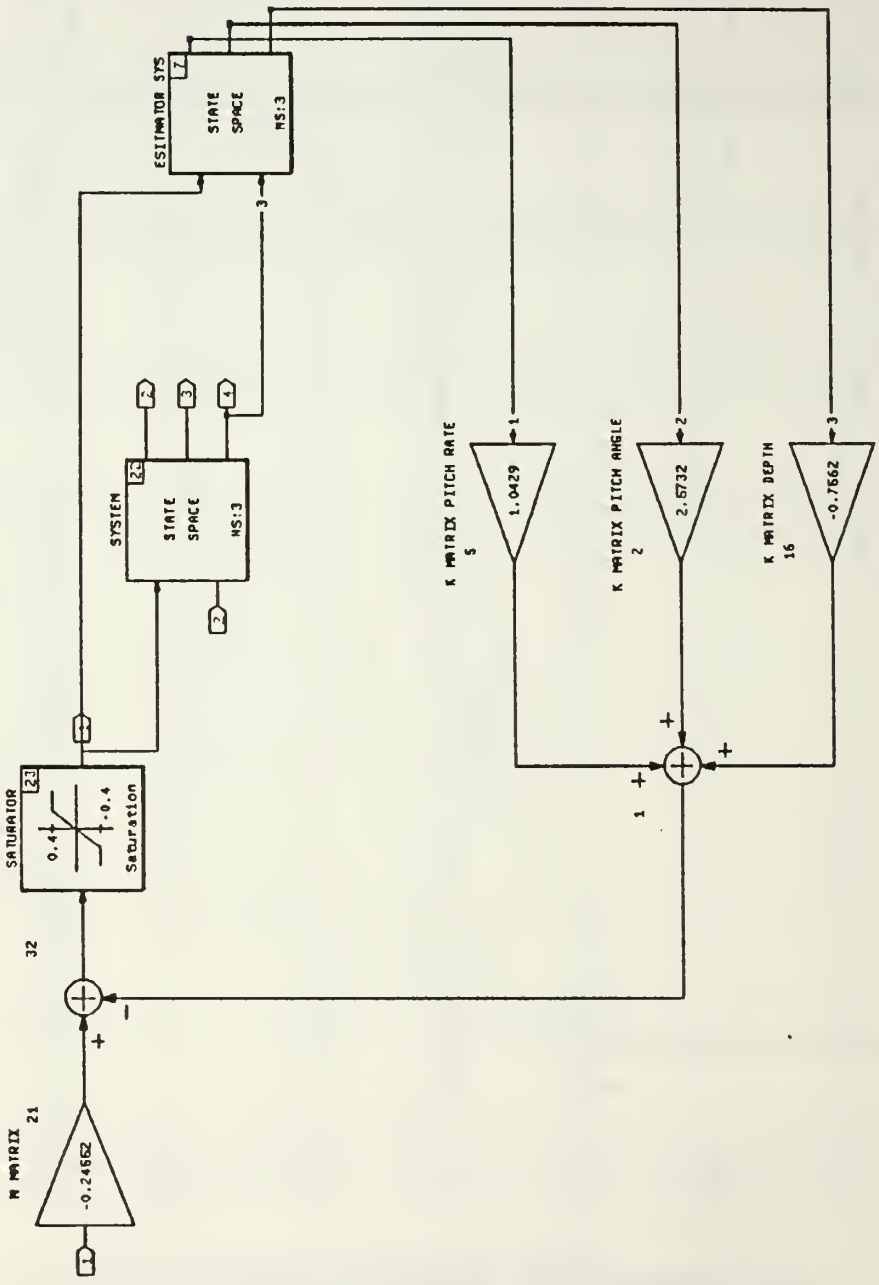

Figure Q1. Matrix-x Program "DEPTHIN.MX" Block Diagram

APPENDIX R
"DEPTHIN.MX" Performance Curves

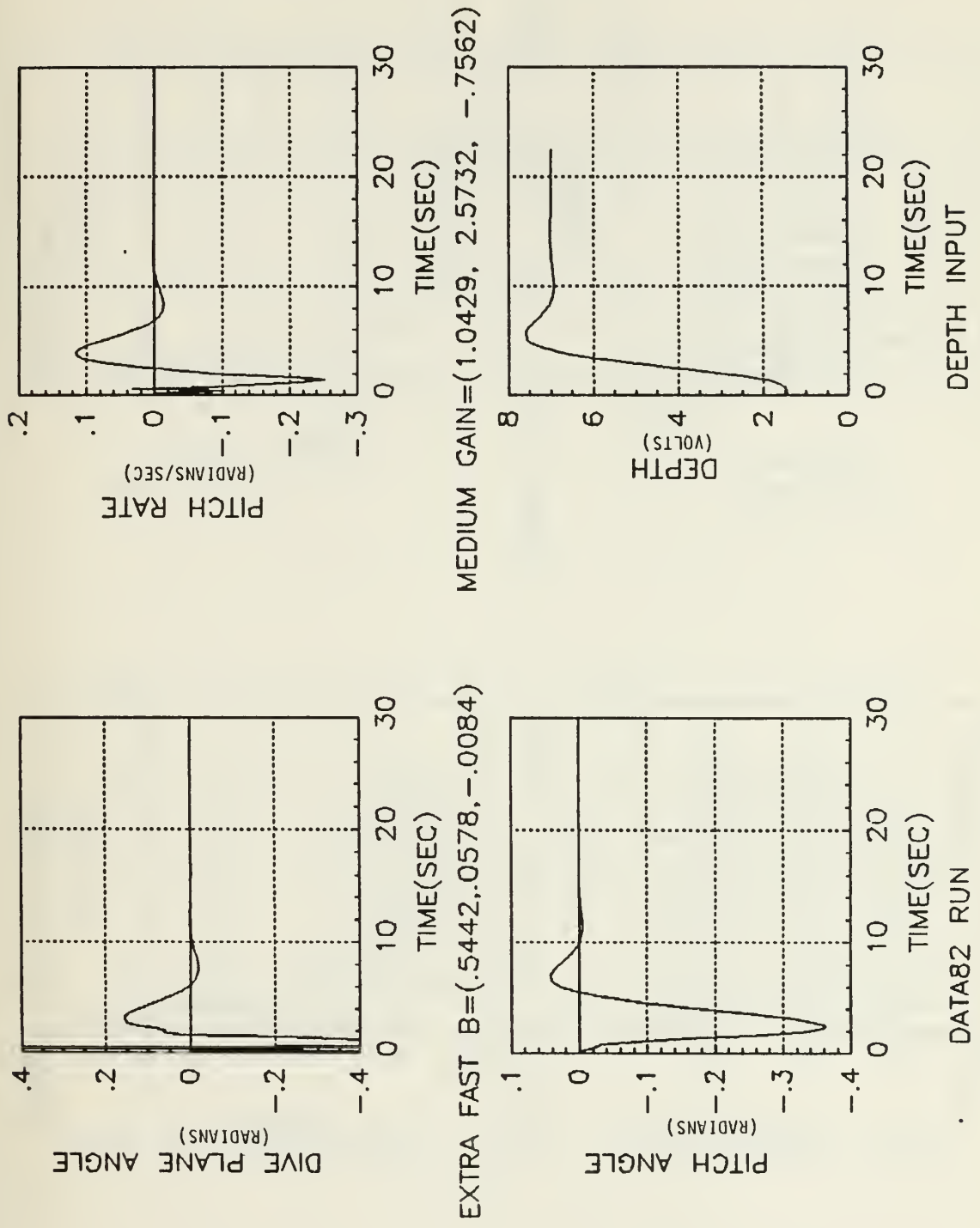

Figure R1. "DEPTHIN.MX" Performance Curves

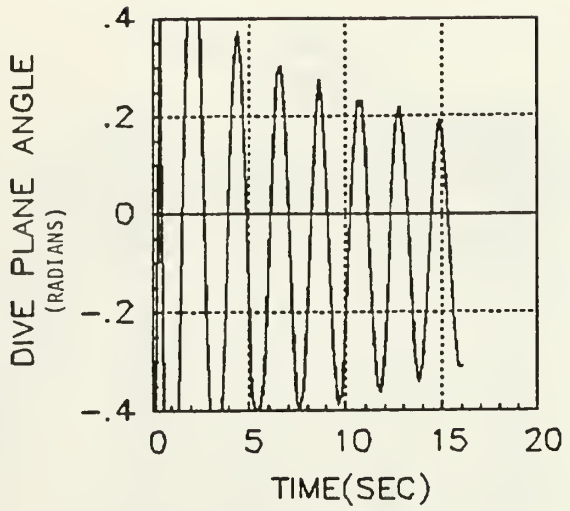

FAST B=(.3628,.0385,-.0056)

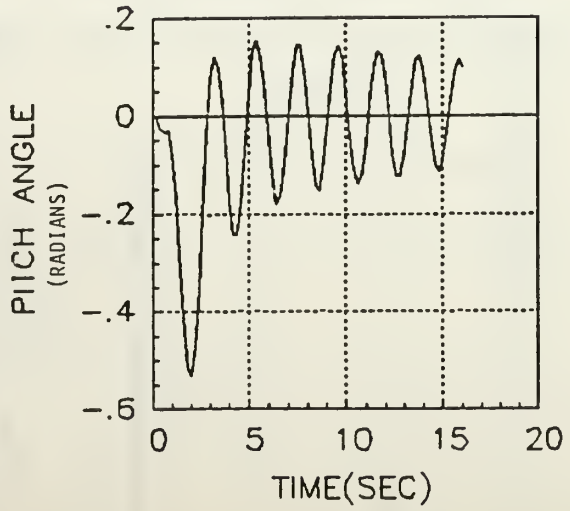

DATA81 RUN DISTURB=.15

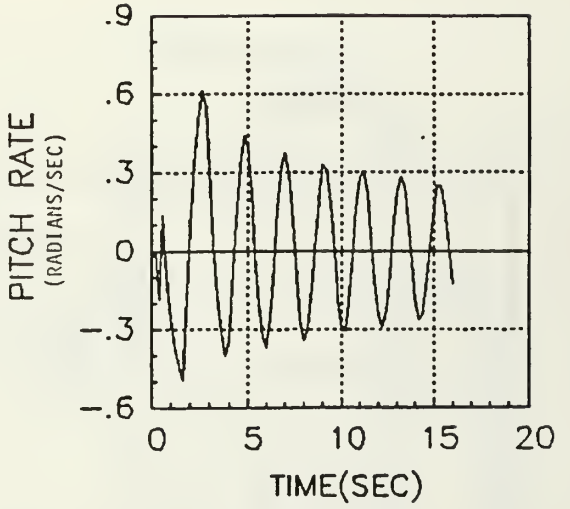

MEDIUM GAIN=(1.0429, 2.5732, -.7562)

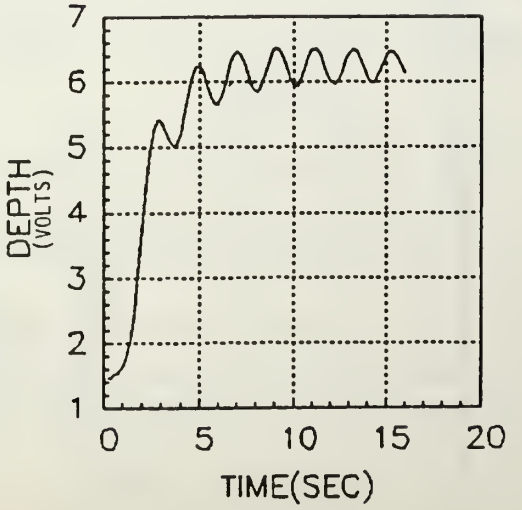

DEPTH INPUT

Figure R2. "DEPTHIN.MX" Performance Curves

Figure R3. "DEPTHIN.MX" Performance Curves

LIST OF REFERENCES

1. Healey, A.J., Cristi, R., Smith, D.L., McGhee, R. B.,"Navigation, Path Planning, Dynamics and Control of Generic Autonomous Underwater Vehicles Proposal," Research Proposal to Naval Postgraduate School Direct Research Fund, Monterey, California, April 1988.

2. NSCS Technical Memorandum 231-78, *SDV Simulator Hydrodynamic Coefficients*, by N.S. Smith, J. W. Crane and D. C. Summey, June 1978

3. Boncal, R., *A Study of Model Based Maneuvering Controls for Autonomous Underwater Vehicles*, M.S.M.E. Thesis, Naval Postgraduate School, Monterey, California, December 1987.

4. Brunner, G., *Experimental Verification of AUV Performance*, M.E. Thesis, Naval Postgraduate School, Monterey, California, March 1988.

5. NSRDC Report 2510, *Standard Equations of Motion for Submarine Simulation*, by M. Gertler and G. R. Hagen, June 1967.

6. Abkowitz, M. A., *Stability and Motion Control of Ocean Vehicles*, M.I.T. Press, 1969.

7. Kwakernaak, H., and Sivan, R., *Linear Optimal Control Systems*, Wiley Interscience, 1972.

8. Reina, J., *AUV Dive Control System Development Including Sensor Bias Compensation and Parameter Estimation*, M.S.M.E. Thesis, Naval Postgraduate School, Monterey, California, December 1988.

9. Young, K. K., and Kwatny, H.G., *Variable Structure Servomechanism Design and Applications to Overspeed Protection Control*, Automatica, vol 18, no.4, pp.385-400, 1982.

10. Corliss, M., and Leitmann, G.,"Transmission Automatic Control",I.E.E.E.Symposium, vol 26, pp.1139, 1981

INITIAL DISTRIBUTION LIST

1.	Defense Technical Information Center Cameron Station Alexandria, Virginia 22304-6145	2
2.	Library, Code 0142 Naval Postgraduate School Monterey, California 93943-5002	2
3.	Chairman, Code 69Hy Department of Mechanical Engineering Naval Postgraduate School Monterey, California 93943-5000	2
4.	Professor D. L. Smith, Code 69Sm Department of Mechanical Engineering Naval Postgraduate School Monterey, California 93943-5000	1
5.	Professor R. McGhee, Code 52Mz Department of Computer Science Naval Postgraduate School Monterey, California 93943-5000	1
6.	Professor R. Christi, Code 62Cx Department of Electrical and Computer Engineering Naval Postgraduate School Monterey, California 93943-5000	1
7.	Dr. G. Dobeck, Code 4210 NCSC Panama City, Florida 32407-5000	1
8.	Russ Werneth, Code U25 Naval Surface Weapons Center White Oak, Maryland 20910	1

9. Paul Heckman, Code 943 — 1
Head, Undersea AI & Robotics Branch
Naval Ocean System Center
San Diego, California 92152

10. Dr. D. Milne, Code 1563 — 1
DTRC, Carderock
Bethesda, Maryland 20084-5000

11. Naval Sea Systems Command — 1
Code PMS-350, Attn: Ms. Judy Runsey
Washington, D.C. 20362-5101

12. Director of Research Administration — 1
Code 012
Naval Postgraduate School
Monterey, California 93943-5000

13. CDR. Gordon S. MacDonald — 1
Nuclear Repair Officer
Portsmouth Naval Shipyard
Kittery, Maine 03904

14. Dick Blidberg — 1
University of New Hampshire
Marine Systems Engineering Lab
SERB Building 242
Durham, New Hampshire 03824

Thesis
M183233 MacDonald
c.1 Model based design and verification of a rapid dive controller for an Autonomous Underwater Vehicle.

Thesis
M183233 MacDonald
c.1 Model based design and verification of a rapid dive controller for an Autonomous Underwater Vehicle.

AMERICAN BINDERY
TOPEKA KANSAS

thesM183233
Model based design and verification of a
3 2768 000 82688 7
DUDLEY KNOX LIBRARY